

8-AT

**GENERATION, MIGRATION, AND TRANSPORTATION
OF GAS CONTAMINATED REGIONS OF DRILLING FLUID**

A Dissertation

**Submitted to the Graduate Faculty of the
Louisiana State University
and Agricultural and Mechanical College
Baton Rouge, Louisiana**

**In partial fulfillment of the requirements
for the degree of
Doctor of Philosophy**

in

The Department of Petroleum Engineering

by

**Vicente Casariego
M.S., Louisiana State University, 1981**

Fall, 1987

ACKNOWLEDGEMENT

The author extends his gratitude to Dr. Adam "Ted" Bourgoyne, Jr. under whose valuable guidance, supervision, trust and encouragement, this work was accomplished.

Special gratitude to Dr. William Holden for his timely suggestions and interest in this work.

Thanks to Dr. Bassiouni and the staff members of the Petroleum Engineering Department.

Appreciation is extended to Kyle Fontenot for his enthusiasm in the experimental determinations of bubble volumes, and to my friend Craig Lilyestrom.

The research was financed through funds made available by the Mineral Management Service, of the United States Department of the Interior.

Thanks to the Mexican Petroleum Institute for granting me complementary student loans.

To my wife Maria Teresa for enduring the difficult times that we found along the accomplishment of my Ph.D. program, and to my daughter Carla and son Vince for their love and "tender smiles" that fill my life at all times, I express my love and gratitude.

The author wishes to dedicate this dissertation to the memory of Dr. Oscar Kimbler[†] for his humane quality, respect towards his fellow men, and for his gentleness, for it is people like him that make this world a better place to live in.

TABLE OF CONTENTS

	Page
Acknowledgement	ii
Table of Contents	iii
List of Tables	vi
List of Figures	vii
Abstract.	xii
 Chapter	
I. Introduction	1
II. Previous Investigations	12
2.1 Flow Patterns	12
2.1.1 Extended Liquids	13
2.1.2 Tubes	14
2.1.3 Annuli	27
2.1.4 Complex Geometries	27
2.2 Bubble Rise Velocity	29
2.2.1 Extended Liquids	30
2.2.2 Tubes	41
2.2.3 Annuli	60
2.3 Liquid Holdup Correlations	67
2.4 Bubble Generation	73
2.5 Bubble Size Distribution for Bubble Flow Pattern	82
2.6 Apparent Migration Rates for Gas Kicks	83
III. Analytical and Experimental Approach	85
IV. Transitional Boundary Lines for Bubble Geometries	87

TABLE OF CONTENTS (continued)

	Page
4.1 Theoretical Development	87
4.2 Analysis of Experimental Data	90
4.3 Significance of the Proposed Correlations	95
V. Bubble Generation	101
5.1 Simulation of Bubble Formation at an Orifice Under Steady State Gas Flow Rate	101
5.2 Experimental Apparatus	112
5.3 Actual and Theoretical Volume of the Bubbles	112
5.3.1 Discussion of Experimental Data	116
5.3.2 Discussion of Theoretical Data	128
5.3.3 Comparison of Actual and Theoretical Bubble Size	132
VI. On the Velocity of a Swarm of Bubbles	137
6.1 Relationships Between Parameter of Single Bubbles and Swarm of Bubbles	141
6.2 Theory of Two-Phase Bubble Flow	142
VII. Principle of Minimum Energy Dissipation	145
7.1 Specific Energy of a Swarm of Bubbles	145
7.2 Equilibrium Bubble Size	151
7.3 Drag Law for a Swarm of Bubbles	154
7.4 Theoretical Gas Concentration	155
VIII. Modelling of Well Control Operations.	164

TABLE OF CONTENTS (continued)

	Page
8.1 Experimental Apparatus and Procedure	166
8.2 Comparison of Actual and Theoretical Casing Pressures	168
IX. Summary and Conclusions	174
Nomenclature	177
References	186
Bibliography	192
Appendix A	198
Appendix B	203
Vita	218

LIST OF TABLES

Table		Page
5.1	Tubing Dimensions	114
5.2	Fluid Properties	114

LIST OF FIGURES

Figure	Page
1.1 History of Water Depth Record for Floating Drilling Vessels	3
1.2 Schematic of Typical Flow Geometry Present for Deep Water Blowout Control Operations (After Bourgoyne et al).	4
1.3 Predicted Well Pressure Response for Example Described in Figure 1.2 (After Bourgoyne et al).	6
1.4 Example of Pressure Control Training Simulators at LSU Blowout Prevention Center	8
1.5 Processes During Well Control Operations	10
2.1 Typical Shapes of Air Bubbles of Several Volumes in Various Liquids (After Haberman and Morton)	15
2.2 Typical Shapes of Air Bubbles in Water (After Levich)	16
2.3 Flow Pattern Description for Vertical Two-Phase Flow Selected by Taitel et al	17
2.4 Flow Pattern Description for Vertical Two-Phase Flow Used by Chierici et al	20
2.5 Flow Regime Numbers of Duns and Ross	22
2.6 Shape Assumed by Large Gas Bubble Rising in Annulus	28
2.7 Angle Subtended of Lenticular Bubbles and Relationship between Curvature and Equivalent Radii	36
2.8 Variation of Bubble Velocity with r_c/r_t (After Collins)	42

LIST OF FIGURES (continued)

Figure	Page
2.9 Values of b as a Function of Tube Diameter and Surface Tension (After Uno and Kintner)	45
2.10 Dimensionless Constant c_1 Versus Bubble Reynolds Number (After Griffith and Wallis)	48
2.11 Dimensionless Constant c_2 as a Function of Liquid Reynolds Number and Bubble Reynolds Number (After Griffith and Wallis)	49
2.12 General Correlation for Velocity of Rise of Cylindrical Air Bubbles (After White and Beardmore)	53
2.13 Bubble Velocity Vs. Surface Tension Parameter for Ranges of Reynolds Numbers (After Zukoski)	56
2.14 Variation of Normalized Velocity with Diameter Number for Angles of Inclination as Measured with Respect to a Horizontal Plane (After Zukoski)	57
2.15 Variation of v_{b0}/v_{∞} with r_c/r_t (After Collins)	59
2.16 Definition of Equivalent Radius and Perimeter for Plane Bubble	63
2.17 Bubble Velocity vs Equivalent Bubble Diameter as Measured in an Open, 6.375-in. by 2.375-in. Annulus	84
4.1 Relationship Between Surface Tension and Inertia Forces for the Stability of Spherical Bubbles	88
4.2 Reynolds Number, at Which a Change in Bubble Geometry Occurs, as a Function of the Liquid Viscosity Number	92

LIST OF FIGURES (continued)

Figure	Page
4.3 Drag Factor vs Reynolds Number. Correlation for Solid Spheres	96
4.4 Drag Factor vs Reynolds Number. Overlay of Solid Spheres Correlation with Data for Oblate Spheroid Bubbles Rising in Both Mineral Oil and Varsol	98
4.5 Karman Number Vs. Bubble Reynolds Number for Oblate Spheroid Bubbles Rising in Varsol and in Mineral Oil.	99
5.1 Two Stage Model of Bubble Formation	103
5.2a Experimental Apparatus to Generate Bubbles	113
5.2b Schematic of Porous Media Used to Generate Bubbles	113
5.3 Volume of Bubble Formed as a Function of Gas Injection Rate When Gas is Injected through Porous Media	118
5.4 Comparison of Bubble Volumes Formed from 0.25-in. Tubing as a Function of Gas Injection Rate. Data Obtained in Low Viscosity Fluids	120
5.5 Comparison of Bubble Volumes Obtained from Horizontal and Vertical Tubings	121
5.6 Comparison of Bubble Volumes Obtained by Injecting Nitrogen Gas and Methane Gas through a 0.25-in. Tubing	122
5.7 Comparison of Bubble Volumes Obtained in Water and in a Solution Containing 5% Sodium Chloride	123
5.8 Comparison of Bubble Volumes Obtained in Water by Injecting Gas through Tubings of Various Diameters	124

LIST OF FIGURES (continued)

Figure	Page
5.9 Comparison of Bubble Volumes Obtained in Water and in a 5 Poise Glycerine Solution by Injecting gas through a 0.25-in. Tubing	125
5.10 Comparison of Bubble Volumes Obtained in Glycerine by Injecting Gas through Tubings of Various Diameters.	126
5.11 Comparison of Bubble Volumes Obtained in Glycerine by Injecting Gas through a Porous Media, and through Tubings of Various Diameters	127
5.12 Theoretical Bubble Volumes Obtained for 0.25-in., and 0.50-in. Diameter Tubings in Water	129
5.13 Theoretical Bubble Volumes Obtained for 0.25-in., and 0.50-in. Diameter Tubings in a 5 Poise Fluid	130
5.14 Theoretical Bubble Volumes Obtained for Water and for a 5 Poise Fluid Tubing of 0.25-in. Diameter	131
5.15 Comparison of Theoretical vs Actual Bubble Volumes Formed in Water by Injecting N ₂ Gas through a 0.25-in. Diameter Tubing	133
5.16 Comparison of Theoretical vs. Actual Bubble Volumes Formed in 500cp Glycerine Solution by Injecting N ₂ Gas through a 0.25-in. Diameter Tubing	135
6.1 Individual Bubble Rising in a Swarm of Bubbles	138
7.1 Voidage vs Superficial Gas Velocity as Predicted by Equation 7.16	156
7.2 Superficial Gas Velocity vs Voidage as Predicted by Equation 7.16	156

LIST OF FIGURES (continued)

Figure	Page
7.3 Typical Superficial Gas Velocity vs Voidage Obtained with Richardson and Zaki's Correlation. Exponent 2.39.	158
7.4 Superficial Gas Velocity vs Voidage from Experimental Data	159
7.5 Gas Velocity vs Voidage as Predicted by Equation 7.18 for an Unweighted Water Base Mud	161
8.1 Comparison of Theoretical Casing Pressure Profile as Obtained by Existing Well Control Simulators and Measured Casing Pressure Profile for 15 bbl Gas Kick (After Bourgoyne, Holden, and Langlinais).	165
8.2 Schematic of the LSU-Goldking No. 1 Research Well, and the Gas Storage and Compression Wells (After Bourgoyne, Holden, and Langlinais).	167
8.3 Comparison of Theoretical and Measured Casing Pressure Profiles for Gas Migration of a 14.8 bbl Gas Kick	169
8.4 Comparison of Theoretical and Measured Casing Pressure Profiles for the 11.18 bbl Gas Kick Circulation Run	170
8.5 Comparison of Theoretical and Measured Casing Pressure Profiles for the 11.16 bbl Gas Kick Circulation Run	171

Casariago, Vicente, B. S. National University of Mexico, 1969

M.S., Louisiana State University, 1981

Doctor of Philosophy, Fall Commencement, 1987

Major: Petroleum Engineering; Minor: Mathematics

Generation, Migration, and Transportation of Gas Contaminated Regions of Drilling Fluid

Dissertation directed by Professor Adam T. Bourgoyne, Jr.

Pages in Dissertation, 218. Words in Abstract, 266

ABSTRACT

The control of high pressure gas encountered while drilling for hydrocarbon reservoirs is one of the more expensive and potentially dangerous problems of the oil producing industry. When the control of high pressure gas is not accomplished flow of gas from the formation to the wellbore occurs. Once detected, the gas influx is stopped by shutting-in the well. This is the first measure taken in a series of operations which are designed to bring back the well under control. These operations are referred to as well control procedures. Well control simulators are used both for evaluating well control procedures and for training of drilling personnel. Current well control simulators assume that the gas enters a wellbore as a continuous plug and travels at the same velocity of the drilling fluid. Unfortunately, these assumptions often lead to inaccurate results.

This study includes a review of the literature on bubble rise velocity in both extended and bounded systems, liquid holdup and flow pattern correlations, and bubble generation. A new method, obtained by applying the minimum energy dissipation principle, was developed to predict the size, shape, concentration, and velocity of gas bubbles within a wellbore during well control operations. The new method was then integrated into a well control simulator computer program that was developed as a part of an ongoing research effort towards the understanding of the behavior of a gas kick for the flow geometry present on a floating drilling vessel. Experiments were performed in a 6000 ft well to determine the accuracy of the computer program. Excellent agreement was seen between the observed and computed results.

ABSTRACT

The control of high pressure gas encountered while drilling for hydrocarbon reservoirs is one of the more expensive and potentially dangerous problems of the oil producing industry. When the control of high pressure gas is not accomplished flow of gas from the formation to the wellbore occurs. Once detected, the gas influx is stopped by shutting-in the well. This is the first measure taken in a series of operations which are designed to bring back the well under control. These operations are referred to as well control procedures. Well control simulators are used both for evaluating well control procedures and for training of drilling personnel. Current well control simulators assume that the gas enters a wellbore as a continuous plug and travels at the same velocity of the drilling fluid. Unfortunately, these assumptions often lead to inaccurate results.

This study includes a review of the literature on bubble rise velocity in both extended and bounded systems, liquid holdup and flow pattern correlations, and bubble generation. A new method, obtained by applying the minimum energy dissipation principle, was developed to predict the size, shape, concentration, and velocity of gas bubbles within a wellbore during well control operations. The new method was then integrated into a well control simulator computer program that was developed as a part of an ongoing research effort towards the understanding of the behavior of a gas kick for the flow geometry present on a floating drilling vessel. Experiments were performed in a 6000 ft well to determine the accuracy of the computer program. Excellent agreement was seen between the observed and computed results.

CHAPTER I

INTRODUCTION

One of the more expensive and potentially dangerous problems associated with the oil producing industry is the control of high pressure formation fluids encountered while drilling for hydrocarbon reservoirs. When the control of high pressure formation fluids is not accomplished a blowout may occur. A blowout is the uncontrolled flow of formation fluids during drilling operations. When this uncontrolled flow discharges to the atmosphere or seafloor, it is called a surface blowout. The uncontrolled flow of fluids from one subsurface formation, through the wellbore, to a second more shallow, subsurface formation is called an underground blowout.

Surface blowouts are extremely dangerous, frequently resulting in injury of drilling personnel, and almost always causing damage of drilling equipment and the environment. In some cases, additional wells must be drilled in order to flood the high pressure formation causing the flow. On the other hand, underground blowouts are not usually as dangerous as surface blowouts, but they are more common because the flow cannot be controlled by surface blowout prevention equipment. Usually subsurface control can be established only by sealing off the lower portion of the well. Many expensive wells have to be redrilled because of this problem.

As the search for petroleum reserves has moved into the offshore environment, the blowout control problem has continued to increase in complexity. In addition, the difficulties in confining an offshore oil spill makes the environmental consequences of a blowout more important. Most modern blowout prevention equipment was

developed for land based drilling operations. With only minor modifications, this equipment has been applied to bottom-supported exploratory drilling rigs such as jack ups and development rigs operating on an offshore platform. However, more significant modifications in blowout prevention equipment and procedures are required for floating vessels, which are used almost exclusively for deep water operations. The first major modification for deep water operation was the location of the blowout preventer stack at the seafloor rather than the surface. The current trend of the oil industry to much greater water depths (See Figure 1.1) emphasizes the importance of the blowout control problem on floating drilling vessels.

The schematic presented in Figure 1.2 is based in part on a well drilled off the coast of Africa in 1978⁶⁶. In this schematic it was assumed that an influx of gas into the borehole was experienced after drilling into a high pressure formation at 11,540 ft. Note that well closure is accomplished by blowout preventers located at the sea floor.

A threatened blowout or "kick" starts if the pressure exerted by the column of drilling fluid in the well is less than the formation pore pressure. The influx of formation fluid into the well can be detected at the surface because of the drilling fluid which is displaced or "kicked" from the surface wellbore annulus into the surface drilling fluid pits. Once detected, the influx of formation fluid is stopped by closing the subsea blowout preventer which seals the annular space around the drill pipe. Before normal drilling operations can be resumed, the formation fluids must be removed from the well and the density of the drilling fluid in the well increased sufficiently to prevent further influx of formation fluids. This is accomplished by circulating the well against a back-pressure

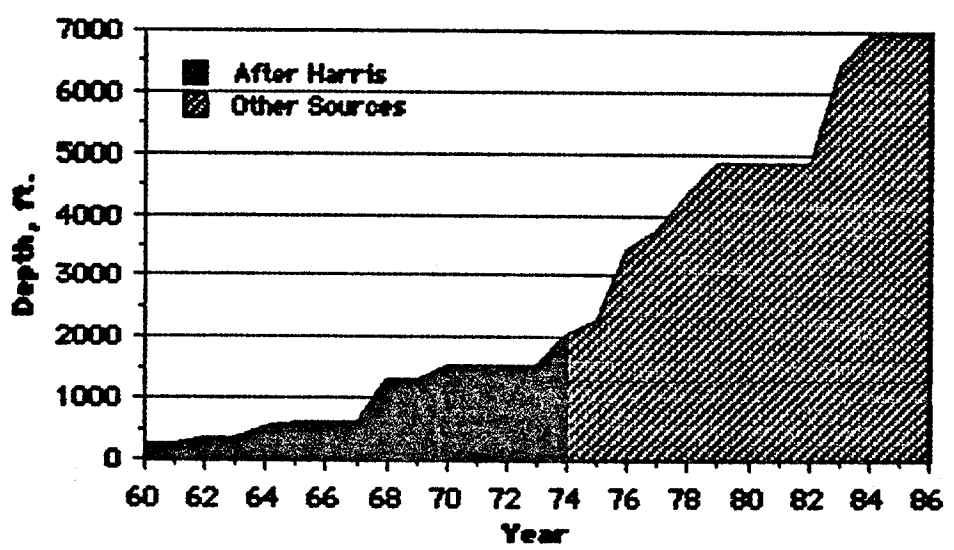


Figure 1.1 History of Water Depth Record for Floating Drilling Vessels

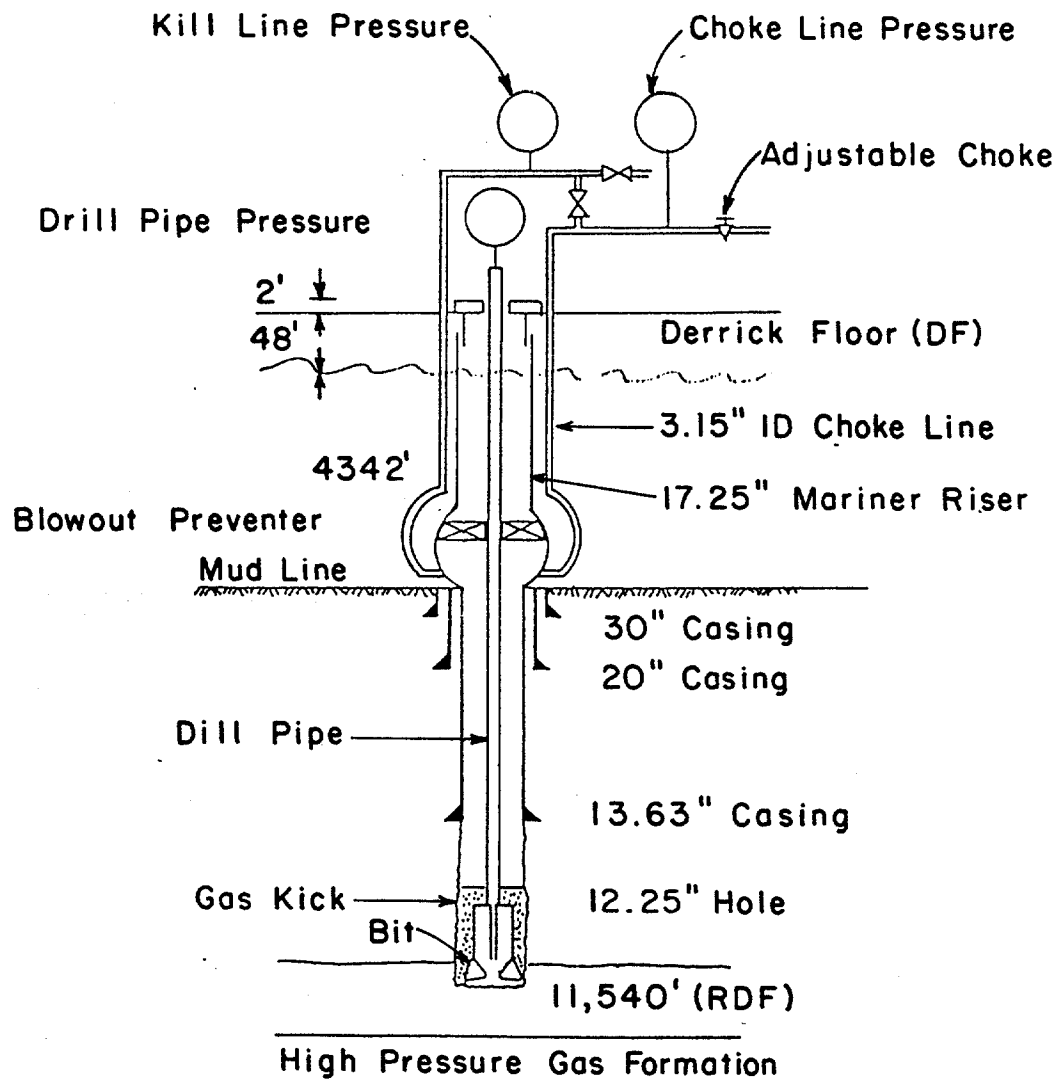


FIGURE I.2. SCHEMATIC OF TYPICAL FLOW GEOMETRY PRESENT FOR DEEP WATER BLOWOUT CONTROL OPERATIONS (After Bourgoyne et al)

provided by an emergency high pressure flow-line and an adjustable choke. The operations required to (1) close the well and (2) circulate the formation fluid from the well and higher density mud into the well are called well control procedures or pressure control procedures.

Pressure control procedures have been developed by the oil industry to provide guidance to the field personnel who must ultimately handle threatened blowouts under a wide variety of circumstances. Most of these procedures, like the blowout prevention equipment which must be employed, were largely developed for land based drilling operations, and modified as required as the search for oil and gas moved offshore. It is anticipated that further modifications in pressure control procedures will be needed as drilling operations are extended to much greater water depths.

Most modern pressure control procedures are evaluated, at least in part, by computer studies predicting the pressure response of the well during various phases of the pressure control operations. Shown in Figure 1.3 are predicted surface choke pressures⁶⁶ for the example of Figure 1.2 for various assumed initial gas influx volumes. One major problem predicted in this example is the rapid increase in choke pressure required when the gas reaches the seafloor and enters the small diameter choke lines. Computer simulations of well control operations can give much insight both in predicting operational conditions and in evaluating alternative pressure control procedures.

Computer simulations of pressure control operations are also carried out on a real time, interactive basis to train field personnel in those pressure control procedures selected for routine applications. Several pressure control simulators are manufactured specifically for such training exercises. Two of the commercially available pressure control training simulators are shown in Figure 1.4. These simulator

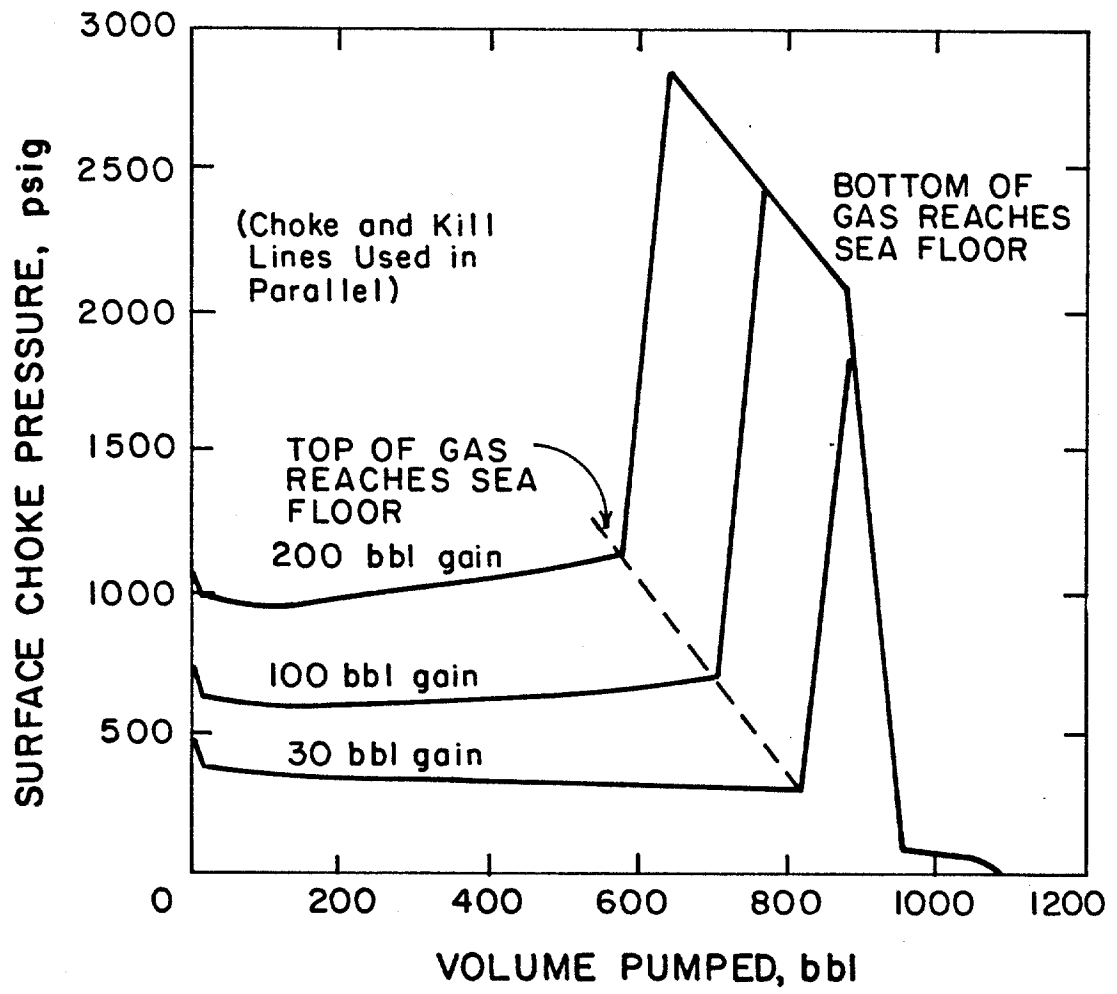


FIGURE I.3. PREDICTED WELL PRESSURE RESPONSE FOR EXAMPLE DESCRIBED IN FIGURE I.2 (After Bourgoyne et al)

facilities are part of the LSU Blowout Prevention Training Center and are used in industry courses leading to certification in pressure control operations.

Accurate computer simulation of pressure control operations require an accurate knowledge of fluid behavior in the well. Preliminary research at Louisiana State University has already shown that the assumptions used at present in blowout control simulations do not always predict actual well behavior when gas is present. Two assumptions found to be at fault are (1) that gas influx enters the wellbore as a continuous slug which occupies the entire annular cross section of the well and remains in this configuration during subsequent pressure control operations and (2) that the gas zone does not migrate upward through the column of drilling fluid but moves instead at the same velocity as the circulating drilling fluid.

This study is a part of a large ongoing research effort whose goal is the development of improved pressure control procedures for floating drilling operations. The main thrust of this study is aimed at determining the velocity and concentration of gas contaminated regions during pressure control operations for the flow geometry present on a floating drilling vessel. Ultimately, it is hoped that a more complete understanding of the gas contaminated zones behavior will lead to very accurate computer simulations of pressure control operations.

The primary objectives of the current study are to determine:

(1) The initial concentration of gas during the generation of a two-phase region in the wellbore due to gas influx from the formation.

(2) The two-phase flow patterns occurring during pressure control operations.

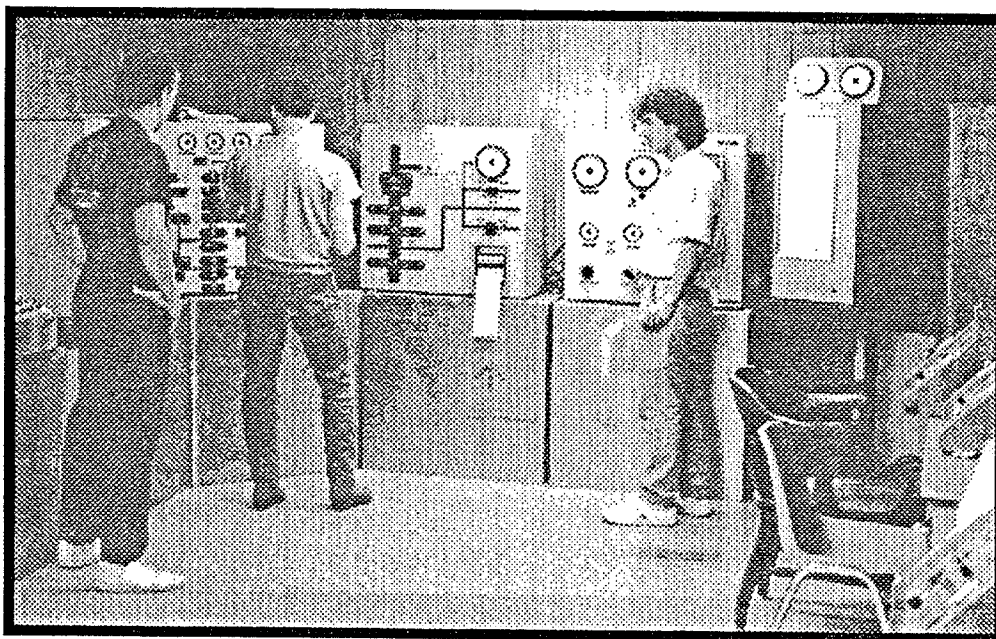


Figure 1.4 Example of Pressure Control Training
Simulators at LSU Blowout Prevention
Center.

(3) The rise velocity of the gas contaminated zone when the drilling fluid is not being circulated by a pump.

(4) The velocity of the gas contaminated zone during pump circulation.

It is important to point out that the problem of gas influx in the wellbore during conventional well drilling operations differs from the classical co-current upwards two-phase flow applied to oil and gas production. Simultaneous, upward two-phase flow in vertical pipes implies steady-state flow of gas and liquid. The radial and axial distribution of gas determine the flow patterns along the pipe which in turn determine the pressure distribution. This previously studied co-current two-phase flow condition is generally approached only in the bottom portion of the borehole during the time prior to the detection of the gas influx. Upon detection of the gas influx, the well is shut-in. At this point, the gas contaminated zone will migrate upwards due to its buoyancy. Finally, the procedures of well control operations call for the circulation or transportation of the gas kick or gas contaminated region. The gas concentration and flow pattern can change with time and position during both gas migration and transportation. The pressures experienced at the surface and at various critical points within the wellbore depend greatly on the gas distribution within the well. A proper engineering design of the well equipment and well-control procedures requires a knowledge of these pressures. Figure 1.5 shows the different phases of the well control operations which must be modelled. Figure 1.5.a refers to the generation of a two-phase region by gas flowing from a porous zone into the borehole while drilling is under way. Here, we must define the initial flow pattern, bubble size, and gas concentration. Figure 1.5.b refers to a shut-in period after the gas influx is detected and the blowout preventers are closed. Figure 1.5.c

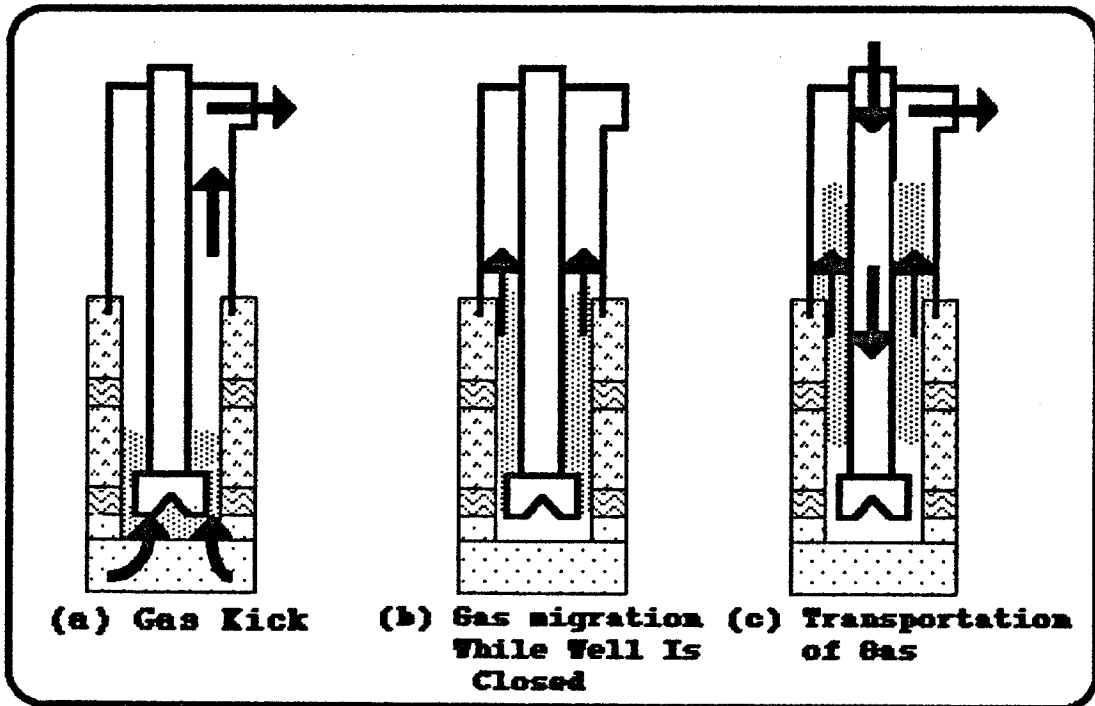


Figure 1.5 Processes During Well Control Operations

refers to a circulation period where the gas contaminated zone is transported through the annular geometry towards the choke line.

CHAPTER II

PREVIOUS INVESTIGATIONS

Two-phase flow is a topic found in many engineering disciplines and is important in a wide range of engineering problems. Because of this, a large body of literature is available in many engineering and scientific journals not normally followed by Petroleum Engineers. Thus an extensive literature review was the appropriate starting point for this study.

It was hoped that major improvements in the accuracy of computer simulations of pressure control operations associated with gas kicks could be made through the development of more realistic algorithms for predicting:

- (1) The two-phase flow patterns present in the wellbore annulus.
- (2) The upward slip velocity of the contaminated region relative to the drilling fluid either when circulating the well or when the well is not being circulated.
- (3) The gas concentration in the gas contaminated region.

Thus, the literature review will be presented for these three important areas.

2.1 FLOW PATTERNS

Previous work on two-phase flow patterns was classified in this study according to the following four geometries.

- (1) Extended liquids
- (2) Tubes

(3) Annuli

(4) Complex Geometries

The extended liquid case includes gas rising in a liquid media which is large enough so that no significant effect of the liquid boundaries can be observed. The next two cases investigated include the effect of bounding the liquid in a tube or annulus. The effect of confining the liquid in a conduit becomes more pronounced as the size of the individual gas bubbles approaches the size of a given conduit.

The last case considered previous work which may provide some insight on the effect of a complex geometry similar to that present on a floating drilling vessel. A floating drilling vessel operating in deep water typically has several long sections of different size annuli connected in series. The upper annular section is in turn connected at the sea floor with one or more vertical tubes which serve as the high pressure choke lines to the surface. Gas is introduced at the bottom of the well from porous media. Before pressure control operations can be accurately modelled, the effect of such a complex flow geometry and associated end effects on the two phase flow patterns must also be determined.

2.1.1 Extended Liquids

When gas is released in an infinite liquid media, the resulting flow pattern is generally described as bubble flow. A qualitative subclassification of this regime, based on the shape of the bubbles is generally used. This kind of classification is useful because the geometry of the bubble is related to the forces controlling the phenomenon of bubble motion. The bubble shape classification used in this study includes:

- (1) Spherical bubbles
- (2) Oblate spheroid bubbles

(3) Lenticular bubbles

Bubbles of a given gas in a given liquid tend to progress from small spherical bubbles to oblate spheroid bubbles and finally to large lenticular bubbles as the bubble volume is increased. Large lenticular bubbles can be unstable, breaking into smaller spherical or oblate spheroid bubbles. Examples of typical air bubble shapes observed by Haberman and Morton² in different liquids are shown in Figure 2.1. Similar observations for air bubbles rising in water described by V. G. Levich³ are shown in Figure 2.2.

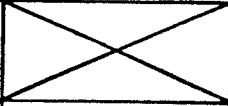
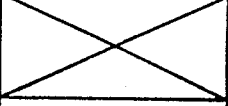
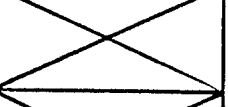
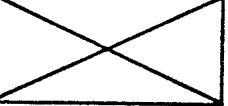
An excellent summary discussion on bubble behavior in extended liquids is given by Haberman and Morton². In addition to bubble volume, the shape of a bubble also depends upon the interfacial tension between the gaseous and liquid phases, the densities of the gaseous and liquid phases, and the viscosity of the gaseous and liquid phases.

2.1.2 Tubes

Flow conduits having a circular cross sectional area are of particular interest in this study because the flow pattern in the subsea choke lines between the blowout preventer stack at the sea floor and the floating drilling vessel at the surface can have a very large effect on the observed pressure behavior of the well. In general, the description of each flow pattern is characterized by the radial or axial distribution of liquid and gas. Taitel et al⁴ in a very recent summary publication used the following flow pattern descriptions in conjunction with the classification shown in Figure 2 .3:

Bubble Flow. The gas phase is approximately uniformly distributed in the form of discrete bubbles in a continuous liquid phase.

Slug Flow. Most of the gas is located in large bullet shape bubbles which have a diameter almost equal to the pipe diameter. They move uniformly upward and are sometimes

LIQUID	EQUIVALENT RADIUS,* cm.		
	0.05	0.2	0.7
METHYL ALCOHOL	-		
VAR SOL	-		
TURPENTINE	-		
WATER 6° C (Filtered)	-		
WATER 19° C (Filtered)	.		
MINERAL OIL	.		
62% CORN SYRUP - WATER	.		
68% CORN SYRUP - WATER	.		

* Equivalent radius is radius of sphere of equal volume.

FIGURE 2.1. TYPICAL SHAPES OF AIR BUBBLES OF SEVERAL VOLUMES IN VARIOUS LIQUIDS (After Haberman and Morton)

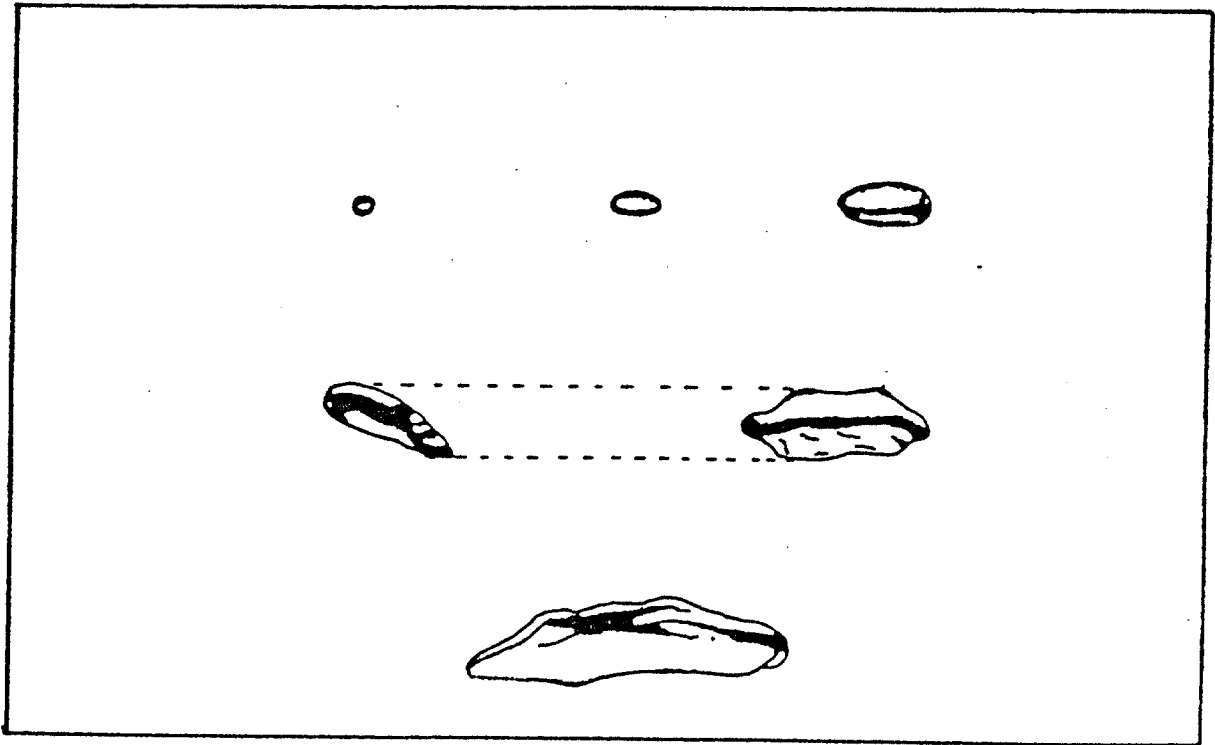


FIGURE 2.2. TYPICAL SHAPES OF AIR BUBBLES IN WATER
(After Levich)

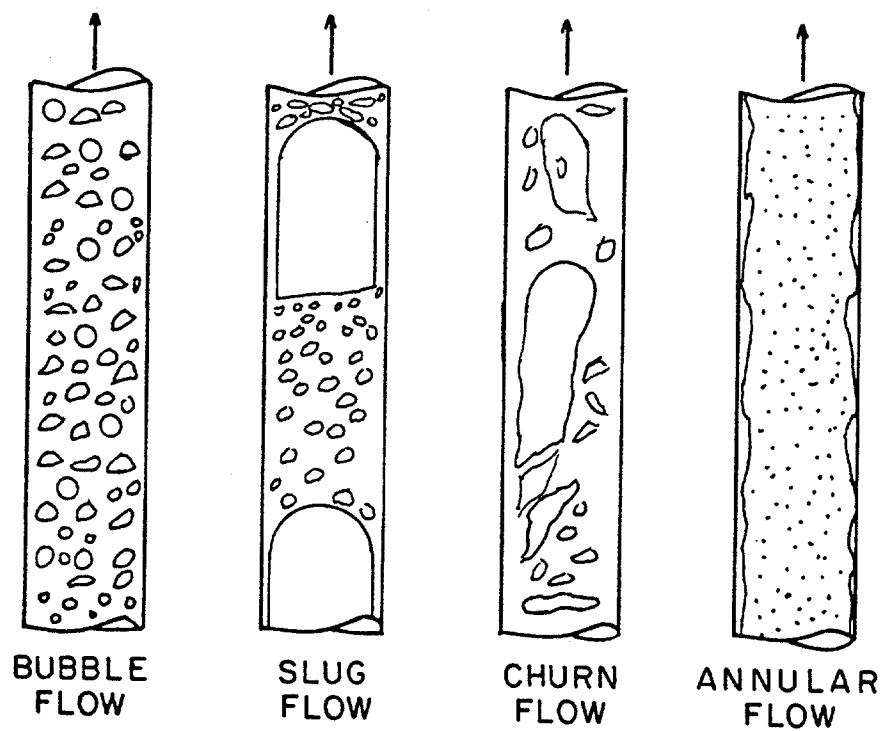


FIGURE 2.3. FLOW PATTERN DESCRIPTION FOR VERTICAL TWO PHASE FLOW SELECTED BY TAITEL et al.

designated as "Taylor Bubbles", after one of the first investigators who studied this flow pattern⁵. Taylor bubbles are separated by slugs of continuous liquid which bridge the pipe and contain small gas bubbles. Between the Taylor bubbles and the pipe wall liquid flows downward in the form of a thin falling film.

Churn Flow. Churn flow is somewhat similar to slug flow. It is however, much more chaotic, frothy and disordered. The bullet-shaped Taylor bubble becomes narrow and its shape is distorted. The continuity of the liquid in the slug between successive Taylor bubbles is repeatedly destroyed by a high local gas concentration in the slug. As this happens and the liquid slug falls, this liquid accumulates, forms a bridge and is again lifted by the gas. This oscillatory or alternating direction of motion of the liquid is typical of churn flow.

Annular Flow. Annular flow is characterized by the continuity of the gas phase along the pipe in the core. The liquid phase moves partly as a wavy liquid film and partly in the form of drops entrained in the gas core.

The annular flow pattern fits the assumption generally made in computer simulation of pressure control operations closer than the other three flow patterns described.

Steady state flow pattern prediction relies on a wide variety of flow pattern correlations. Among the published flow pattern correlations are those given by:

- (1) Griffith and Wallis (1961)⁶
- (2) Duns and Ross (1963)⁷
- (3) Sternling (1965)⁸
- (4) Wallis (1969)⁹
- (5) Hewitt and Roberts (1969)¹⁰
- (6) Govier and Aziz (1972)¹¹
- (7) Gould (1974)¹²
- (8) Oshinawa and Charles (1974)¹³
- (9) Chierici, Ciucci, and Schloechi (1974)¹⁴

(10) Taitel, Bornea, and Dukler (1980)⁴

A typical approach has been to correlate experimental observations by plotting transitional boundary lines on a two dimensional plot called a flow pattern map. An example of this approach is shown in Figure 2.4. There has not been uniformity on the parameters selected for the coordinates of the flow pattern maps although the abscissa is often directly related to the gas flow rate and the ordinate is often related to the liquid flow rate.

Usually there is not good agreement in results obtained using the various flow pattern correlations available. This is not too surprising since maps prepared from experimental data on one pipe size and for a limited range of fluid properties are not necessarily valid for other conditions. For sake of brevity, only the correlations judged to have the most promising potential will be presented. The correlations are classified according to the flow pattern boundaries which they represent.

Transition to Slug Flow Pattern

Griffith and Wallis were the first to discuss the bubble flow to slug flow transition. They were not sure that the bubble flow pattern was a stable pattern in long systems, reasoning that since different size bubbles travel at different rates, there is a natural tendency for small bubbles to link up and form slugs. However, based on previous experimental observations by Bailey et al¹⁵, they presented a correlation for the transition from bubble flow to slug flow when the gas volume fraction, in the column surpasses 0.18 for a 1" diameter tube. This implies that slug formation is not stable for gas volume fractions below 0.18.

Taitel et al⁴ in a very recent publication made a similar recommendation but placed the limiting gas volume fraction at 0.25. Taitel pointed out that spherical bubbles could be theoretically packed

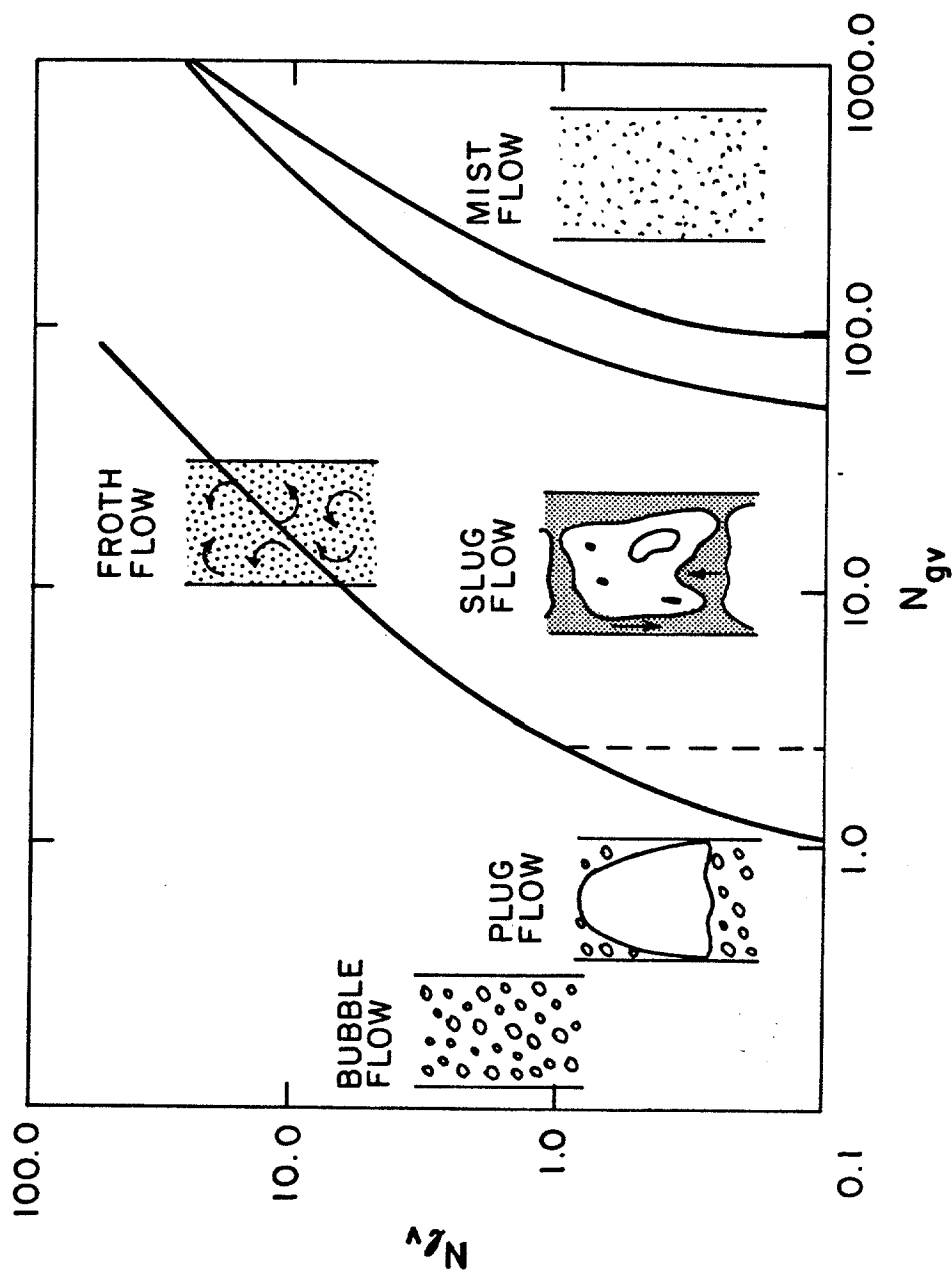


FIGURE 2.4. FLOW PATTERN DESCRIPTION FOR VERTICAL TWO PHASE FLOW USED BY CHIERICI et al.

so as to occupy a maximum of 52% of the volume, but bubble coalescence begins to increase sharply when the spacing between the bubbles is less than half their radius. This corresponds to a gas volume fraction of 0.25.

Duns and Ross⁷ presented the following criteria for the transition from bubble flow to slug flow:

$$N_{gV} \leq L_1 + L_2 N_{lV} \dots \dots \dots (2.1a)$$

$$N_D = D \sqrt{(\rho_l g / \sigma_l)} \dots \dots \dots (2.1b)$$

$$N_{gV} = (q_g / A) \sqrt[4]{(\rho_l / (g \sigma_l))} \dots \dots \dots (2.1c)$$

$$N_{lV} = (q_l / A) \sqrt[4]{(\rho_l / (g \sigma_l))} \dots \dots \dots (2.1d)$$

where

q_g = upward gas volume flow rate at existing conditions

q_l = upward liquid volume flow rate at existing conditions

A = Area of tube

D = tube diameter

ρ_l = liquid density

g = acceleration of gravity

σ_l = interfacial tension

L_1, L_2 = parameters defined by N_D and Figure 2.5

Use of this correlation does not require prior knowledge or calculation of the gas volume fraction. The criteria is most sensitive to the gas flow rate, the liquid flow rate, and the tube diameter, with the liquid density and interfacial tension being much less important. The criteria is completely independent of the liquid viscosity.

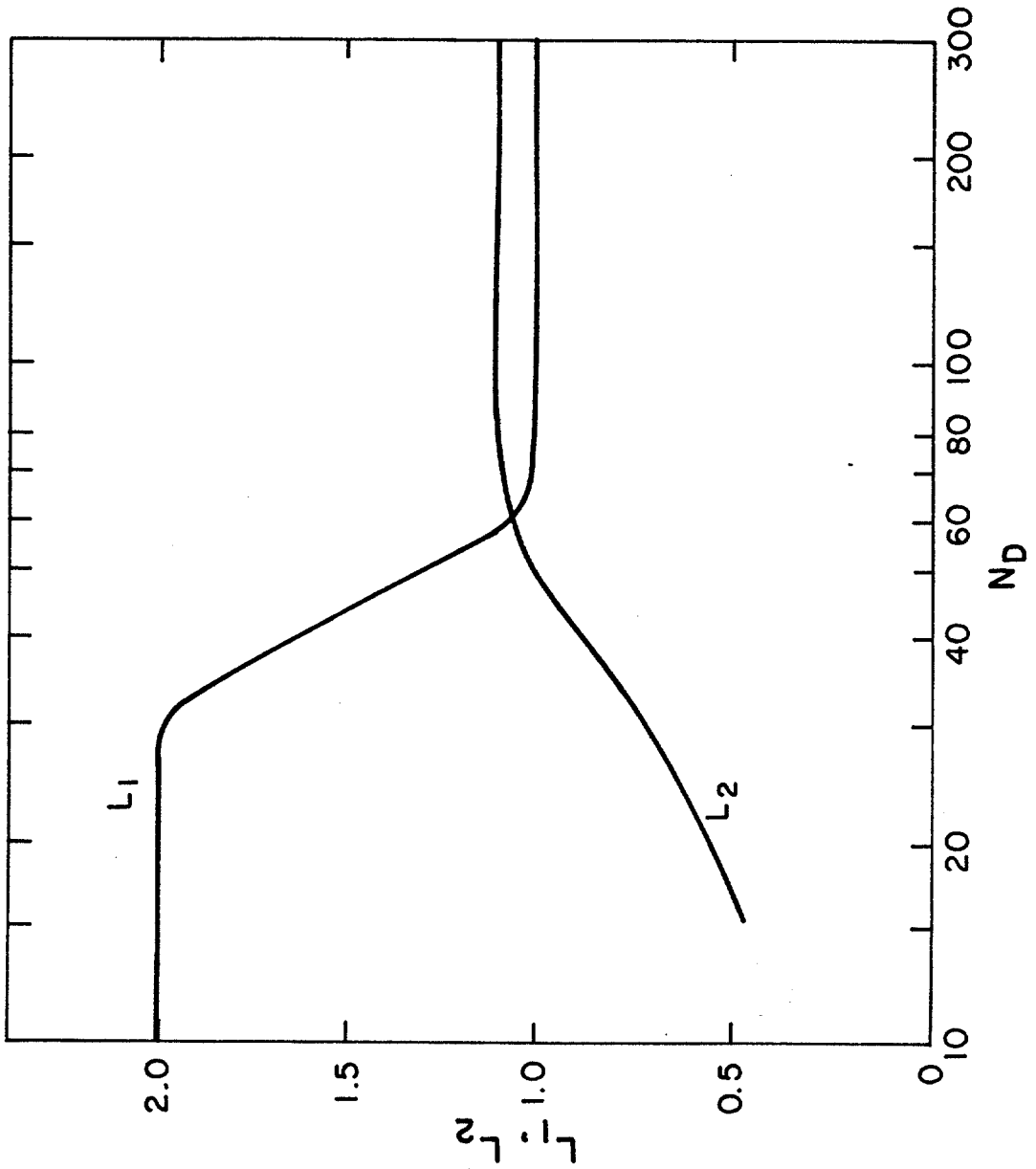


FIGURE 2.5. FLOW REGIME NUMBERS OF DUNS AND ROSS

Orkiszewski¹⁶ suggested the transition from bubble flow to slug flow occurs when a parameter L_B becomes greater than the gas fraction in the output stream of the system, as it is expressed by the following inequality:

$$L_B \geq q_g / (q_g + q_l) \dots \dots \dots (2.2a)$$

where L_B is defined by:

$$L_B = \begin{cases} 0.13 & \text{for } L_x \leq 0.13 \\ L_x & \text{for } L_x > 0.13 \dots \dots \dots (2.2b) \end{cases}$$

$$L_x = 1.071 - 0.2281 v_{sm}^2 / D \dots \dots \dots (2.2c)$$

where

v_{sm} = the mixture velocity obtained by dividing the total gas and liquid volume flow rate at the existing conditions by the tube area, ft/sec

D = the tube diameter, ft

Chierici et al¹⁴ used essentially this same criteria with a limiting value of 0.18 for L_B rather than 0.13. This criteria is sensitive only to the gas and liquid flow rates and the tube diameter.

Govier and Aziz¹¹ predict the onset of a slug flow pattern when

$$N_x \geq N_1 \dots \dots \dots (2.3a)$$

where

$$N_x = q_g/A (g/0.0764)^{1/3} [(72 \rho_l) / (62.4 \sigma_l)]^{1/4} \dots \dots \dots (2.3b)$$

$$N_1 = 0.51 (100 N_Y)^{0.172} \dots \dots \dots (2.3c)$$

$$N_Y = q_1/A (g/0.0764)^{1/3} [(72 \rho_l) / (62.4\sigma_1)]^{1/4} \dots \dots \dots (2.3d)$$

where

q_g = gas volume flow rate at existing conditions, ft³/sec

q_l = liquid volume flow rate, ft³/sec

ρ_g = gas density, lb/ft³

ρ_l = liquid density, lb/ft³

σ_1 = interfacial tension, dynes/cm

This criteria is primarily sensitive to gas flow rate, liquid flow rate, and tube area and has a weak dependence on liquid density and interfacial tension.

Transition to Churn Flow Pattern

It is difficult to compare different criteria for predicting the onset of churn flow because of differences as to the description of this flow pattern by different investigators. Some identify churn flow on the basis of froth that appears within the gas region. In this study, we have adopted the description of Taitel et al⁴ which is based on an oscillatory motion of the liquid region between gas slugs that are too short to remain stable.

Taitel et al provide a convincing argument backed by experimental observation that churn flow is actually due to entrance effects and if the system is long enough, eventually a stable slug flow will be produced. Churn flow is caused when a Taylor bubble breaks through a short liquid slug to another Taylor bubble above, resulting in a coalescence of two gas bubbles and two liquid slugs into one larger gas bubble and one larger liquid slug. Eventually a long enough liquid slug is created to form a stable bridge between the

Taylor bubbles. A liquid slug length approximately 16 times the tube diameter was found to be stable.

For low viscosity liquids and/or tube sizes of several inches or greater, the length of the system, l_E , above the entrance in which churn flow can exist is given approximately by:

$$l_E = 40.6 D (v_{sm} / \sqrt{gD} + 0.22) \dots \dots \dots (2.4)$$

where the tube diameter D , mixture velocity, v_{sm} , and gravitational acceleration, g , are defined in any consistent units. For systems of finite lengths less than l_E , churn flow could exist throughout the entire system. Since we are dealing with extremely long systems in pressure control operations, churn flow is probably of significance only over the bottom several hundred feet of each section of uniform geometry.

Transition to Annular Flow Pattern

For high gas flow rates, the flow becomes annular. A liquid film flows adjacent to the wall and gas travels rapidly upward carrying entrained liquid droplets. The liquid film tends to be wavy and liquid droplets tend to be broken off the wave peaks by the upward moving gas core. For this flow pattern to be stable, the liquid droplets must be carried upward. If they are allowed to fall and accumulate into a liquid bridge, slug flow or churn flow results.

Duns and Ross⁷ predict the transition to the annular flow pattern occurs when

$$N_{gV} \geq 75 + 84 N_{lV}^{0.75} \dots \dots \dots (2.5)$$

where N_{gV} and N_{lV} are given by Equations (2.1a) and (2.1d) respectively. This criteria is most sensitive to gas flow rate, liquid flow rate, and tube area, with liquid density and interfacial tension playing a minor role. The criteria is independent of liquid viscosity. Orkiszewski¹⁶ as well as Chierici et al¹⁴ also used this same criteria for predicting the transition to annular flow.

Govier and Aziz¹¹ predict the onset of annular flow when:

$$N_x \geq \begin{cases} 70/(100N_y)^{0.152} & \text{for } N_y < 4 \\ 26.6 & \text{for } N_y \geq 4 \end{cases} \dots \dots \dots (2.6)$$

where the variables N_x , N_y , q_g , A , ρ_l , and σ_l have the same units as defined for Equation (2.3). This criteria is highly sensitive to gas flow rate and tube area, with liquid flow rate, liquid density, and interfacial tension playing a minor role.

Taitel et al⁴, developed an expression for onset of annular flow based on the slip velocity of the largest drop size felt to be stable. The critical drop size is based on a critical Weber number of 30 and a drag coefficient of 0.44 for the liquid drop. The resulting criteria is given by:

$$q_g = 3.1A [\sigma g (\rho_l - \rho_g)]^{0.25} / \rho_g^{0.5} \dots \dots \dots (2.7)$$

This criteria depends primarily on gas flow rate and tube area, with liquid density, gas density, and interfacial tension having a minor role. The criteria is independent of liquid flow rate and liquid viscosity.

2.1.3 Annuli

Vertical two phase flow patterns have not been studied previously in annuli. The work done in tubes is sometimes extended to annuli through use of an equivalent hydraulic radius concept, but this approach has not been verified experimentally.

Zukoski¹⁷ in reporting some work on the slip velocity of long bubbles in tubes mentioned that D. Fluck and J. Gille of North American Aviation, Downey, California had observed in unpublished experiments an unsymmetric bubble shape in the emptying of an annular space between cylinders. These individuals are reported by Zukoski to have observed that gas moves up one side of the annulus with liquid falling down the opposite side. For large ratios of the outer to inner radius of the annulus, the width of the liquid fluid flow area near the bubble nose was reported approximately equal to the diameter of the inner tube.

Rader, Bourgoyne, and Ward¹⁸ worked with an annular geometry on a previous LSU study of gas slip velocity for a wide variety of tube sizes and fluid properties. However, this previous work considered only the flow pattern resulting from a very rapid gas injection into the system, attempting to be as close as possible to the conventional assumption that the gas enters the well as a continuous plug. It was noted that in all cases, the gas did not occupy the entire cross sectional area, but instead the gas slug traveled up on side of the annulus with liquid backflow occupying an area opposite the bubble. The fractional area of the liquid backflow was found to increase as the viscosity of the fluid was increased. The observed bubble shapes are shown in Figure 2.6.

2.1.4. Complex Geometries

Although it is widely recognized that end effects due to changing geometry are important, little experimental work has been

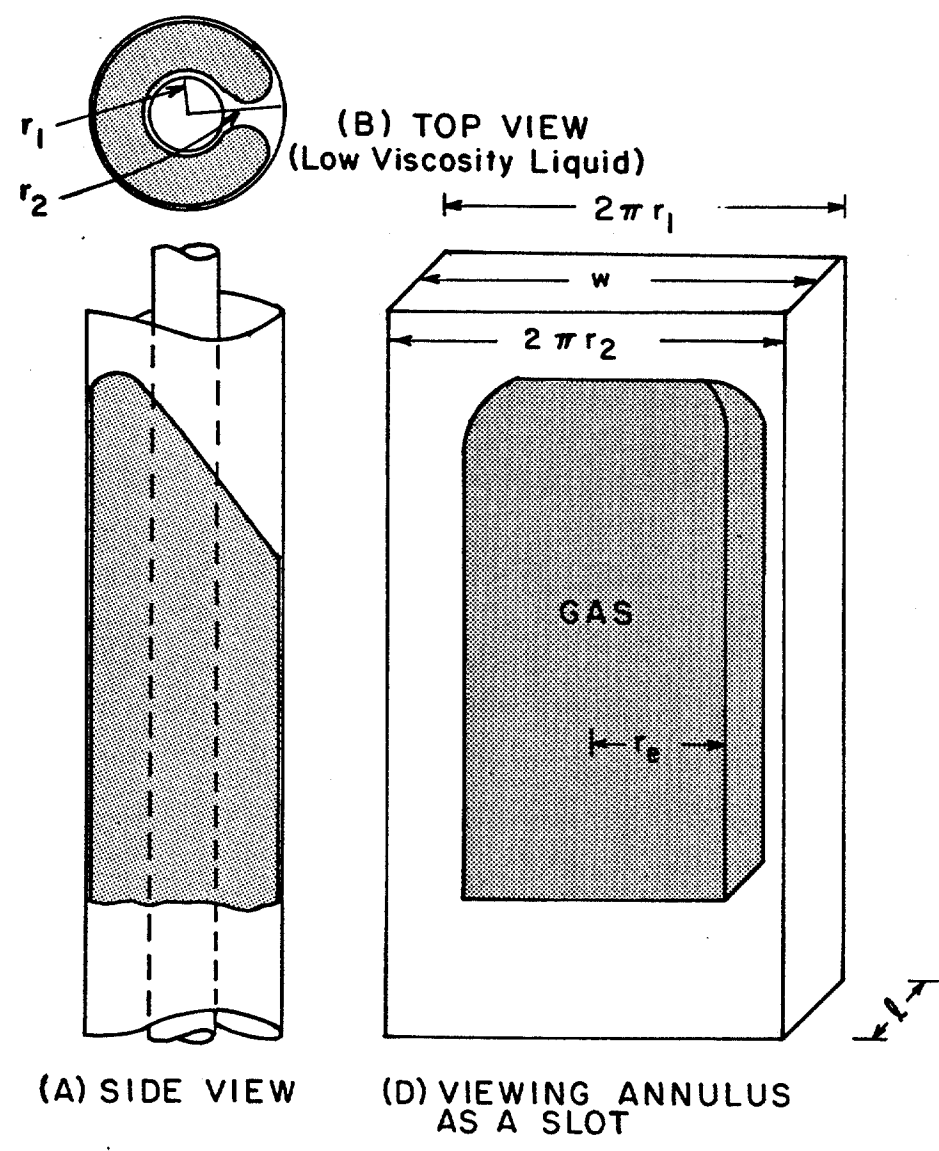


FIGURE 2.6. SHAPE ASSUMED BY LARGE GAS BUBBLE RISING IN ANNULUS

reported. An example of a change in geometry in the well control problem would be the change from a large annulus to a small choke line at the seafloor (See Figure 1.2). Griffith and Wallis⁶ pointed out that entrance effects can persist over great lengths, and that long periods of time are often required to achieve steady-state two-phase flow. Taitel et al⁴ reported that the churn flow pattern was due primarily to entrance effects. Flow exit conditions can also affect upstream flow patterns. For non vertical tubes, the angle of deviation has a large effect on the bubble shape and fluid distribution¹⁸.

Since a gas kick is taken from an open formation, the gas travels directly from a porous media to the wellbore. A large number of small streams of gas converging in the wellbore to form a gas kick may cause different entrance effects than a single stream of gas from a pipe. It is well known that a porous media is an excellent bubbler device.

Nicklin¹⁹ used a porous plate to generate bubble flow patterns in a vertical tube having 3.75 in. internal diameter and 6 ft. of length he injected gas through a porous bronze disk at flow rates up to about 1.8 ft³/min measured at average test conditions. This corresponded to a superficial gas velocity of about 0.4 ft/sec. Over the short length of pipe used, bubble flow was observed up to a superficial gas velocity of about 0.2 ft/sec. At higher gas rates, the formation of gas slugs was noted.

2.2 BUBBLE RISE VELOCITY

Previous work on the velocity at which a gaseous zone moves upward through a liquid was classified in this study according to the following three main geometries:

(1) Extended liquids

(2) Tubes

(3) Annuli

The importance of flow pattern on the bubble rise velocity for these three geometries was also researched. The velocity of a bubble in such three geometries is reviewed next.

2.2.1 Extended Liquids

The velocity of gas bubbles rising through a relatively infinite liquid media has been widely studied. Some of the more significant work done in this area include those of:

1. Hadamard²⁰ - Rybezynski (1911)²¹
2. Davies and Taylor (1949)⁶
3. Peebles and Garber (1953)²²
4. Haberman and Morton (1956)²
5. Mendelson (1967)²³
6. Acharya, Mashelkar and Ulbrecht (1977)²⁴
7. Ishii and Pei (1980)²⁵

In several of these works, experimental bubble slip velocity measurements were presented in terms of a bubble drag coefficient which was correlated with a bubble Reynolds number. Unfortunately, the correlations of drag coefficients versus bubble Reynolds number lack generality.

Recall from Section 2.1.1 that the injection of gas in an infinite liquid media results in a bubble flow pattern and that a qualitative subclassification of this regime, based on the shape of the bubbles, is generally used. The same subclassification is also useful in discussing the upward velocity of the gas bubbles except that the spherical bubble shape is further subdivided into a rigid sphere and a fluid sphere case. Very small gas bubbles behave much like a solid particle and hence the term rigid sphere is applied.

Thus, the gas bubble rise behavior in extended liquids will be discussed for the four following sub categories:

- (1) rigid spherical bubbles
- (2) fluid spherical bubbles
- (3) oblate spheroid bubbles
- (4) lenticular bubbles

Rigid Spherical Bubbles

Several investigators have shown experimentally that very small gas bubbles rising in an extended liquid behave much like solid spherical particles in that the bubbles drag coefficient is predicted by Stokes' Law. Thus, bubble rise velocity can be developed using the following relationship for drag force F_D :

Stokes' Law

$$F_D = (6\pi / g_c) \mu_l r_e v_\infty \dots \dots \dots (2.8)$$

For a bubble rising at its terminal velocity, the drag force, F_D , is also expressed by:

$$\begin{aligned} F_D = F_B - W_b &= V_b \rho_l (g/g_c) - V_b \rho_g g/g_c \\ &= (4/3) \pi (g/g_c) r_e^3 (\rho_l - \rho_g) \dots \dots \dots (2.9) \end{aligned}$$

where

F_B = buoyancy force

W_b = weight of the spherical bubble

V_b = volume of the spherical bubble

ρ_l, ρ_g = liquid and gas density respectively

μ_1 = fluid viscosity

r_e = equivalent radius of sphere having the same volume of the gas bubble

v_∞ = velocity of the bubble in an extended liquid

g = gravitational acceleration

g_c = conversion factor between mass and force units

From equations (2.8) and (2.9), the terminal velocity can be expressed by

$$v_\infty = (2/9) g r_e^2 (\rho_l - \rho_g) / \mu_1 \dots \dots \dots (2.10)$$

By definition, the drag coefficient is

$$\begin{aligned} f_D = (F_D/E_K) A &= 6 \pi \mu_1 r_e v_\infty / [(\rho_l / 2) v_\infty^2 \pi r_e^2] \\ &= 24 / N_{Reb} \dots \dots \dots (2.11) \end{aligned}$$

where

$$N_{Reb} = 2 r_e v_\infty \rho_l / \mu_1 \dots \dots \dots (2.12)$$

Peebles and Garber²² following the trend of many investigators recommended application of Stokes' Law for $N_{Reb} \leq 2$. However, Haberman and Morton proved that the transition to the fluid sphere region can happen at bubble Reynolds numbers as low as 2×10^{-6} .

Fluid Spherical Bubbles

The transition to the fluid sphere region is marked by slightly lower drag coefficients than that predicted for a solid sphere of equal

volume. This occurs because of circulation patterns taking place within the gaseous phase.

Peebles and Garber²⁴ presented the following drag correlation for the fluid spherical bubble region

$$f_D = 18.7 N_{Reb}^{-0.68} \dots \dots \dots (2.13)$$

Also, f_D can be expressed as

$$\begin{aligned} f_D &= F_D / (E_K A) \\ &= (4/3) \pi g r_e^3 (\rho_l - \rho_g) / ((\rho_l v_\infty^2 / 2) \pi r_e^2) \end{aligned}$$

From the former two equations, the velocity of the bubble becomes

$$v_\infty = 0.33 g^{0.76} r_e^{1.28} (\rho_l / \mu_l)^{0.52} (\rho_l - \rho_g / \rho_l) \dots \dots \dots (2.14)$$

Equations (2.13) and (2.14) apply for the following range of bubble Reynolds numbers:

$$2 \leq N_{Reb} \leq 4.03 [(g / \mu_l^4) / (\rho_l \sigma_l^3)]^{-0.214}$$

where all variables are defined as above and

$$\sigma_l = \text{surface tension}$$

This correlation was based on experimental work done for air bubbles rising in over 22 different liquids.

Haberman and Morton² also did experimental work in the fluid sphere region. They found that a theoretical development by Hadamard²⁰ and by Rybezynsky²¹ could be applied. The Hadamard and Rybezynsky equation is defined by

$$F_D = 4 \pi \mu_l r_e v_\infty / g_c \dots \dots \dots (2.15)$$

From Equations (2.15) and (2.19), the terminal velocity for fluid sphere results to be

$$v_\infty = (1/3) g r_e^2 (\rho_l - \rho_g) / \mu_l \dots \dots \dots (2.16)$$

and from Equation (2.15) and the definition of drag coefficient

$$f_D = 16/N_{Reb} \dots \dots \dots (2.17)$$

Oblate Spheroid Bubbles

The oblate spheroid region is marked by sharply increasing drag coefficients with increasing Reynolds number. The most extensive work done in the oblate spheroid region was presented by Peebles and Garber²². They provided the following expressions to correlate the drag coefficient and the velocity of slightly deformed bubbles

$$v_\infty = 1.35 (\sigma_l / (\rho_l r_e))^0.5 \dots \dots \dots (2.18)$$

$$f_D = 0.44 g r_e^4 v_\infty^4 \rho_l^3 / \sigma_l^3 \dots \dots \dots (2.19)$$

Equations (2.18) and (2.19) apply for the following conditions

$$16.32 \left[(g \mu_1^4) / (\rho_1 \sigma_1^3) \right]^{0.144} \leq g r_e^4 v_\infty^4 \rho_1^3 / \sigma_1^3 \leq 5.75$$

Lenticular Bubbles

In 1949, Davies and Taylor⁵ found that the flow near the front of large lenticular bubbles in extended liquids was very close to the theoretical flow near the front of a complete sphere in an inviscid fluid. Also, they noticed that the angle subtended at the center of curvature of the stagnation point of a bubble changes during the growth of the bubble (See Fig. 2.7).

The following expression to calculate the slip velocity of lenticular bubbles was given by Davies and Taylor:

$$v_\infty = \frac{2}{3} (g r_c)^{0.5} \dots \dots \dots (2.20)$$

where

v_∞ = velocity of the bubble

r_c = curvature radius of the top portion of the bubble

g = acceleration of gravity

The curvature radius, r_c , was determined from photographed bubbles.

Davies and Taylor also derived the following relationship between volume and rate of rise of a bubble.

$$v_\infty = 24.8 V_b^{1/6} \dots \dots \dots (2.21)$$

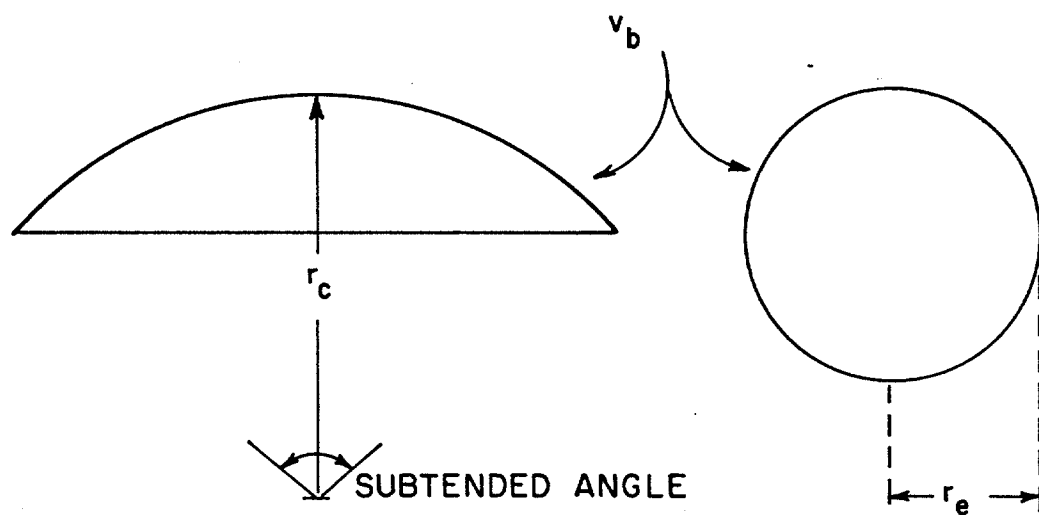


FIGURE 2.7. ANGLE SUBTENDED OF LENTICULAR BUBBLES
AND RELATIONSHIP BETWEEN CURVATURE
AND EQUIVALENT RADII

where

V_b = volume of bubble, cm^3

v_∞ = bubble velocity, cm/sec

If we define an equivalent radius, r_e , as that of one sphere having the same volume of the lenticular bubble, we can write

$$V_b = (4/3) \pi r_e^3 \dots \dots \dots (2.22)$$

$$v_\infty = 24.8 [(4/3) \pi r_e^3]^{1/6} \dots \dots \dots (2.23)$$

Dividing Equation (2.20) by Equation (2.23) yields the following relationship between radius of curvature and equivalent radius

$$r_c / r_e = 2.275 \dots \dots \dots (2.24)$$

In terms of the equivalent radius, the velocity of the flattened-shape bubbles becomes

$$v_\infty = 1.01 (g r_e)^{0.5} \dots \dots \dots (2.25)$$

Haberman and Morton found that for lenticular bubbles the drag coefficient is a constant, e.g., $f_D = 2.6$. Since $f_D = (8/3) g r_e / v_\infty^2$, the bubble rise velocity is given by the same expression found by Davies and Taylor, which was reported previously as Equation (2.25).

Harvey D. Mendelson²³ found an equation to determine the terminal velocity of the bubbles in pure liquids of low viscosity. Based on the work of Haberman and Morton, he observed an analogy

between the propagation of surface waves over deep water and the lenticular bubbles rising in pure liquids. By substituting the wave length, λ , for the perimeter of an equivalent circumference in the wave velocity equation, he arrived at the following expression:

$$v_{\infty} = [\sigma_1 / (r_e \rho_1) + g r_e]^{0.5} \dots \dots \dots (2.26)$$

where

v_{∞} = velocity of the bubble

σ_1 = surface tension

ρ_1 = liquid density

g = acceleration of gravity

r_e = equivalent spherical radius of the bubble

Non-Newtonian Fluids

Fluids that do not exhibit a direct proportionality between applied shear stress and rate of shear are classified as non-Newtonian fluids. Among these, pseudoplastic fluids are of interest to the drilling industry. Fortunately some work has been done on bubble motion in pseudoplastic fluids.

Rigid Spherical Bubbles

Using variational methods, Wasserman and Slattery²⁶ determined upper and lower bounds on the drag coefficient of a sphere in a power law-model fluid. The drag coefficient f_D was expressed by:

$$f_D = 24 F_S (n) / N_{RPL} \dots \dots \dots (2.27)$$

where

$$N_{RPL} = d^n v_\infty^{2-n} \rho_l / k \dots \dots \dots (2.28)$$

and $F_S(n)$ is a function of the pseudoplasticity index, n .

Unfortunately, Wasserman and Slattery reported poor agreement between their calculated drag coefficient and experimental data.

Recently, A. Acharya et al²⁷ found the following relationship between the drag coefficient of a bubble, f_D , and the generalized Reynolds number N_{RPL} for a power law fluid:

$$f_D = 24 F_S(n) / N_{RPL} \dots \dots \dots (2.29)$$

where

$$F_S(n) = 3 [(3n-3) / 2] \{ 33 n^5 - 63 n^4 - 11 n^3 + 97 n^2 + 16n \} / (4 n^2 (n+1) (n+2) (2n+1)) \dots \dots \dots (2.30)$$

They reported good agreement between experimental data and their theory.

Fluid Spherical Bubbles

T. Hirose and M. Moo-Young²⁸ proposed the following equations to describe the drag coefficient of a bubble in a power-law fluid:

$$f_D = (16 / N_{RPL}) F_f (n) \dots \dots \dots (2.31)$$

where the correction factor $F_f(n)$ is a function of the pseudoplasticity index given as:

$$F_f(n) = 2^{n-1} 3^{(n-1)/2} \left\{ \frac{(13+4n-8n^2)}{[(2n+1)(n+2)]} \right\} \dots \dots \dots (2.32)$$

Recently, S. M. Bhavaraju et al²⁹ also determined a correction factor for the drag coefficient for a single bubble moving in a power law fluid. This result is expressed by previous Equation (2.31), except that now $F_f(n)$ is given as:

$$F_f(n) = 3^{(n-1)/2} 2^{n-1} [1-7.66(n-1)/2] \dots \dots \dots (2.33)$$

Also, they presented the following correction factor, $F_{fp}(N_B)$ for drag coefficient for a single bubble moving in a Bingham plastic fluid:

$$F_f(N_B) = 1 + 3.22 N_B/2 \dots \dots \dots (2.34)$$

where the Bingham number, N_B , is defined as

$$N_B = d_e \tau_y / (v_\infty \mu_p) \dots \dots \dots (2.35)$$

Oblate Spheroid Bubbles and Lenticular Bubbles

Acharya, Mashelkar, and Ulbrecht²⁷ reported good agreement between experimental data and the values of bubble velocity predicted by Mendelson's equation for bubbles rising in non-Newtonian fluids. This equation was presented as Equation (2.26)

in the previous section. Note that this equation assumes that bubble velocity is independent of fluid viscosity.

Fragmentation of Bubbles

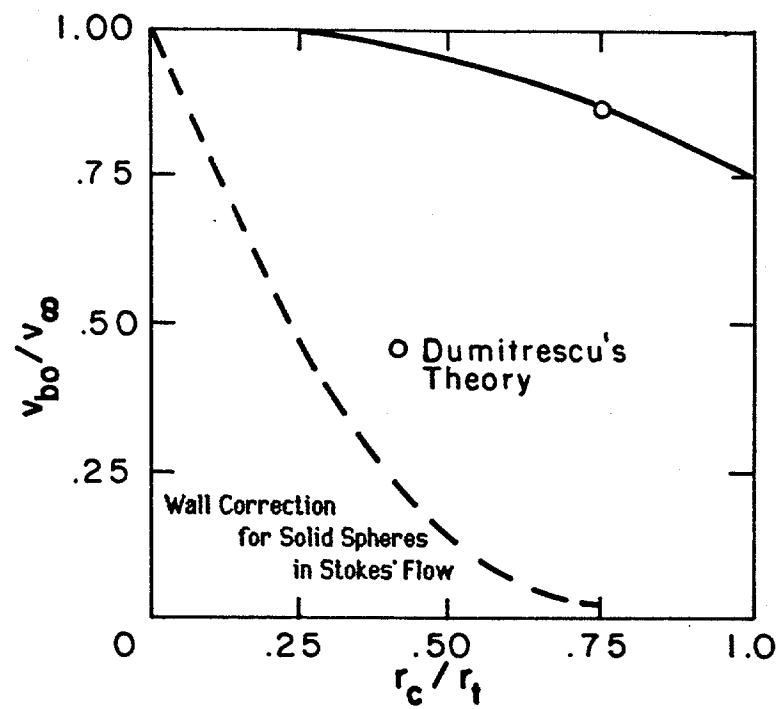
Regardless of the rheological fluid classification of the continuous phase, eventually the bubbles will fragmentate. In general, as the size of the bubbles increase, the bubbles increase their velocity until they begin to deform, and finally they become unstable. At this point the bubbles go into a process of fragmentation.

Levich³ reported fragmentation of gas bubbles to occur at equivalent radius of around 3 cm (1.18-in). Bryn³⁰ reported that large air bubbles in water at room temperature assume a lenticular shape, become very unstable, and finally tend to break easily into numerous smaller bubbles. Haberman and Morton also reported bubble rise velocities up to 60 cm/sec for lenticular bubbles (equivalent radius around 3 cm) rising in water at room temperature.

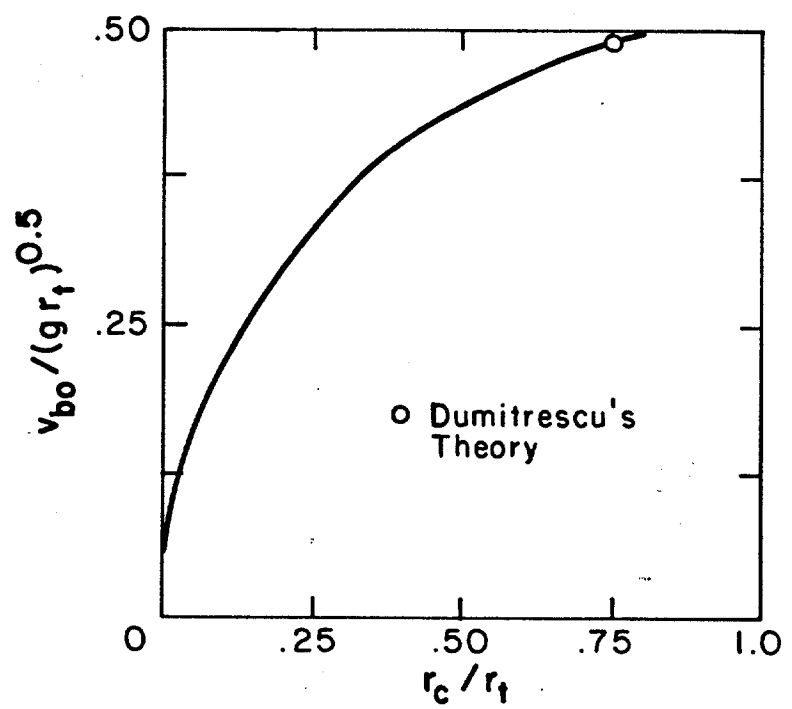
2.2.2 Tubes

When bubbles rise in a restricted media, the boundary affects their velocities. The net effect is a lower bubble rise velocity than that obtained for infinite media. The reduction in bubble rise is not important for small bubble diameters in large tubes. However, as the size of the bubbles approaches the size of the tube the boundary effect becomes significant. This phenomenon is illustrated in Figure 2.8. Among the first works published on gas bubbles moving in restricted media was that of O'Brien and Gosline.

O'Brien and Gosline³⁰ made a study of the velocity of large bubbles in vertical tubes. Their experimental work was performed in three tubings having diameters of 1.18-in., 2.24-in., and 6.0-in. The properties of the fluids covered a range of viscosities from 1 to 96 cp.



(a) NORMALIZED BUBBLE VELOCITY VS. NORMALIZED BUBBLE CURVATURE RADIUS



(b) DIMENSIONLESS BUBBLE VELOCITY VS. NORMALIZED BUBBLE CURVATURE RADIUS

FIGURE 2.8. VARIATION OF BUBBLE VELOCITY WITH r_c/r_t (After Collins)

They found that for bubble radius greater than 3 mm the effect of the pipe walls becomes noticeable. Also they reported a limiting velocity beyond which no increase resulted from an increase in the volume of the bubble. They also performed experiments on the velocity of a stream of bubbles in a stationary liquid. They observed that the bubble velocities increased linearly with increases in air flow through the tube. The maximum velocities found for continuous gas injection was found to be far greater than the velocity of the largest single bubbles released in the same tube.

In 1943 D. T. Dumitrescu³¹, made a theoretical analysis of an infinitely long bubble in a tube. He arrived to the following equation for the limiting velocity of a bubble in an inviscid fluid.

$$v_{b0} = 0.496 (g r_t)^{0.5} \dots \dots \dots (2.36)$$

Also, he supported this equation with experimental investigation. Using tubes of 0.99 cm, 2 cm, 3.76 cm, and 7 cm in diameter, he found a value of 0.49 for the constant of proportionality of his equation. Equation (2.36) is valid for larger diameters where the surface tension and viscous forces are insignificant.

Later, Davies and Taylor⁵ also derived an equation for the velocity of slugs rising through perfect fluids contained in cylindrical tubes. They arrived to the following equation:

$$v_{b0} = 0.464 (g r_t)^{0.5} \dots \dots \dots (2.37)$$

They also provided experimental data to support this equation. The value 0.464 was slightly lower than that obtained by Dumitrescu (See Equation 2.36).

Laird and Chisholm³² reported measured velocities of cylindrical bubbles in vertical tubes. The values obtained were on the average 10% greater than those obtained from the equations of Davies and Taylor. Their experiments were conducted in a 2-in. diameter tube with the upper end open to the atmosphere.

In 1956, Uno and Kintner³³ conducted a study to determine the effect of wall proximity on the velocity of air bubbles rising in a static liquid. They measured terminal velocities of bubbles rising in distilled water, 65% glycerine, diethylene glycol, and a surfactant solution in vertical cylindrical tubes, having internal diameters of 2.09, 3.64, 4.91, 6.90, 9.50 and 15.25 cm. Diethylene glycol, having a viscosity of 24.5 cp was the most viscous fluid included in the study. They obtained an empirical correlation which is defined by the following equation:

$$v_{bo} / v_{\infty} = \{ [1/b] (1 - r_e/r_t) \}^{0.765} \dots \dots \dots (2.38)$$

where

r_e = the equivalent spherical radius for the given bubble volume

r_t = the tube radius

b = a function of the tube radius and the surface tension

v_{bo} = actual terminal velocity of the bubble

v_{∞} = velocity of the bubble in a liquid of infinite extent

Figure 2.9 gives the values of b for the liquids used by Uno and Kintner. This figure illustrates the importance of the surface tension. Note that the effect of surface tension decreases for the larger tube sizes.

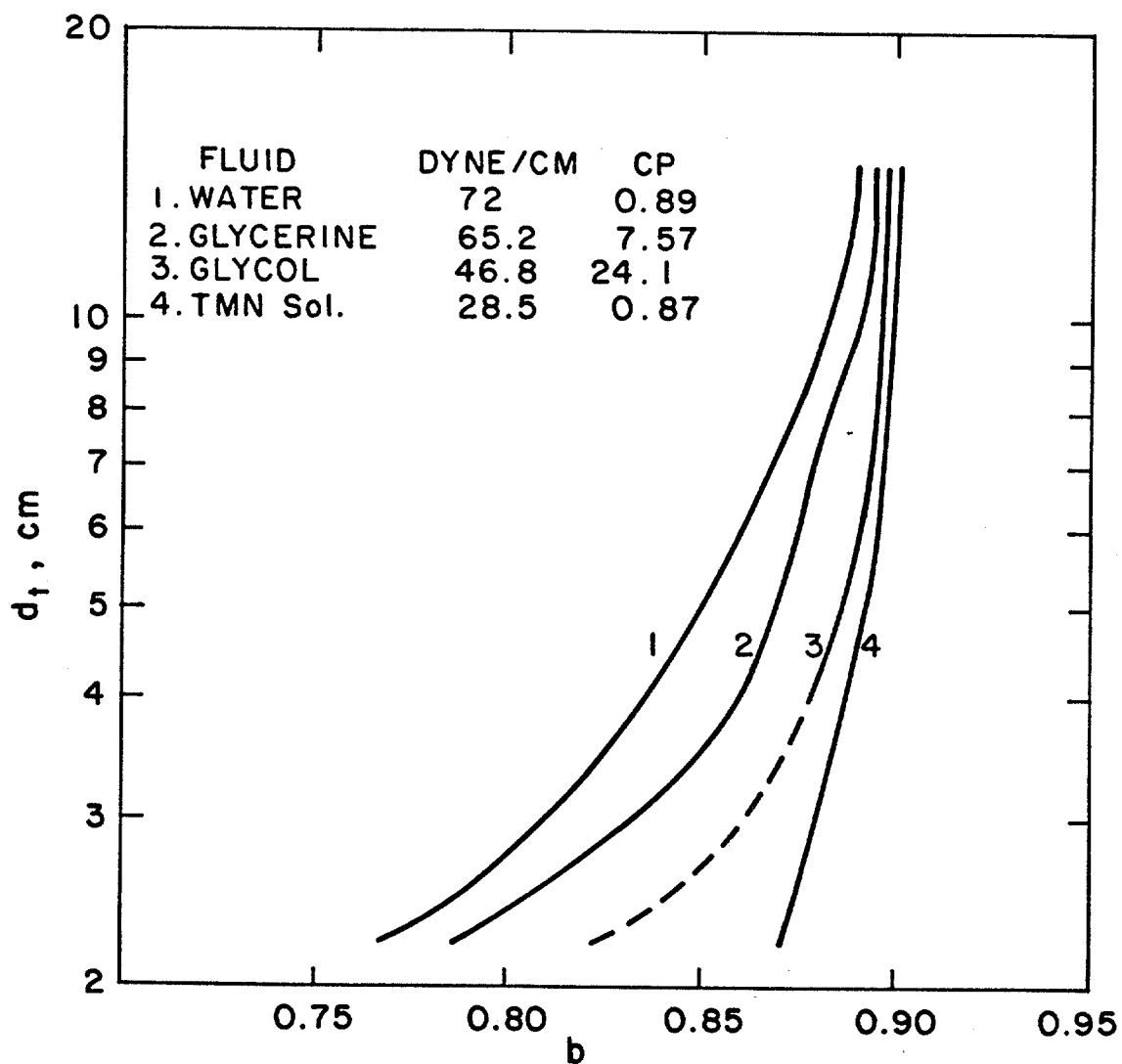


FIGURE 2.9. VALUES OF b AS A FUNCTION OF TUBE DIAMETER AND SURFACE TENSION (After Uno and Kintner)

In 1961, Griffith and Wallis⁶ studied experimentally the effect of water velocity on the rise velocity of large air slugs in vertical tubes with diameters of 0.5, 0.75 and 1.0-in. They presented their results in terms of a gas slip velocity defined as

$$v_{b+} = v_b - v_{sm} \dots \dots \dots (2.39)$$

where

v_b = the bubble rise velocity with respect to the tube.

v_{b+} = the bubble velocity with respect to the liquid ahead of the bubble, assuming incompressible fluids.

v_{sm} = the mean mixture velocity due to continuous injection into the tube.

The bubble velocity was found to be given by

$$v_{b+} = c_1 c_2 (g r_t)^{0.5} \dots \dots \dots (2.40)$$

where c_1 is a function of the bubble Reynolds number, and c_2 is a function of both the bubble Reynolds number and the liquid Reynolds number.

The bubble Reynolds number was defined by

$$N_{Rb} = d_t v_{b+} \rho_l / \mu_l \dots \dots \dots (2.41)$$

and the fluid Reynolds number by

$$N_{Rf} = d_t v_{sm} \rho_l / \mu_l \dots \dots \dots (2.42)$$

where

d_t = tube diameter

v_{b+} = the bubble rise velocity with respect to the liquid ahead
of the bubble

v_{sm} = the mean mixture velocity

ρ_l = the liquid density

μ_l = the liquid viscosity

The resulting correlation for c_1 and c_2 are shown in Figures 2.10 and 2.11.

Equations (2.39) and (2.40) can be combined to obtain

$$v_b - v_{sm} = c_1 c_2 (g r_t)^{0.5}$$

solving for v_b yields

$$v_b = c_1 c_2 (g r_t)^{0.5} + v_{sm} \dots \dots \dots (2.43)$$

For inviscid liquids, large tube diameters, and cylindrical bubbles, c_1 reaches the value of 0.496 obtained by Dumitrescu to describe the slug velocity in closed end tubes.

In 1962 Nicklin, Wilkes and Davidson³⁴ performed a study on cylindrical bubbles flowing through either stagnant liquid or moving liquid. To prevent the viscous effects from becoming important, they used water as the liquid phase and a 1.02-in. internal diameter

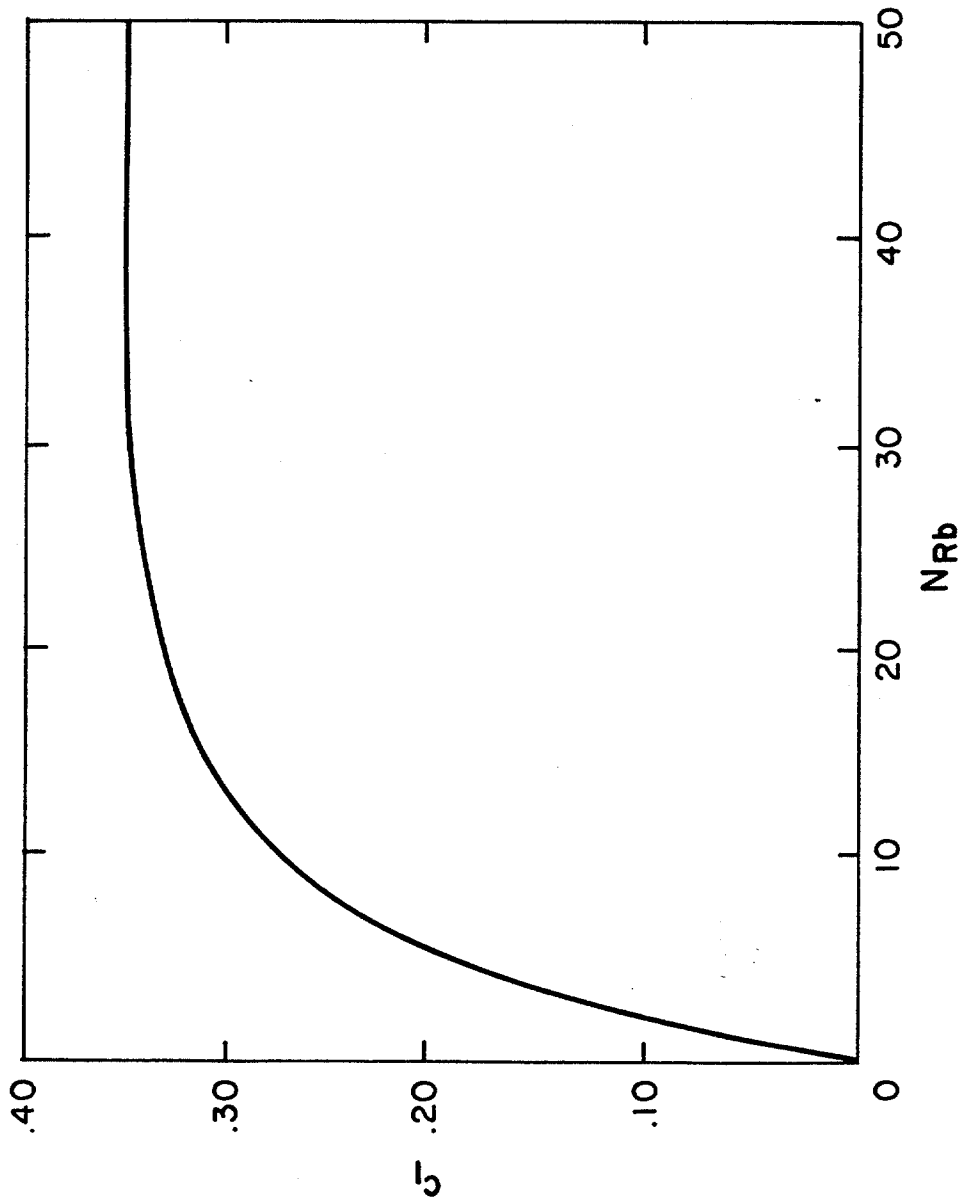


FIGURE 2.10. DIMENSIONLESS CONSTANT c_1 VERSUS BUBBLE REYNOLDS NUMBER (After Griffith and Wallis)

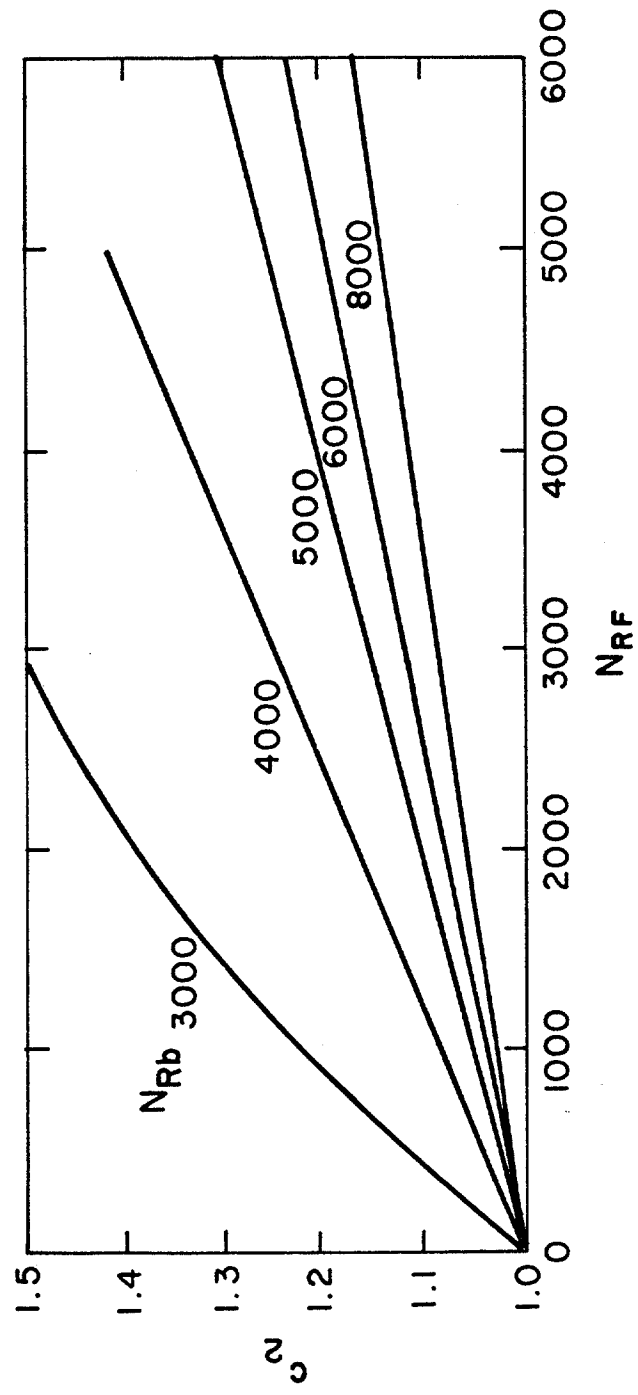


FIGURE 2.11. DIMENSIONLESS CONSTANT c_2 AS A FUNCTION OF LIQUID REYNOLDS NUMBER AND BUBBLE REYNOLDS NUMBER (After Griffith and Wallis)

tubing. They observed that the rising velocity of the gas slugs through stagnant liquid in an open tube increased with the length of the slugs as it has already been observed by other investigators. Furthermore, Nicklin et al found that increase in velocity to be related to the movement of the liquid caused by the expansion of the bubble itself. The investigators experimentally found that in a moving liquid stream the velocity of the cylindrical bubbles is given by the expression

$$v_b = 0.496 (g r_t)^{0.5} + K_{IV} v_{sm} \dots \dots \dots (2.44)$$

where

v_b = the upward gas slug velocity.

v_{sm} = the average upward mixture velocity.

K_{IV} = a coefficient having a value of 1.48 for liquid Reynolds number below of 2000.

The liquid Reynolds number, N_{RL} , is given by

$$N_{RL} = d_t v_{sm} \rho_l / \mu_l \dots \dots \dots (2.45)$$

where

d_t = internal diamer of the tube

v_{sm} = average velocity of the fluid

ρ_l = density of the liquid

μ_l = viscosity of the liquid

The first term of the right side of the equation is the Dumitrescu's equation for cylindrical bubbles in a static liquid. The second term accounts for the effect of the moving liquid. The factor K_{lv} , in front of the liquid velocity is greater than one because the average liquid velocity in the central core of the tube where the gas tends to reside is greater than the average liquid velocity in the complete section of the tube. When both liquid and gas were continuously injected in the bottom of the tube, the steady state bubble rise velocity for turbulent flow was found to be predicted by

$$v_b = 0.496 (g r_t)^{0.5} + 1.2 (v_{sl} + v_{sg}) \dots \dots \dots (2.46)$$

where

v_{sl} = the superficial liquid velocity

v_{sg} = the superficial gas velocity

and the remaining terms are as previously defined. When liquid was injected in the top of the tube to obtain a countercurrent process, the factor K_{lv} was reduced to values lower than one. By analogy, the authors extended the use of their equation for small bubbles.

Equation (2.44) of Nicklin et al and Equation (2.43) of Griffith and Wallis define the bubble rise velocity in a moving liquid stream. The expressions differ in the way the effect of liquid velocity on the velocity of the bubble is taken into account. Griffith and Wallis chose to take this effect into account using an empirical coefficient placed in the first term of the right side of equation rather than through use of a second term.

Also in 1962, White and Beardmore³⁵ performed experimental work on large bubbles rising in tubes. They used glass tubes of

diameters ranging from 0.5 to 3.87 cm. The fluids used had specific gravities ranging from 0.997 to 1.40, viscosities ranging from 0.87 to 20, 900.00 cp, and surface tensions ranging from 30.8 to 77.7 dyne/cm. A correlation for velocity of rise of cylindrical bubbles in vertical tubes was presented using dimensionless groups. Their correlation is presented in Figure 2.12. The correlation is given in terms of (1) the diameter number N_D , (2) the Froude number, N_{Fr} ; and (3) a property group, or liquid viscosity number, N_μ .

These groups are defined by

$$N_D = (\rho_l g d_t^2 / \sigma_l)^{0.5} \dots \dots \dots (2.47)$$

$$N_{Fr} = v_{bo}^2 / (g d_t) \dots \dots \dots (2.48)$$

$$N_\mu = [g \mu_l^4 / (\rho_l \sigma_l^3)]^{0.25} \dots \dots \dots (2.49)$$

where

ρ_l = the density of the liquid

g = gravitational acceleration

d_t = internal tube diameter

σ_l = interfacial tension between fluid and bubble

v_{bo} = terminal velocity of the bubble, relative to undisturbed liquid

μ_l = viscosity of the liquid

The correlation can be used in the following way.

(1) Calculate the property group, or liquid viscosity number, N_μ .

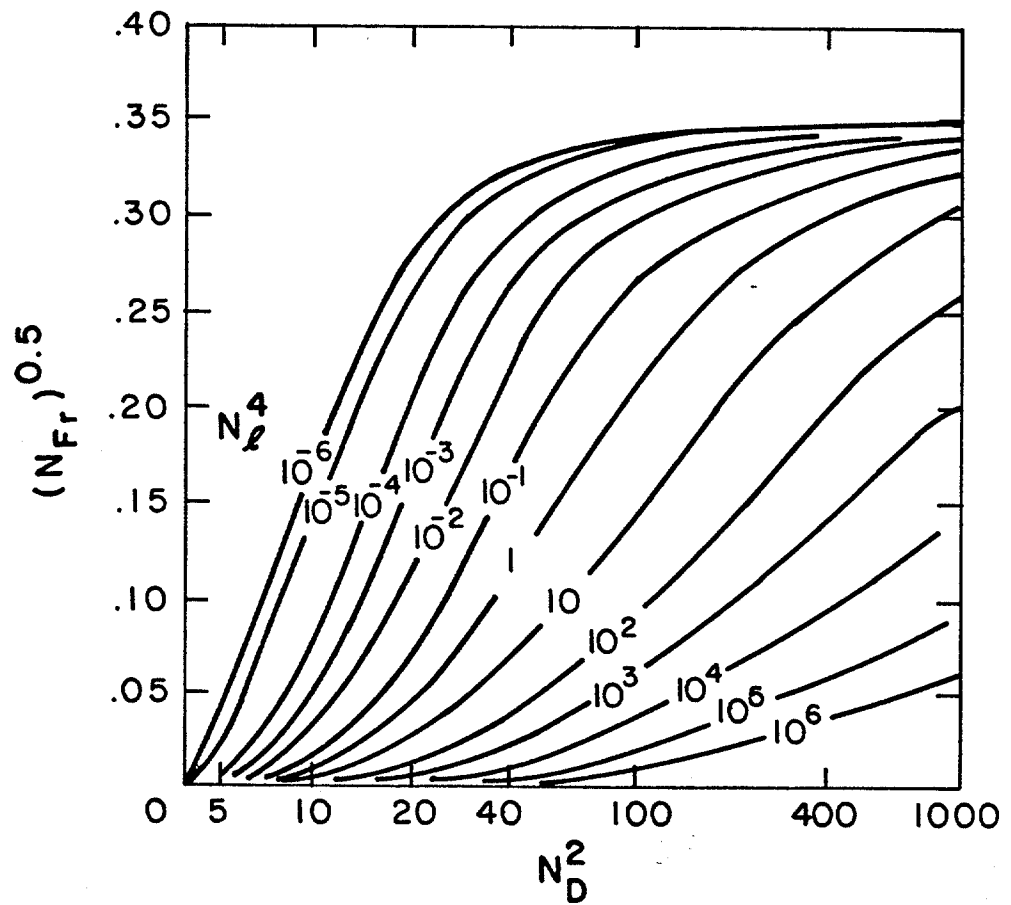


FIGURE 2.12. GENERAL CORRELATION FOR VELOCITY OF RISE OF CYLINDRICAL AIR BUBBLES (After White and Beardmore)

and the diameter number, N_D , which only are function of the continuous phase properties and the geometry of the tube. (2) With these two parameters, determine the maximum of the square root of the Froude number, from Figure 2.12. Solving this equation, the velocity of a cylindrical bubble in such a system will be determined.

Brown³⁶ also published a correlation of large bubbles rising in vertical tubes. The velocity of the bubble in a stagnant liquid was expressed as follows:

$$v_{b0} = 0.496 (g r_t)^{0.5} [(1 - (-1 + (1 + 2 N r_t)^{0.5}) / N r_t] \dots \dots (2.50)$$

where

N = Dimensional property parameter, ft^{-1} ,

$$= (14.5 g \rho_l^2 / \mu_l^2)^{1/3}$$

ρ_l = liquid density, lbm/ft^3

μ_l = liquid viscosity, $lbm/(ft \text{ sec})$

g = gravity acceleration, ft/sec^2

r_t = tubing radius, ft

The author limited this equation for the following conditions:

1) Surface tension parameter:

$$(\rho_l g r_t^2 / \sigma_L) (1 - (r_t - r_o) / r_t) > 5.0$$

2) Viscosity parameter

$$2 N r_t > 60$$

In these expressions, $(r_t - r_0)$ is the equilibrium liquid film thickness falling past the large lenticular bubble of radius r_0 in a tube of radius, r_t .

Zukosky¹⁷ performed a series of experiments in order to determine the influence of viscosity, surface tension and tube inclination on motion of long bubbles in closed tubes. He determined two dimensionless parameters to assure similarity between two systems. These parameters are given by the following expressions:

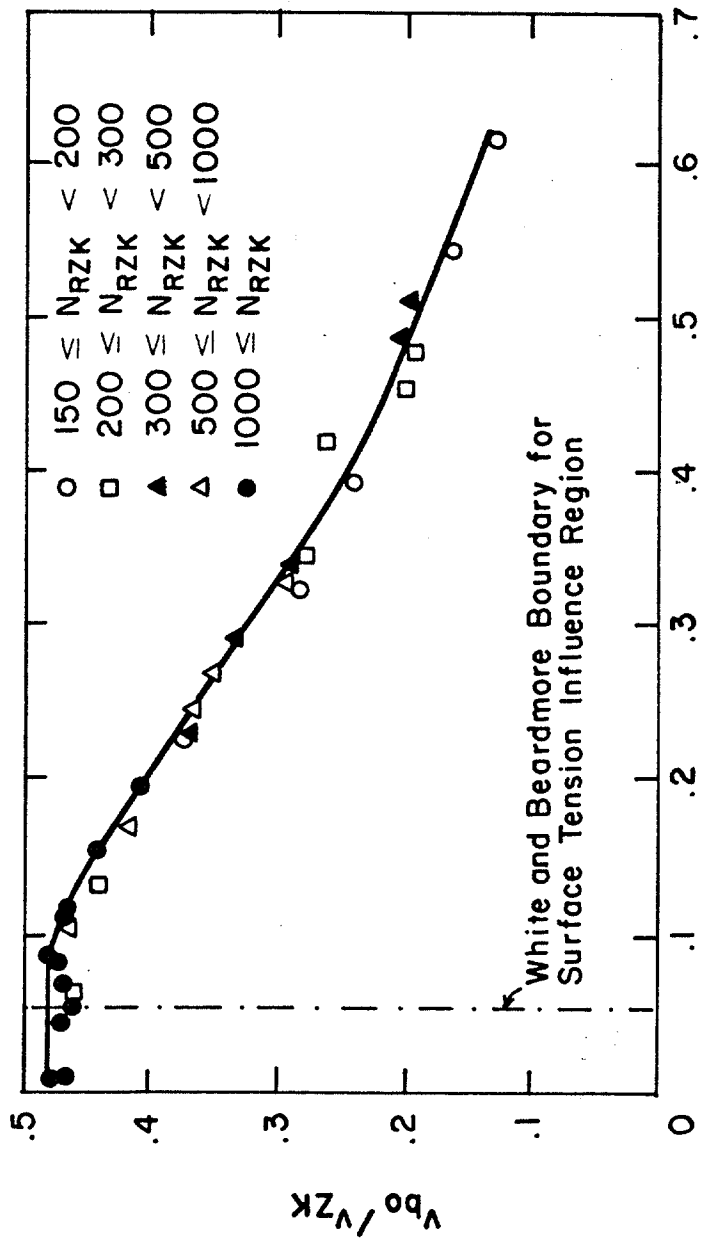
$$v_{zk} = [g r_t (\rho_l - \rho_g) / \rho_l]^{0.5} \dots \dots \dots (2.51)$$

$$N_{Rzk} = r_t v_{zk} \rho_l / \mu_l \dots \dots \dots (2.52)$$

$$\Sigma = \sigma_l / (g (\rho_l - \rho_g) r_t^2) = 4 / N_D^2 \dots \dots \dots (2.53)$$

He concluded that for bubble Reynolds numbers greater than about 200, the velocities are substantially independent of viscous effects. He also pointed out that the surface tension parameter Σ tended to increase with decreasing bubble Reynolds number so that it was difficult to ascertain if Σ or N_{Rzk} is the controlling factor. However, Figure 2.13 was presented as evidence that the surface tension has very large effect for Σ values above 0.1. With respect to the tube inclination, Zukosky found that the velocity increases with the angle of inclination (measured from the vertical), and it reaches a maximum at around 45°. The effect of tube inclination is shown in Figure 2.14.

In 1967, Collins³⁷ presented a work dealing with the effect of a



$$\Sigma = 4/N_D^2$$

FIGURE 2.13. BUBBLE VELOCITY VS. SURFACE TENSION PARAMETER FOR RANGES OF REYNOLDS NUMBERS (After Zukoski)

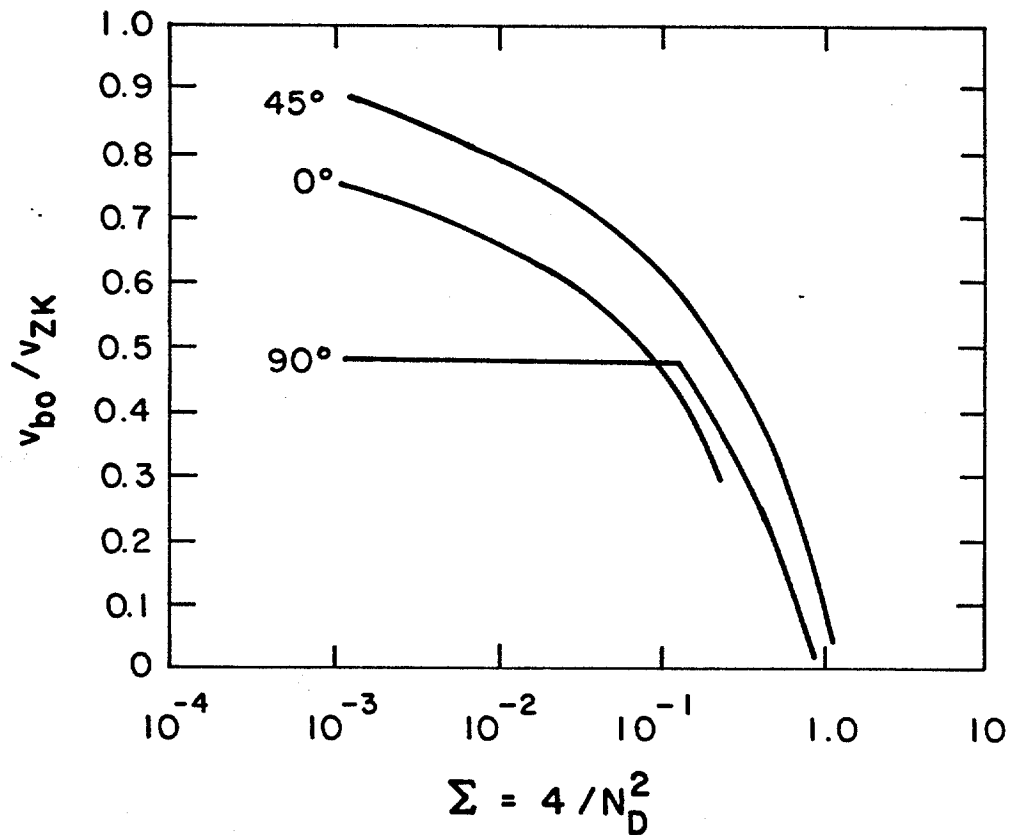


FIGURE 2.14 . VARIATION OF NORMALIZED VELOCITY WITH DIAMETER NUMBER FOR ANGLES OF INCLINATION AS MEASURED WITH RESPECT TO A HORIZONTAL PLANE (After Zukoski)

cylindrical boundary on the velocity of large gas bubbles in a liquid. The solid lines in Figure 2.8 represent the theoretical solution found by the author. This theoretical solution is a function of the curvature radius of the bubble at the forward stagnation point of the bubble. Using the empirical relation derived by Davies and Taylor relating the bubble velocity with volume of lenticular bubbles, he arrived to the semi-empirical line shown in Figure 2.15. Here, v_{b0} is the bubble velocity in a restricted media and v_{∞} is the Davies-Taylor velocity of bubbles in an infinite media, given by Equation (2.20). The geometry and the volume of the bubble were correlated by the equation:

$$r_c/r_t = 0.71 \tanh^{0.5} [4.25 (v_b^3 / r_t)^2] \dots \dots \dots (2.54)$$

where

r_c = the average curvature radius

r_t = the tube radius

An alternate expression for the slip velocity of cylindrical bubbles was found by V. Casariego³⁸:

$$v_b = 1.27 v_{b0}^{0.9457} v_{l+}^{0.0543} + v_{sm} \dots \dots \dots (2.55)$$

where

v_b = the bubble velocity with respect to the tube

v_{l+} = the velocity of the liquid ahead of the bubble

v_{b0} = the limiting gas slug velocity

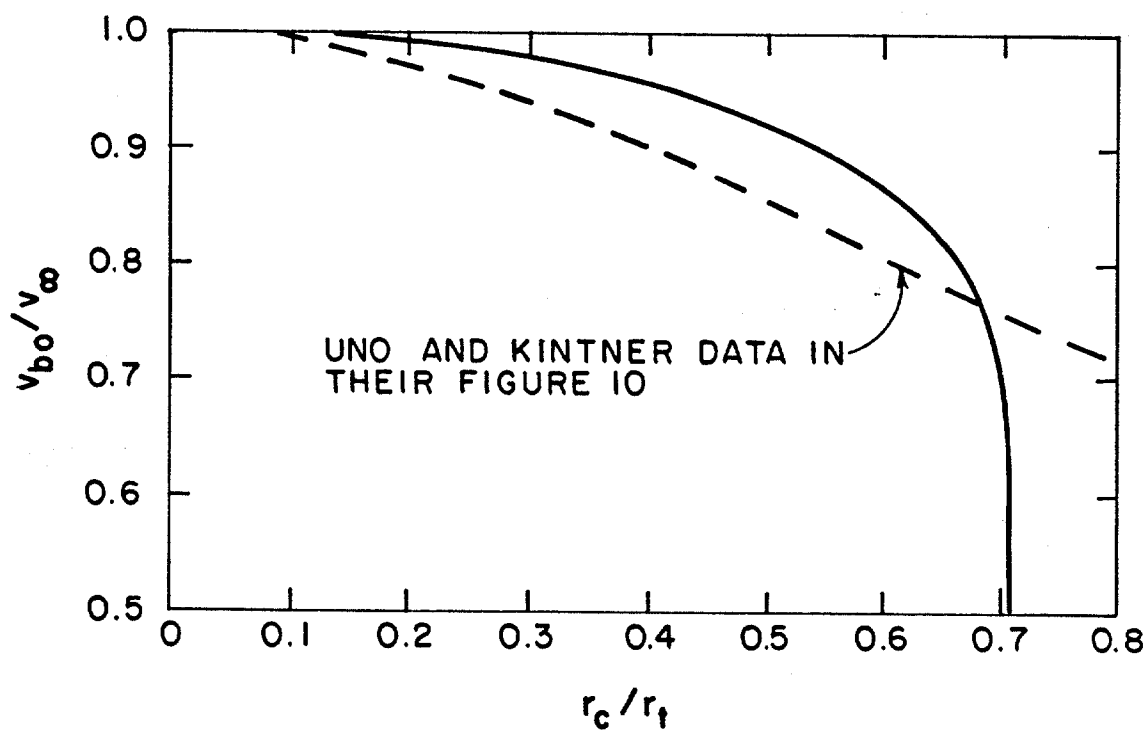


FIGURE 2.15. VARIATION OF v_{bo}/v_{∞} WITH r_c/r_t
(After Collins)

The correlation was obtained in a 32 ft, 6.375-in. internal diameter tube. Tap water and a 146 cp solution of glycerine were used as liquid phase. Air was the dispersed phase. The vertical tube was open ended. Use of the liquid velocity above of the cylindrical bubble accounts for the departure of the Dumitrescu's potential theory.

2.2.3 Annuli

Only a very limited number of investigators have studied the rise of gas in an annular geometry. However, since the transversal section of annuli may be approximately as a rectangle, a review of bubbles rising in rectangular channels was also included in the literature review.

Griffith³⁹ determined experimentally that the limiting gas slug velocity, $v_{bo \square}$, is given by

$$v_{bo \square} = (0.23 + 0.13 \ell/w) (gw)^{0.5} \dots \dots \dots (2.56)$$

where

w = the channel width

ℓ = the channel length

g = the gravity acceleration

If the channel is thought of as an annulus, (See Figure 2.6) the width and the thickness of the channel can be approximated by the following equations:

$$2 \ell = d_2 - d_1$$

$$w = \pi (d_2 + d_1) / 2$$

and Equation (2.56) can be expressed by

$$v_{bo\Box} = [0.2883 + 0.05186 (d_2 - d_1) / (d_2 + d_1)] [g (d_2 + d_1)]^{0.5}$$

..... (2.56a)

In 1965, R. Collins⁴⁰ derived the velocity of a two-dimensional gas bubble rising in liquid along the axis of a channel of finite width. He chose as asymptotes of the two-dimensional solution

$$v_{b\infty\Box} = 0.5 (g r_c)^{0.5} \dots \dots \dots (2.57)$$

$$v_{bo\Box} = 0.238 (g w)^{0.5} \dots \dots \dots (2.58)$$

where

$v_{b\infty\Box}$ = velocity of lenticular plane bubbles between infinitely wide parallel plates

$v_{bo\Box}$ = gas slug velocity in a rectangular channel of width w

g = acceleration due to gravity

r_c = curvature radius of a lenticular bubble

w = width of a rectangular channel

Equation (2.58) is the Garabedian solution for the limiting velocity of a plane bubble. Using these expressions to normalize his results, Collins obtained the expressions:

$$v_{bo} / v_{bo\Box} = \{ (3w / (2 \pi r_c)) [3 + (3w / (2 \pi r_c))^2] \}^{0.5} - (3w / (2 \pi r_c))^{1.5} \dots \dots \dots (2.59)$$

$$\frac{v_{bo}}{v_{b\infty}} = \left(\frac{w}{\pi r_c} \right) \left[3 + \left(\frac{3w}{2\pi r_c} \right)^2 \right]^{0.5} - 6 \left(\frac{w}{2\pi r_c} \right)^2 \dots \dots \dots (2.60)$$

where

$$r_c / w \leq 3/2$$

Maneri and Mendelson⁴¹ wrote a paper in 1968. They used a wave theory analogy and arrived to the following equation for bubbles rising in rectangular channels:

$$\frac{v_{bo}}{v_{b\infty}} = \left\{ \tanh \left[\pi C_3 \left(r_e w/2 \right) / \left(2 + \ell/r_e \right) \right] \right\}^{0.5} \dots \dots \dots (2.61)$$

where

$$v_{b\infty} = \left[\pi \sigma_1 / \left(2 r_e + \ell \right) \rho_1 + \left(g \left(2 r_e + \ell \right) / \pi \right) \right]^{0.5} \dots \dots \dots (2.62)$$

$$C_3 = \left(\left(2 + 2 \ell/w \right) / \pi \right) \tanh^{-1} \left\{ 2 \pi \left[0.23 + 0.13 \ell/w \right]^2 / \left(2 + 2 \ell/w \right) \right\} \dots \dots \dots (2.63)$$

Here, the equivalent radius r_e , describes that of one plane bubble having a length ℓ and a curvature radius, r_c . The transformation from r_c to r_e given by the authors is illustrated in Figure 2.16. The relationship between r_c and r_e is given by Equation (2.24). The former equations adapted for an annular space limited by radii r_1 and r_2 , can be expressed:

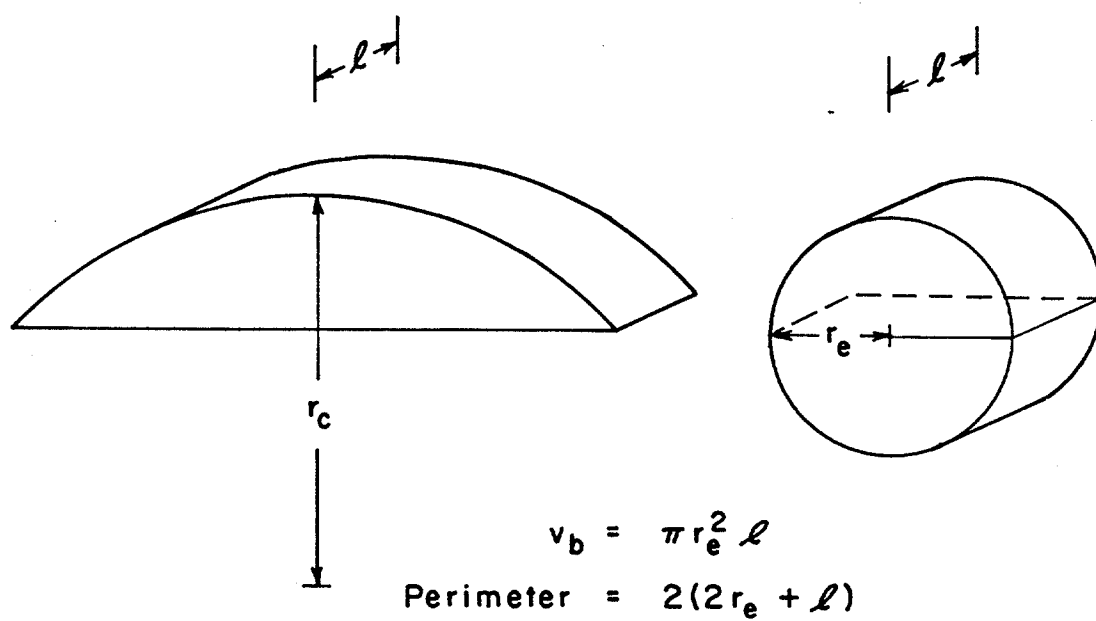


FIGURE 2.16. DEFINITION OF EQUIVALENT RADIUS AND PERIMETER FOR PLANE BUBBLE

$$v_{bo} / v_{b\infty} = \left\{ \tanh \left[\frac{\pi^2 C_3 (r_2 + r_1)}{r_e} / (4 + 2 (r_2 - r_1) / r_e) \right] \right\}^{0.5} \dots \dots \dots (2.61a)$$

$$v_{b\infty} = \left\{ \frac{2 \sigma_1}{(2 r_e + (r_2 - r_1) \rho_l) + g (2 r_e + (r_2 - r_1) / \pi)} \right\}^{0.5} \dots \dots \dots (2.62a)$$

$$C_3 = 2/\pi + (2/\pi^2) (r_2 - r_1) / (r_2 + r_1)$$

$$\tanh^{-1} \left\{ \frac{2\pi \left[(0.23 + 0.130 (r_2 + r_1) / (\pi (r_2 + r_1)))^2 \right]}{2 + 2 (r_2 - r_1) / (\pi (r_2 + r_1))} \right\} \dots \dots \dots (2.63a)$$

In 1975, D.W. Rader, A.T. Bourgoyne, and R.W. Ward¹⁸ introduced a correlation to calculate annular bubble rise velocity. The parameters experimentally studied were (1) annular geometry, (2) liquid viscosity, (3) gas and liquid densities, (4) gas expansion, (5) liquid velocity, (6) slanted wells, (7) bubble length, (8) interfacial tension, and (9) eccentricity of the annulus. They showed that the first six parameters affect significantly the rise velocity of a simple continuous bubble whereas the remaining three parameters have little or no effect on the slip velocity of a continuous bubble. Furthermore, they arrived at the following conclusions:

1. A large gas bubble rising in a vertical annulus will travel up on side of the annulus with liquid backflow occupying an area opposite to the bubble.

2. The fractional area of liquid backflow increases as the viscosity of the fluid increases.

3. The effect of slanted wells on the slug velocity is to increase the gas slug velocity. This is in agreement with the trend observed

by Sukosky¹⁷ for circular pipes.

Their experimental work covered annular spaces bounded by inner diameters, d_1 , from 0.2 in to 7.94 in and by outer diameters, d_2 , from 0.58 in to 9.58 in. Both Newtonian and non-Newtonian fluids were used as liquid phase. The viscosity range of Newtonian fluids was from 1 to 1050 cp. Non-Newtonian fluids covered the following range of rheologic characteristics: (1) yield point from 1.3 to 129 lb/100 ft², and (2) plastic viscosity from 11 to 111 cp.

Rader, Bourgoyne and Ward arrived at the following correlation for gas slug velocity, expressed in field units:

$$v_{b+} = \{ 0.163 + 0.0920 \log N_{RB} \} (d_1 + d_2)^{-5} \left[\frac{(\rho_l - \rho_g)}{\rho_l} \right]^{-5} \dots \dots \dots (2.64)$$

$$1 \leq N_{RB} \leq 100\,000$$

$$N_{RB} = [928 \rho_l v_{b+} (d_2 - d_1)] / \mu_l \dots \dots \dots (2.65)$$

where

v_{b+} = velocity of the slug with respect to the tube, ft/sec

d_1 = outside diameter of the inner tube of the annulus, in.

d_2 = inside diameter of the outer tube of the annulus, in.

ρ_l = liquid density, lb/gal

ρ_g = gas density, lb/gal

μ_l = liquid viscosity, cp

In 1981, V. Casariego³⁸ extended the above discussed work to large diameter tubes. He used a 32 ft. length 6.625-in. of internal diameter model. In order to obtain annular geometry, a 2.375 inch diameter tube of PCV could be placed inside the 6.625-in. pipe. The upper end of the apparatus was open. Tap water, 80 and 146 cp. glycerin solution was used as liquid phase. He arrived at the following expression for the velocity of a gas slug with respect to the tube:

$$v_b = v_{sm} + 1.22 v_{bo}^{0.9712} v_{1+}^{0.0287} \dots \dots \dots (2.66)$$

where

v_{1+} = the average velocity of the liquid ahead of the bubble

H.V. Nikens⁴² did a theoretical study on the rising velocity of gas slugs in closed vertical rectangular channels. He presented approximate theoretical solutions for both two dimensional channels and three dimensional channels. Also, he made experimental measurements of the velocity of gas slugs in water for channels of 7.62 cm. of length and of various widths. Nikens found that for large diameter numbers, the slug velocity can be expressed as:

$$v_{bo\Box} = 0.337 [2g (\ell + w) / \pi]^{1/2} \dots \dots \dots (2.67)$$

where

ℓ = length of the channel

w = width of the channel

2.3 LIQUID HOLDUP CORRELATIONS

An important parameter needed in the quantitative characterization of two phase flow patterns is the average fractional volume of the conduit which is occupied by gas, α , or conversely, the fractional volume occupied by liquid, H_l .

The fractional liquid volume is commonly called the liquid holdup. Many previous investigators who have presented empirical correlations for determining flow patterns also have presented liquid holdup correlations.

The liquid holdup can be related to the average slip velocity of the gas bubbles relative to the liquid. The average slip velocity is defined by

$$v_s = v_g - v_l \dots \dots \dots (2.68)$$

The average upward gas flux called the gas superficial velocity is given by

$$v_{sg} = q_g / A \dots \dots \dots (2.69)$$

The true upward average gas velocity is given by the gas volume flow rate divided by the average area available to the gas. Thus

$$v_g = q_g / A^\alpha = v_{sg} / \alpha = v_{sg} / (1 - H_l) \dots \dots \dots (2.70)$$

Similarly, the upward liquid superficial velocity is given by

$$v_{sl} = q_l / A \dots \dots \dots (2.71)$$

and the true upward average liquid velocity is given by

$$v_l = q_l / A H_l = v_{sl} / H_l \dots \dots \dots (2.72)$$

A convenient grouping of terms called the mixture velocity is defined by

$$v_{sm} = v_{sg} + v_{sl} \dots \dots \dots (2.73)$$

Employing Equations (2.61) - (2.66) it can be shown that:

$$H_l = \left\{ (v_s - v_{sm}) + \sqrt{(v_{sm} - v_s)^2 + 4 v_s v_{sl}} \right\} / (2v_s) \dots \dots (2.74)$$

It must be remembered in employing Equation (2.74) that an upward direction was assumed for both the gas and liquid flow.

Hagedorn and Brown⁴³ published a correlation to find a theoretical liquid holdup. Their correlation requires the calculation of four dimensionless numbers. These numbers depend on the liquid phase properties, the geometry of the tube and the superficial velocity of the fluids. Three of the dimensionless numbers are defined by Equations (2.1b), (2.1c), and (2.1d); the fourth number, N_μ , is defined

$$N_\mu = \mu_l (g / (\rho_l \sigma_l^3))^{1/4} \dots \dots \dots (2.75)$$

where

μ_l = viscosity of the liquid

σ_1 = surface tension of the liquid

ρ_1 = liquid density

g = gravity acceleration

The holdup in Hagedorn and Brown's correlation was determined as that required to make the calculated pressure losses agree with the measured pressure losses. The measured pressure losses were obtained from tests performed in small diameter tubings of 1500 ft of length.

Duns and Ross⁷ measured directly the liquid holdup. They published correlations of dimensionless functions against the viscosity number, N_μ , defined by Equation (2.75). The dimensionless functions determine the slip velocity number, N_s , which is defined

$$N_s = v_s \left(\rho_1 / \sigma_1 g \right)^{0.25} \dots \dots \dots (2.76)$$

The slip velocity obtained from this equation is substituted in Equation (2.74) to obtain the liquid fraction.

Griffith and Wallis⁶ defined the gas fraction as

$$\alpha = v_{sg} / (v_{sm} + v_{b+}) \dots \dots \dots (2.77)$$

where α , v_{sg} and v_{sm} are defined as above, and v_{b+} is the bubble rise velocity with respect to the liquid. This velocity includes a correction factor to take into account the compressibility of the gas phase. The expression to obtain v_{b+} is Equation (2.40) which was already discussed.

Nicklin, Wilkes and Davidson³⁴ derived the following expression to determine the "equivalent" length of liquid around a gas slug:

$$L_{el} = 0.495 (d_t L_s)^{0.5} \dots \dots \dots (2.78)$$

where

d_t = tube diameter.

L_s = gas slug length.

L_{el} = equivalent length of liquid around a slug.

The equivalent length of liquid is the volume of liquid around a slug divided by the area of the tube. Clearly, the voidage can be obtained in terms of the pipe diameter and the slug length. The authors showed experimentally that Equation (2.78) holds for short slugs.

Some investigators have worked out theoretical calculations for a single flow pattern. They relate the liquid holdup and single bubble velocity to the average velocity of a swarm of bubbles. These will be discussed next.

Marrucci⁴⁴ proposed an expression relating the velocity of rise of a swarm of spherical bubbles to the velocity of a single bubble. Based in an analysis of a cellular spherical model, he derived the following equation

$$v_{sw} = v_{\infty} (H_l)^2 / (1 - \alpha^{5/3}) \dots \dots \dots (2.79)$$

$$1 < N_{Rb} < 300$$

where

v_{sw} = velocity of a swarm of bubbles with respect to the liquid

v_{∞} = velocity of a single bubble in an extended liquid

α = volume fraction occupied by the gas

$$H_1 = 1 - \alpha$$

Equation (2.76) is restricted to the range of high but subcritical Reynolds numbers, and pure, ideal fluids.

Bhatia⁴⁵ derived a method to predict the gas holdup or gas fraction of a swarm of bubbles based on the bubble velocity in a restricted media as developed by Mendelson and Maneri⁴¹. Therefore, this method is applicable to pure inviscid liquids. The relationship between volumetric gas fraction and bubble velocity given by Bhatia is:

$$v_{sw} = v_{\infty} \sqrt{\tanh(0.25 (1/\alpha)^{1/3})} \dots \dots \dots (2.80)$$

where

v_{sw} = velocity of a swarm of bubbles in a stagnant liquid

v_{∞} = velocity of the bubble in an infinite media as defined by Equation (2.26)

α = volumetric gas fraction

Non-Newtonian Fluids

Bhavaraju, Mashelkar and Blanch⁴⁶ made a theoretical study on the motion of a swarm of bubbles in a power law fluid. In the case of fluid spheres, they presented the following equation:

$$v_{sw} = v_{\infty} [F_f(n) / F_{f,sw}(n)]^{1/n} \dots \dots \dots (2.81)$$

where

$$F_f(n) = [13 + 4n - 8n^2] / [(2n + 1)(n+2)]$$

$$F_{f,sw}(n) = a [bA_1 - cA_3 + 12A_4 + e]h$$

$$a = 1 / [1 - \alpha^{1/3}]^{n-1}$$

$$b = 4n(2n + 1)$$

$$c = 2(2n + 1)/n$$

$$e = (n - 1) / (1 - \alpha^{1/3})$$

$$g = 1/n + [g(1 - 2n)] / [2(1 + 2n)]$$

$$h = 1/(n + 2)$$

$$A_1 = \{ [6n(n - 1)] / [4n(2n + 1)^2(1 - \alpha^{1/3})] \} \\ (1 - \alpha^{2/3}) / (1 - \alpha - (2n + 3)/3)$$

$$A_3 = \{ [6n(n - 1)] / [(2n + 1)(1 - \alpha^{1/3})^2] \} \\ \{ (1 - \alpha^{1/3}) / (2n + 1) + (3 - 5\alpha^{1/3}) / 24 \\ + \alpha^{-2/3} / 12 - (\alpha^{1/3} \ln \alpha^{1/3}) / 2 \\ + [(1 - \alpha^{-2/3})(1 - \alpha^{-2n/3})] / [4n(2n + 1)(1 - \alpha^{-(2n+3)/3})] \\ + n(2n+1)\alpha^{-2n/3}(1 - \alpha^{-1/3}) / 3 \} - 1 / [2(1 - \alpha^{1/3})]$$

$$A_4 = [6n(n - 1)] \alpha^{-2/3} (1 - \alpha^{-(2n+1)/3}) / [12(2n+1)(1 - \alpha^{1/3}) \\ (1 - \alpha^{-(2n+3)/3})]$$

and for rigid spheres they proposed the following relationship:

$$v_{sw} = v_{\infty} [F_s(n)]^{1/n} / F_{s,sw}(n) \dots \dots \dots (2.82)$$

where $F_s(n)$ and $F_{s,sw}(n)$ are correction factors defined by Wasserman and Slattery and by Mohan and Raghukaman, respectively.

Equations (2.81) and (2.82) indicate that the bubble swarm velocity increases as the pseudoplasticity of the fluid increases for a given gas holdup. This is opposite to the trend for single bubble velocity where the bubble velocity decreases as the pseudoplasticity of the fluid increases (See Equations 2.29-2.32).

From all the literature reviewed on liquid holdup correlation, it appears that the determination of the individual size (or average size) of the bubbles is needed for obtaining the velocity and concentration of the gas contaminated region.

2.4 BUBBLE GENERATION

Gas kicks are taken from open formations where the gas enters the wellbore directly from a porous media. A large number of small streams of gas converging in the wellbore to form a gas kick may cause different entrance effects than a single stream of gas from a pipe. Nicklin used a porous plate to generate bubble flow patterns in a vertical tube having 3.75-in. internal diameter and 6 ft. of length. He injected gas through a porous bronze disk at flow rates up to about 1.8 ft³/min measured at average test conditions ($v_{sg} = 0.4$ ft/sec). Over the short length of pipe used, bubble flow was observed up to a superficial gas velocity of about 0.2 ft/sec. At higher gas rates the formation of gas slugs was noted.

A porous media may be represented by a large number of small diameter tubes closely packed. Some investigators have worked on the prediction of the volume of the bubbles released from

a nozzle. Acharya et al²⁷ performed a review of the available models of bubble formation in Newtonian fluids. They found that the models for inviscid fluids may be simplified to the form of

$$V_b = c (q_{gN}^2/g)^{3/5} \dots \dots \dots (2.83)$$

where

V_b = volume of the bubble

q_{gN} = volumetric gas flow rate per nozzle

$c = 0.976$

Also, they found that this equation could be safely extended to predict the bubble sizes in highly viscous non-Newtonian fluids provided the flow rates were in the order to 10^{-6} m³/sec. (35.3×10^{-6} ft³/sec) per nozzle opening.

Bhatia chose Patrick's correlation for determining the average bubble diameter d_{eav} in cocurrent two phase flow. The average bubble diameter is expressed in terms of the liquid velocity v_l .

$$d_{eav} = 0.52/v_l^{2/3} \dots \dots \dots (2.84)$$

$0.5 \text{ ft/sec} \leq v_l \leq 5 \text{ ft/sec}$

where

$$v_l = v_{sl}/H_l \dots \dots \dots (2.85)$$

v_{sl} = superficial liquid velocity, ft/sec

H_l = liquid volume fraction

d_{eav} = average bubble diameter, cm

v_l = liquid velocity with respect to the tube

Apparently, this correlation works for inviscid fluids only.

Ramakrishnan, Kumar and Kuloor⁴⁷ worked out a model based on a two step mechanism of bubble formation. The model considered an expansion stage and a detachment stage. During the first stage the bubble expands and it is attached to the tip of the orifice. During the second stage the bubble base moves away from the tip but it remains in contact with the orifice through a gas neck. The final volume of the bubble is expressed as the sum of the gas volumes delivered through the orifice in each step. The first step is obtained by a balance of forces. It includes forces of buoyancy, viscous drag, surface tension, and inertia. The second step is obtained by expressing the bubble-movement by Newton's second law of motion. They obtained the following equations:

$$V_{bl}^{5/3} = [47.4 \times 10^{-3}/g] q_{gN}^2 + \{ [2.42 \mu_l] / [g \rho_l] \} q_{gN} V_{bl}^{1/3} \\ + [(\pi d_N \sigma_l) / (g \rho_l)] V_{bl}^{2/3} \dots \dots \dots (2.86)$$

$$r_{el} = B (V_{bf}^2 - V_{bl}^2) / (2q_{gN}^{(A+1)}) - C (V_{bf} - V_{bl}) / (Aq_{gN}) \\ - 3G (V_{bf}^{2/3} - V_{bl}^{2/3}) / (2q_{gN}^{(A-1/3)}) \dots \dots \dots (2.87)$$

where

V_{bl} = volume of the bubble at the end of the first stage, cm^3

g = acceleration due to gravity, cm/sec^2

q_{gN} = volumetric flow rate of air, cm^3/sec

θ = contact angle, deg

μ_l = viscosity of the liquid, $\text{g}/\text{cm}\text{-sec}$

ρ_l = density of the liquid, g/cm^3

d_N = nozzle diameter, cm

σ_1 = surface tension, dyne/cm

r_{e1} = radius of the bubble at the end of the first stage, cm

V_{bf} = final volume of the bubble, cm^3

$$A = 1 + 14.6 V_{bf}^{1/3} \mu_1 / [(11/16) \rho_1 q_{gN}]$$

$$B = 16g / (11q_{gN})$$

$$C = 16\pi d_N \sigma_1 \cos \theta / (11 \rho_1 q_{gN})$$

$$G = 3.52 \mu_1 / \rho_1$$

Their model was tested with experimental work. The range of variables covered by the authors was:

- (1) Liquid viscosity of 1 to 552 cp
- (2) Surface tension of 41.1 to 71.7 dyne/cm
- (3) Density of 0.987 to 1.257 g/cm^3
- (4) Air flow rate of 1 to 80 cm^3/sec
- (5) Orifice diameter of 0.1378 to 0.7042 cm

Their model explains most of the discrepancies existing in the literature regarding the influence of viscosity, surface tension, and density on bubble formation. They reported that calculated values and experimental values were in good agreement.

Recently, Tsuge and Hibino⁴⁸ proposed a two-stage model to determine the size of bubbles formed at a single orifice. Their model takes into account fluctuations of gas pressure on the gas chamber. However, the solution of this model is a numerical one.

Also, Takahashy and Miyahara⁴⁹ worked out a correlation to determine the volume of a bubble at a single orifice. Their model is also a two-stage model. It takes into account the effect of the gas

chamber volume, liquid physical properties, gas flow rates and orifice diameters. Their equations are:

a) Low gas flow rates

$$V_{bl} = [4 \sigma_l V_{ch}] / [1.41 d_N P_{avg}] \dots \dots \dots (2.88)$$

b) High gas flow rates:

$$V_{bl}^{5/3} = 47.4 \cdot 10^{-3} q_{gN}^{2/3} + 1.61 \mu_l q_{gN} V_{bl}^{1/3} / (g \rho_l) \dots \dots \dots (2.89)$$

$$d_{el} = B(V_{b2}^2 - V_{bl}^2) / [2q_{gN}(A+1)] \\ - 3G(V_{b2}^{2/3} - V_{bl}^{2/3}) / [2q_{gN}(A-1/3)] \dots \dots \dots (2.90)$$

$$V_{bf} = V_{bl} + V_{b2} \dots \dots \dots (2.91)$$

$$1 \leq N_{ch} \leq g$$

where

V_{bl} = bubble volume either in region of low gas flow rates or
in first stage of high flow rates, cm^3

V_{b2} = bubble volume in region of high gas flow rates, cm^3

V_{ch} = chamber volume, cm^3

$N_{ch} = 4 V_{ch} g (\Delta \rho) / d_N^2 P_{avg}$

$\Delta \rho = \rho_l - \rho_g$

ρ_g = gas density at average operating conditions, g/cm^3

P_{avg} = average pressure, $dyne/cm^2$

$$A = [1 + 7.80 V_{bl}^{1/3} \mu_1] / [(11/16) \rho_1 q_{gN}]$$

$$B = 16 g / 11q_{gN}$$

$$G = 6.72 \mu_1 / \rho_1$$

and the remaining variables are defined as the previous Ramakrishnan et al model.

In 1981, Pinczewski⁵⁰ developed a numerical model to describe the formation and growth of bubbles at a submerged orifice. The model describes the effect of gas momentum by assuming that the flow field inside the bubble is a circulating toroidal vortex. The author reported good agreement between computed bubble growth rates, formation times and chamber pressure fluctuations with experimental data. Also, the predicted bubble shapes were similar to those observed experimentally.

In 1955, J. O. Hinze⁵¹ derived a formula to determine the maximum drop size for emulsification in a turbulent flow. From dimensional analysis he obtained:

$$d_{95g} (\rho_1 / \sigma_1)^{3/5} E_I^{2/5} = C$$

Using a value of 0.725 for the constant C; the 95% cut point diameter of the dispersed phase is then:

$$d_{95g} = 0.725 (\sigma_1 / \rho_1)^{0.6} (1/E_I)^{0.4} \dots \dots \dots (2.92)$$

$$= 0.725 (\sigma_1^{0.6} / \rho_1^{0.2}) (1 / E_{IV})^{0.4} \dots \dots \dots (2.92a)$$

where

d_{95g} = Globule diameter for which 95% of drops measured have a diameter less than d_{95g}

σ_1 = interfacial tension

ρ_1 = density

E_1 = Energy input per time for a liquid unit of mass, or power dissipation per unit of liquid mass

E_{1V} = Energy input per unit of volume and time, or power dissipation per unit of liquid mass

Bhavaraju et al⁴⁶ found a similar expression to Equation (2.92) for determining the main bubble diameter d_{eav} in turbulent flow.

$$d_{eav} = c_1 (0.6 \sigma_1 / (0.2 \rho_1)) (1/E_{1V})^{0.4} (\mu_1 / \mu_g)^{c_2} \dots \dots \dots (2.93)$$

$$d_{eav} \geq 0.45 \text{ cm for pure liquids}$$

The constants c_1 and c_2 were evaluated with experimental data, and they were found to be 0.7 and 0.1, respectively. The viscosity ratio term accounts for the influence of viscosity on bubble fragmentation. These authors also proposed the following design equation to determine the bubble diameter for moderately high gas rates in both low and high viscosity liquids:

$$d_e = 3.23 d_N N_{RN}^{-0.1} N_{FRN}^{0.25} \dots \dots \dots (2.94)$$

where

d_e = bubble diameter in region near the nozzle, m

d_N = nozzle diameter, m

$N_{RN} = 4 \rho_1 q_{gN} / (\pi d_N \mu_1)$ = modified Reynolds number at the discharge of a nozzle

$$N_{FrN} = q_{gN}^2 / d_N^5 g = \text{nozzle Froude number}$$

$$\rho_l = \text{liquid density, kg/m}^3$$

$$q_{gN} = \text{gas rate per nozzle, m}^3/\text{sec}$$

$$\mu_l = \text{liquid viscosity, N.sec/m}^2$$

$$g = \text{acceleration due to gravity, m/sec}^2$$

From all the previous review on bubble formation, it appears that there are not correlations on bubble behavior at high gas rates in high viscosity liquids.

Elizo Sada et al⁵² worked on the phenomenon of bubble formation in flowing liquids. They found that the bubble size formed in flowing liquids decreases with the superficial liquid velocity. Three types of bubble formation were observed: (a) single bubbles, (b) coalescent bubbles, and (c) gas jets. These types depend on the fluid flow rates. The bubble sizes in the region of single bubbles and coalescent bubbles were correlated by the following empirical equations:

Single bubbles

$$d_{bi} / d_N = 1.55 N_{FrN}^{0.2} \dots \dots \dots (2.95)$$

Coalescent bubbles

$$d_{bi} / d_N = 2.5 N_{FrN}^{0.2} d_N^{0.1} / d_{N0} - 3.5 \dots \dots \dots (2.96)$$

where

$$N_{FrN} = v_{gn} / g d_{bi} + 0.33 v_{sl}^2$$

d_{bi} = diameter of the bubble just after leaving the nozzle, cm

d_N = nozzle diameter, cm

d_{NO} = 0.086 cm

v_{gN} = gas velocity through nozzle, cm/sec

v_{sl} = superficial liquid velocity, cm/sec

g = gravitational acceleration, cm/sec²

The region of single bubbles is determined by

$$d_{bi}^2 N_{Frm} < 6$$

Their experimental work was performed in a 100 cm in height and 5 cm inside diameter pipe made of acrylic. A calming section was installed at the bottom pipe for the purpose of obtaining a uniform distribution of liquid velocity. Two nozzle sparger were used; one was 0.036 cm inside diameter and 0.130 cm outside diameter and the other was 0.305 cm and 0.400 cm. The nozzle submergence was 91 cm. Air or nitrogen was used as dispersed phase. Tap water was the liquid phase. Bubbles were generated under constant flow rate conditions. Gas flow rates ranged from 0.33 cm³/sec to 36.2 cm³/sec. Liquid flow rates ranged from 0 cm³/sec to 3040 cm³/sec. Dimensions of the bubbles were determined just after leaving the nozzle and at 7 cm above the nozzle tip.

When the nozzle of 0.305 cm. internal diameter was used, most of the data belonged to the region of single bubbles. The authors reported that after the superficial liquid velocity reached a value of around 90 cm/sec (3.0 ft/sec), the bubbles were no longer formed at the nozzle tip but at the crest of a gas jet flowing into the liquid.

Equations such as that of Ramakrishnan et al⁴⁷ are useful for determining the bubble size produced for various fluid-orifice

systems. However, these deterministic models are restricted to bubble generation under Stokes regime. Gas flow rates investigated were limited up to $80 \text{ cm}^3/\text{sec}$. Higher gas flow rates will result in gas jet formation at the tip of the nozzle where continuity could be satisfied either by the formation of single bubbles at a given frequency, or by the formation of multiple bubbles from the body of the gas jet⁹.

2.5 BUBBLE SIZE DISTRIBUTION FOR BUBBLE FLOW PATTERN

It has been shown analytically and experimentally that the size of bubbles generated at an orifice depends on the fluid properties and on the gas flow rates. However, non uniform bubble sizes have been observed in the process of intensive bubbling where forced gas convection is obtained by injecting gas into liquid through transverse porous plates or distributor grids with holes of the same diameter. Researchers^{53,54} have measured average bubble diameters in the range of 0.12 cm to 0.6 cm in this process. Particularly, for bubbling in water under various gas flow rates, an average bubble diameter of around 0.60 cm has been reported⁵⁴. The associated minimum and maximum measured diameters were 0.2 cm and 1 cm, respectively. This indicates that all of the bubbles were deformed bubbles.

Assuming that the bubble size is a random variable, some investigators^{53,54} have found that in an intensive bubbling process, the bubble diameter distribution fits closely to a Gaussian curve. This fact has been used to estimate the specific (phase contact) surface area for some chemical processes⁶⁵. While some workers reported a relatively constant average diameter and bubble size distribution⁵⁴ for bubbling in water for different water depths, other authors⁹ reported that the average void fraction changes with the

depth of water for a constant gas flow rate injected through a given gas distributor. Apparently, additional work is required for determining bubble size distribution in systems with larger water depths.

2.6 APPARENT MIGRATION RATES FOR GAS KICKS

Previous experimental work conducted in two 6000 ft wells at Louisiana State University has shed considerable light on the gas migration rates for gas kicks. Simulated well control operations conducted by Rader, Bourgoyne and Ward¹⁸ indicated apparent gas slip velocities of 1440 to 5040 ft/hour. Gas migration experiments conducted by Mathews and Bourgoyne⁵⁶ showed clearly that pressure increases, due to upward gas migration, occurred up to 2.5 hours after gas was injected in the bottom of a 6000 ft well. This gives apparent slip velocities of 2400 ft/hour.

Comparison of the apparent gas migration rates observed to the velocity of gas slugs shows that the flow pattern existing in the well could not be slug flow or plug flow. Casariego³⁸ determined experimentally, in a 30 ft model wellbore, the relationship shown in Figure 2.17 between bubble velocity and bubble equivalent diameter in a 6.375-in. by 2.375-in. annulus. This geometry is close to that present in the 6000 ft wells used by the Rader, Bourgoyne, and Ward, and by Mathews and Bourgoyne. Figure 2.18 indicates that for the apparent gas migration velocities determined in the full scale well experiments, diameter bubble sizes below about 1-in. were present. This diameter is smaller than that of Taylor bubbles, and well below the equivalent diameter required to obtain completely developed gas slugs.

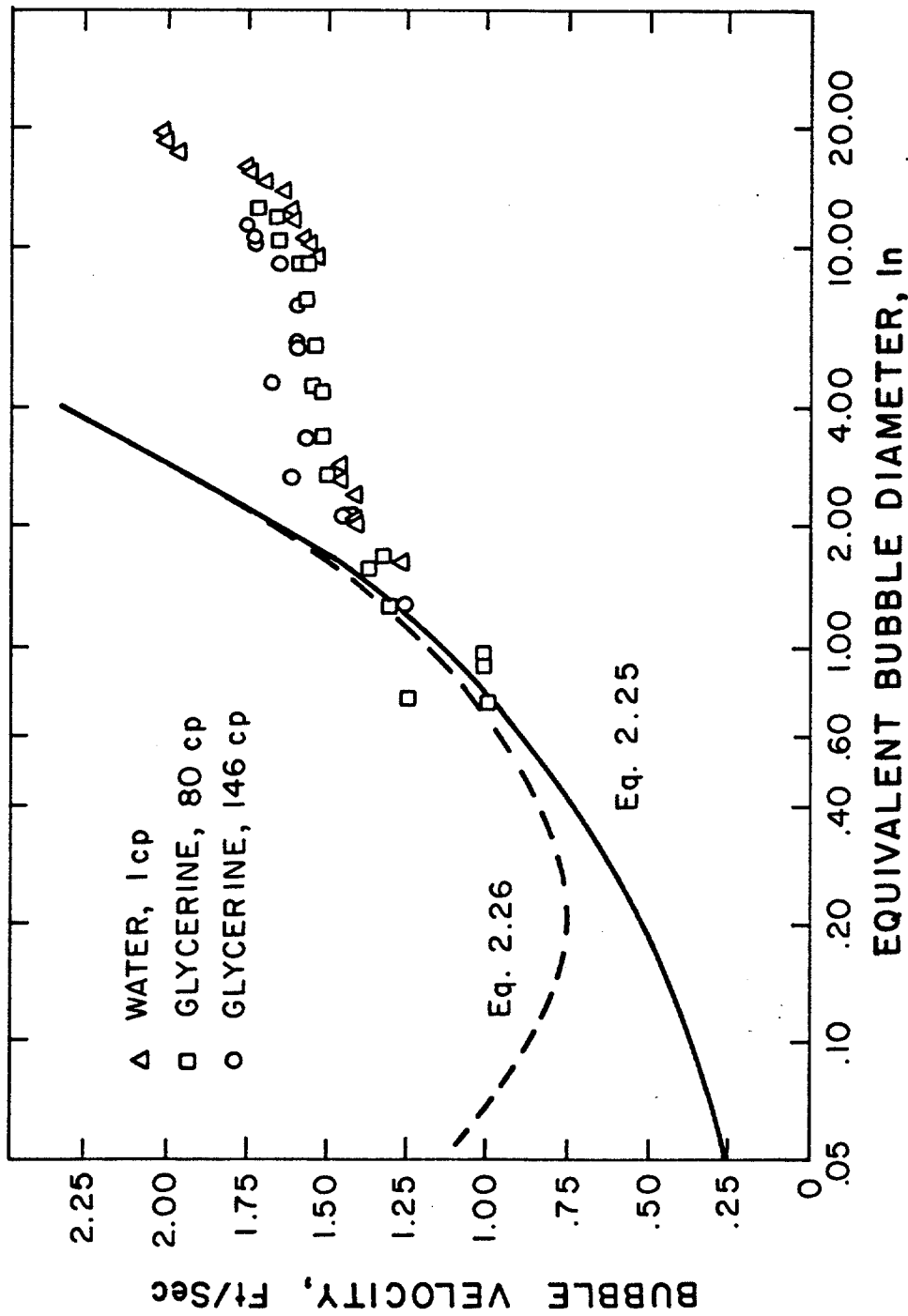


FIGURE 2.17. BUBBLE VELOCITY VS. EQUIVALENT BUBBLE DIAMETER AS MEASURED IN AN OPEN, 6.375-IN. BY 2.375-IN, ANNULUS

CHAPTER III

ANALYTICAL AND EXPERIMENTAL APPROACH

From a study of the previous literature in this area, it was concluded that the ruling flow pattern encountered in well control operations is bubble flow. Also, it was found that the average size of the bubbles is needed for obtaining the velocity and concentration of the gas in the two phase region. Therefore, an extended analytical model for predicting the size of bubbles generated in a non-Stokes regime through submerged orifices or porous media was needed. In order to accomplish this, knowledge of the relationship between bubble volume, bubble shape, and bubble velocity or drag is required.

The general approach in this study was first to define the relationship between the volume of a bubble and its associated drag and shape. Next, a method was developed for determining the initial size of bubbles formed during a gas kick. The method developed was then verified with experimental data obtained in a tank. These contributions are presented in Chapter V.

Chapter VI, contains topics related to the drag law between a single bubble and a swarm of bubbles, together with the review of pressure losses in two-phase flow as an introduction for the use of the minimum energy dissipation theorem.

From the work reported in Chapter V, the size of bubbles generated at the discharge of submerged orifices at high flow rates was found to be in the range of large lenticular bubbles. Moreover, the relationships presented in Chapter IV point out that for common well diameters, the large bubbles are unstable. This implies that regardless of the initial bubble size, an equilibrium bubble size exists

for a given well condition. This subject is developed in Chapter VII, where the minimum energy dissipation principle is applied recursively to obtain an average equilibrium bubble size and an average equilibrium gas fraction.

Chapter VIII discusses the application of this work to the computer simulation of well control operations. The new methods developed in previous chapters are used to improve an existing well control simulator program. Experiments are then conducted in a 6000 ft well to determine the accuracy of the improved computer program.

CHAPTER IV

TRANSITIONAL BOUNDARY LINES FOR BUBBLE GEOMETRIES

In Chapter II, previous work on the gas bubble rise behavior was discussed for the following major regions: rigid spherical bubbles, fluid spherical bubbles, oblate spheroid bubbles, and lenticular bubbles. In addition, the relationship between volume and shape of the bubbles with the dynamic forces acting over them was also discussed. In this chapter, the techniques adopted for describing bubbles rising in extended liquids will be presented.

4.1 THEORETICAL DEVELOPMENT

A simple approach to find the relationship between size and deformation of the bubbles can be done with a Force-Momentum Balance. Consider a spherical bubble to be rising in an extended liquid with a terminal velocity, v_{∞} , under Stokes Law. Assume that we overimpose a velocity v equal in magnitude but opposite to v_{∞} as it is shown in Figure 4.1. Considering an ideal liquid, there should be a force balancing the momentum acting over the spherical control volume. For the bubble to remain spherical, the surface forces should be able to withstand this force acting over its projected area; therefore, we can write:

$$4 \sigma_l A / d_e = v \rho_l v A \dots \dots \dots (4.1)$$

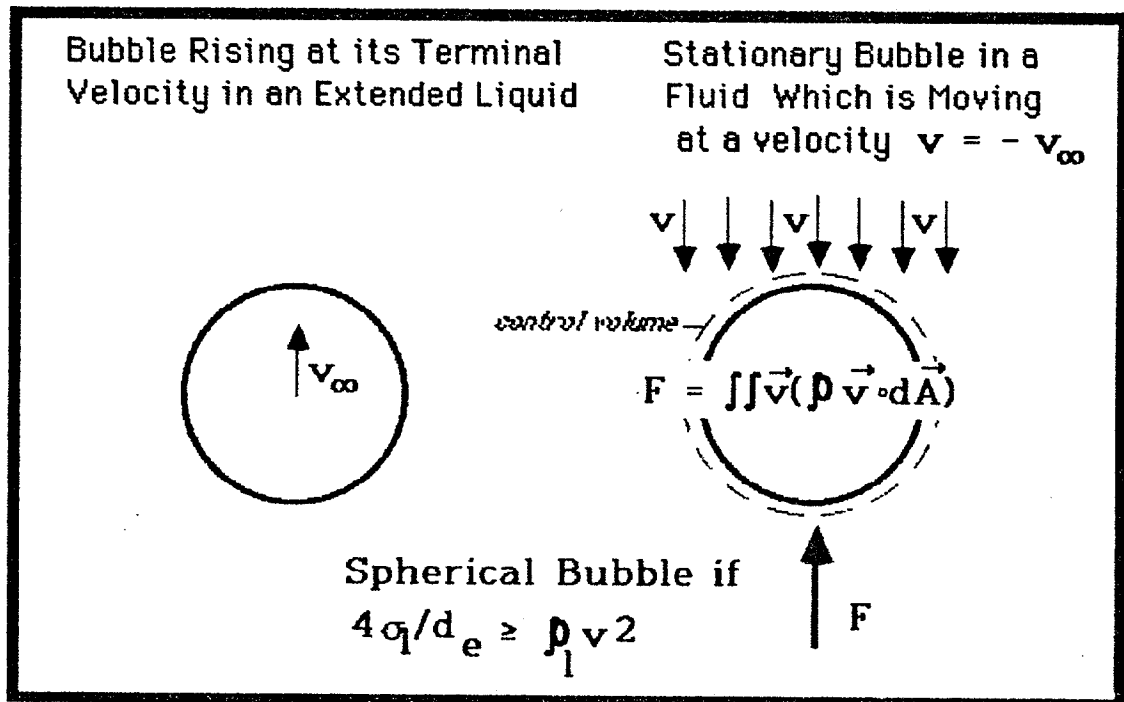


Figure 4.1 Relationship Between Surface Tension and Inertia Forces for the Stability of Spherical Bubbles.

$$d_e = 4 \sigma_1 / (\rho_1 v^2) \dots \dots \dots (4.2)$$

Recall that for rigid spherical bubbles, rising at its terminal velocity, the drag and buoyancy forces are in balance, and the terminal velocity is expressed:

$$v_\infty^2 = (4/3) g \Delta\rho d_e / (\rho_1 f_D) \dots \dots \dots (4.3)$$

particularly, for Stokes regime

$$v_\infty = g \Delta\rho d_e^2 / (18 \mu_1) \dots \dots \dots (4.4)$$

From equations (4.2) and (4.4).

$$d_e^5 = 4 \cdot 18^2 \sigma_1 \mu_1^2 / (g^2 \rho_1 \Delta\rho^2) \dots \dots \dots (4.5)$$

This equation describes the critical bubble diameter or the diameter at which a rigid spherical bubble starts to be deformed when it is rising in an extended liquid. The bubble Reynolds number associated to this critical bubble diameter, $(N_{Reb})_s$ is found from Equations (4.2), (4.4), and (4.5) to be

$$(N_{Reb})_s = 4.095 \{ \rho_1^2 \sigma_1^3 / (g \Delta\rho \mu_1^4) \}^{1/5} \dots \dots \dots (4.6)$$

Equation (4.6) shows that the critical Reynolds number is a function of a dimensionless viscosity number or the viscosity number, N_μ . Note that this term is the same as that previously

presented as Equations (2.49) and (2.75) except that the numerator contains a density difference. At low pressures, the density of the gas phase can be neglected and the density difference is approximately equal to the liquid density. Equation (4.6) gives the Reynolds number up to which a spherical bubble is stable. It is worthy to point out that similar dependence of the critical Reynolds number on the viscosity number has been observed in phenomena related to the stability of interphases. For example, Stephen Whitaker found that the critical Reynolds number for the stability of a falling liquid film is proportional to the viscosity number raised to the $-4/5$ power. The expression that he found differs from Equation (4.6) only by a constant.

Unfortunately, the relationship between volume, shape and velocity for oblate spheroid bubbles becomes too complex for a theoretical analysis similar to the one already done for spherical bubbles. However, the above discussion suggests that a criteria to predict the stability of the bubbles may be obtained by analyzing experimental data. A logarithmic plot of bubble Reynolds number against viscosity number of the liquid should display a straight line if an exponential relationship exists. Fortunately, data on bubbles rising in various liquids has already been published^{2, 22}.

4.2 ANALYSIS OF EXPERIMENTAL DATA

Haberman and Morton² did an extensive experimental work on the velocity of bubbles rising in extended liquids. Their work, already reviewed in Chapter II, covered a range of viscosity numbers of the liquids from 10^{-3} to 1. These researchers also reported the range of bubble Reynolds numbers where a given geometrical shape of the bubble was observed. Their data, together with some points

obtained from other work²² will be analyzed.

The selected data is represented by the points plotted in Figure 4.2. This figure, with logarithmic scales, displays in the vertical axis the bubble Reynolds number, and in the horizontal axis the viscosity number of the liquid raised to the fourth power. The points in the plot represent the conditions where a given geometrical shape of the bubble vanishes in the process of adopting a new geometrical shape in response to the dynamic forces acting over the bubble. For example, for water, the viscosity number raised to the fourth power is 2.63×10^{-11} . The critical (maximum) Reynolds number for spherical bubbles, rising in water, is 800. Above of this Reynolds number, the shape of the bubble starts to change to oblate-spheroid bubble. The aspect ratio of this bubble (the ratio of its vertical dimension to its horizontal dimension) decreases as the bubble Reynolds number increases until a Reynolds number of about 7000 is reached. At this point, the bubble is completely deformed and becomes a lenticular or Taylor bubble. This shape will remain unchanged as the bubble Reynolds number increases, until bubble fragmentation occurs at about a Reynolds number of 30,000.

The points mentioned above lay in the vertical line at the viscosity number of water, raised to the fourth power. The lines joining the points where a similar change occurs for bubbles rising in liquids with different viscosity numbers are here called transitional boundary lines.

Transitional line between spherical bubbles and oblate spheroid bubbles

The points in the lower half of Figure 4.2 represent the value of Reynolds numbers up to which a spherical shape was observed for bubbles rising in liquids with various viscosity numbers. Haberman and Morton's data shows: a cluster of points around a Reynolds

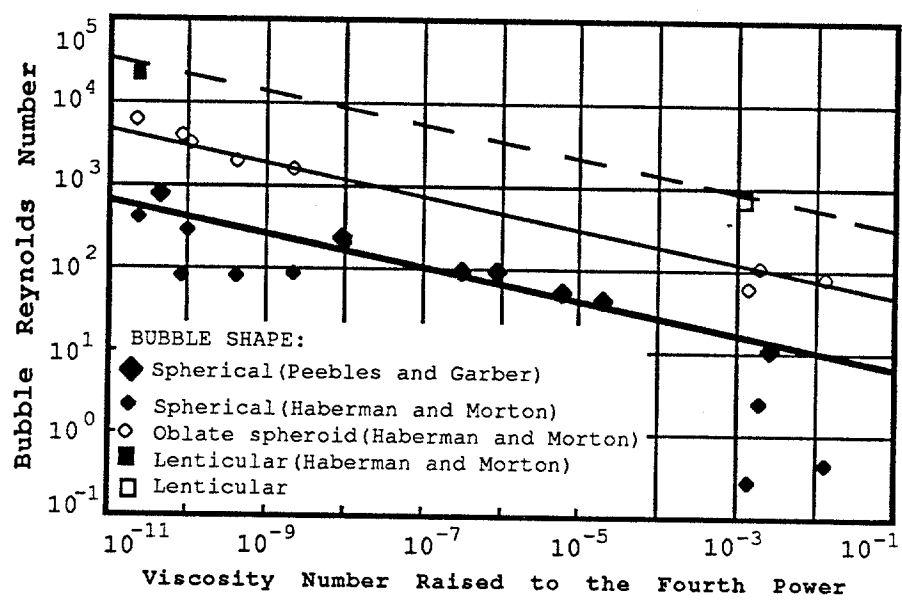


Figure 4.2. Reynolds Number, at Which a Change in Bubble Geometry Occurs, as a Function of the Liquid Viscosity Number.

number of 250 for bubbles rising in liquids with low viscosity number; and a cluster of points around a Reynolds number of 0.5 for liquids with high viscosity number. The scattered data does not show a clear trend for defining an exponential relationship as that of Equation (4.6). However, by adding points from data of Peebles and Garber²² for liquids with intermediate viscosity numbers to Figure 4.2, a trend is defined. This trend is shown by the lower straight line on the mentioned figure. The line defines the following exponential relationship between the viscosity number of the liquid and the critical spherical bubble Reynolds number, $(N_{Reb})_s$.

$$(N_{Reb})_s = 4.573 (N_\mu)^{-4/5} \dots \dots \dots (4.7)$$

Equation (4.7) confirms that the bubble Reynolds number depends on the $-4/5$ power of the viscosity number of the liquid, already obtained in section 4.1. This equation differs from the theoretical value given by Equation (4.6), only by a factor of 1.12. This relationship gives a range of critical bubble Reynolds number from 900 to 9 for the range of viscosity numbers shown in Figure 4.2.

Transitional line between oblate spheroid bubbles and lenticular bubbles

The next step was to look for a similar dependence of the Reynolds number on the viscosity number of the liquid for oblate spheroid bubbles. In this case, only five points for liquids with low viscosity number and three points for high viscosity numbers were available. However, they display an exponential relationship which runs approximately parallel to that obtained for spherical bubbles in Figure 4.2. The expression for the critical Reynolds number for

oblate spheroid bubbles, $(N_{Reb})_o$, in terms of the viscosity number is

$$(N_{Reb})_o = 6.232 (N_{Reb})_s = 28.5 (N_\mu^4)^{-1/5} \dots \dots \dots (4.8)$$

This correlation gives a range of critical oblate spheroid bubble Reynolds number from 800 to 80 for the range of viscosity numbers covered in Figure 4.2.

Transitional line between lenticular bubbles and multiple bubbles, or bubble fragmentation

The next step was to determine a correlation for the stability of lenticular bubbles. Unfortunately, the only available data point is that of water³. This point is in the left upper corner of the plot. By analogy, we assumed that the critical lenticular bubble Reynolds number, $(N_{Reb})_l$, depends also on the $-4/5$ power of the viscosity number. A constant was determined to satisfy the only data point, and the following expression was obtained

$$(N_{Reb})_l = 6.232^2 (N_{Reb})_s = 177.6 (N_\mu^4)^{-1/5} \dots \dots \dots (4.9)$$

In an attempt to confirm this correlation an experiment was performed in a 2 ft width, 1 ft long, 2 ft high acrylic tank. The following steps describe this experiment: First, the tank was filled with 78 cp glycerine; second, cups filled with air were immersed into the bottom of the tank; third, the cups were suddenly inverted to liberate the gas; fourth, the bubbles rising through the tank were recorded with a video camera. A maximum diameter of the base of lenticular bubbles in the range of 5-in. to 6-in. was obtained.

The average value of the base of these lenticular bubbles, 5.5-in. was used to determine its average equivalent diameter. The

value of this average equivalent diameter, obtained by geometrical relationships, is 3.16-in. The associated bubble Reynolds number for this particular bubble was 670 and the viscosity number of the liquid 0.18. These values give a point with coordinates $(1.04 \times 10^{-3}, 670)$ in Figure 4.2. This point falls close to the proposed correlation represented by the dashed line in the upper part of Figure 4.2.

In short, the two boundary lines as given by Equations (4.7) and (4.8) are proposed for determining: the transition of the geometrical shape of the bubbles from rigid spherical bubbles to oblate spheroid bubbles, and from oblate spheroid bubbles to lenticular bubbles, respectively. In addition, Equation (4.9) is proposed as the boundary line where bubble fragmentation in an extended liquid occurs.

4.3 SIGNIFICANCE OF THE PROPOSED CORRELATIONS

The proposed correlations give parameters which define the zone of bubble Reynolds numbers where a determined type of bubble can exist in an extended liquid. For a given liquid, the viscosity number is defined. This viscosity number defines three critical Reynolds numbers: one for rigid spherical bubbles, a second number for oblate spheroid bubbles and a third number for lenticular bubbles.

Analysis of previous work indicates that the oblate spheroid bubbles region is most important for well control modelling. This region starts at a bubble Reynolds number, $(N_{Reb})_s$, and ends at the bubble Reynolds number, $(N_{Reb})_o$. The drag for spherical bubbles can be obtained from the conventional experimental, f_D , versus, N_{Re} , correlation for solid spheres (see Figure 4.3) until $(N_{Reb})_s$ is reached.

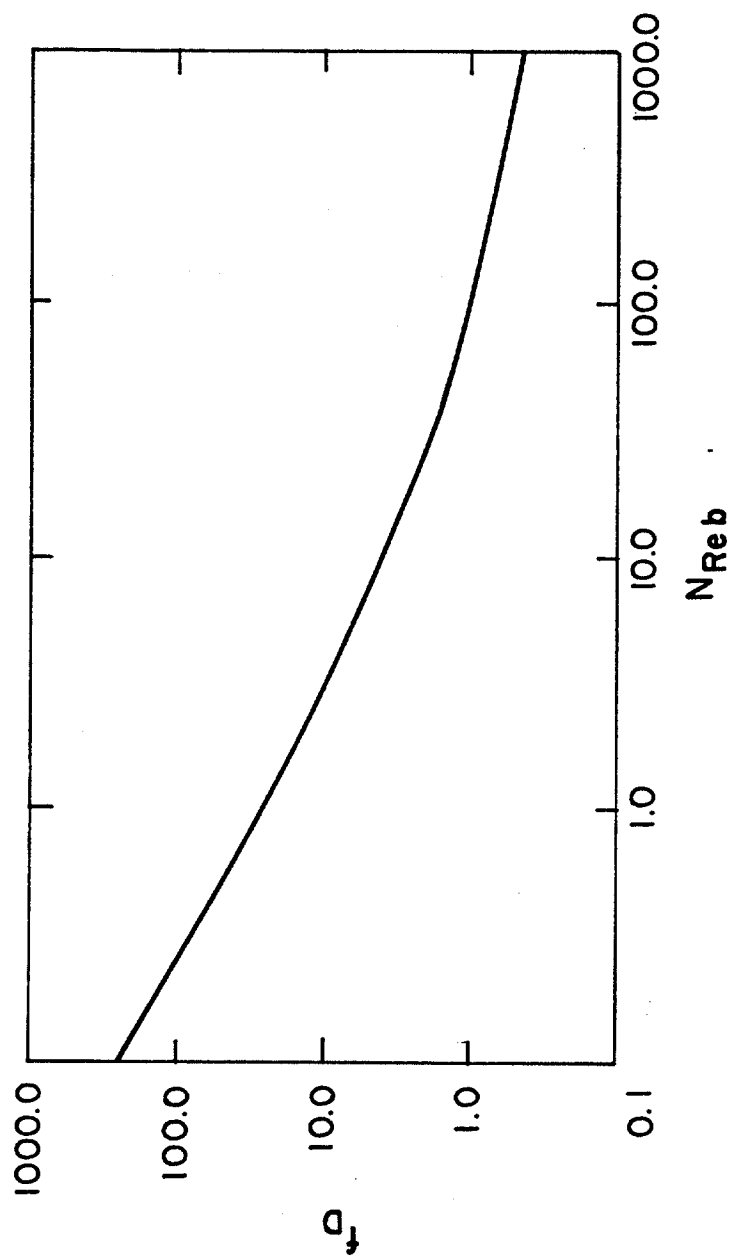


FIGURE 4.3. DRAG FACTOR VS. REYNOLDS NUMBER.
CORRELATION FOR SOLID SPHERES

The associated drag for this Reynolds number is f_{Ds} . The drag for lenticular bubbles is 2.66 and this value is associated to $(N_{Reb})_o$. An additional problem that must be solved is to determine the drag law for bubbles which are changing its aspect ratio in response to the dynamic conditions and the fluid properties. Note from Figure 4.4 that bubbles may start to deform under Stokes-transition regime as in the case of the mineral oil, or they may start to deform under turbulent regime, as in the case of the varsol. Also, note that the starting point of bubble deformation, for both liquids, lies in the rigid sphere drag law, and the final point of deformation lies at the constant drag line 2.66.

An approximation of the drag for oblate spheroid bubbles can be obtained, regardless of the aspect ratio of the bubble, by using a modified Karman number, N_K , defined as $f_D^{1/2}$ times N_{Reb} . It is well known that a plot of the Karman number versus particle Reynolds number can approximately be described by an exponential relationship for reasonable intervals of Reynolds numbers. Such is the case for our correlations, where:

$$(N_{Reb})_o / (N_{Reb})_s = 6.232$$

For example, Figure (4.5) displays the Karman number against the bubble Reynolds number obtained from experimental data for varsol and for mineral oil. A particular exponential law between N_K and N_{Reb} can be determined either for deformed bubbles rising in mineral oil or for deformed bubbles rising in varsol by joining the extreme points of the oblate spheroid bubbles. These straight lines closely fit the actual data for varsol and for mineral oil, respectively.

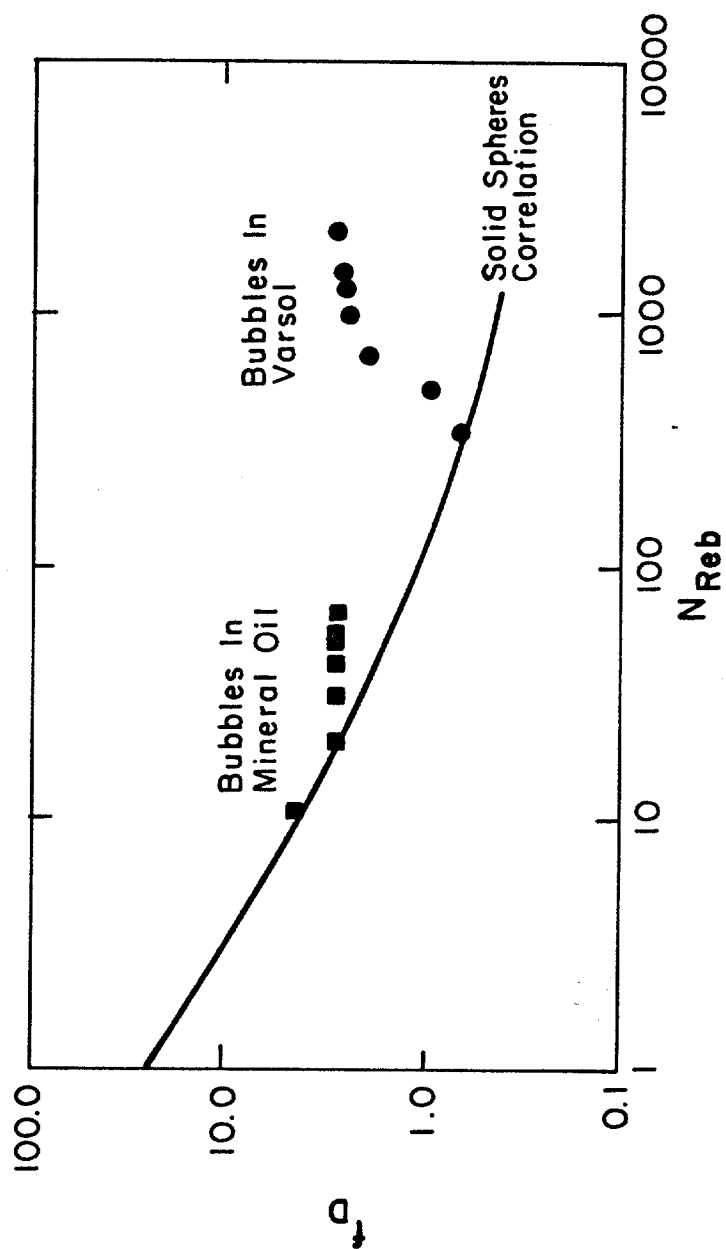


FIGURE 4.4. DRAG FACTOR VS. REYNOLDS NUMBER. OVERLAY OF SOLID SPHERES CORRELATION WITH DATA FOR OBLATE SPHEROID BUBBLES RISING IN BOTH MINERAL OIL AND VARSOL

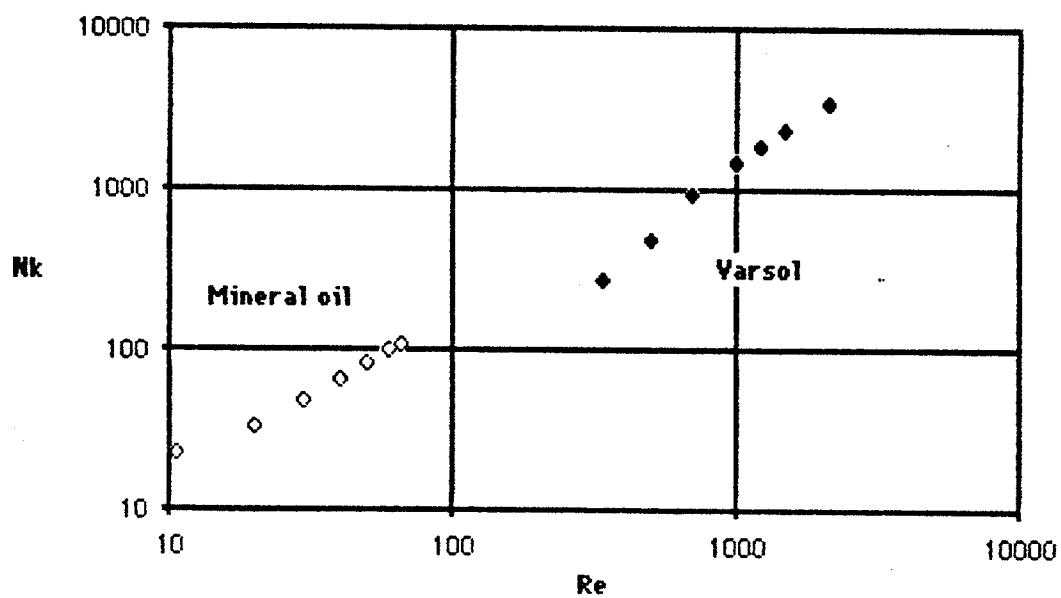


Figure 4.5 Karman Number vs Bubble Reynolds Number for Oblate Spheroid Bubbles Rising in Varsol, and in Mineral Oil

In short, in this chapter, a method was developed for obtaining the drag coefficient for any single bubble from the fluid properties where the bubble is rising. This method applies for rigid spherical bubbles, oblate spheroid bubbles, and lenticular bubbles rising in extended liquids. The method could be of practical importance if a representative bubble size can be defined for the bubble flow pattern which is predominant in well control operations, as it was discussed in Chapter II, section 2.6.

CHAPTER V

BUBBLE GENERATION

In Chapter IV, it was mentioned that one approach to solve the velocity of a swarm of bubbles is to find the effect of the concentration of the dispersed phase on the velocity of one of its elements rising in an infinite liquid. In turn, determination of the velocity of a single bubble rising in an infinite media requires that the average size of the individual bubbles be known. Also, it was said that gas issuing from a porous media can be thought of as gas issuing from a bundle of orifices. Furthermore, some models and correlations on bubble generation were reviewed. Unfortunately, these reviewed models are either limited to Stokes flow regime or they are valid only for inviscid liquids.

Since a method to predict the drag coefficient for any bubble rising in an infinite media had been developed in previous chapter, it was then practical to obtain a generalized model to predict the size of the bubbles generated under constant gas injection throughout an orifice. The analytical model that was obtained, as well as experimental data, gathered from a tank, for verifying this model are presented in this chapter.

5.1 SIMULATION OF BUBBLE FORMATION AT AN ORIFICE UNDER STEADY STATE GAS FLOW RATE

A Force Momentum Balance will be used to analyze the formation of gas bubbles at an orifice immersed in liquid. A theory to describe bubble formation is based on a two stage model. The

first stage consists of the expansion of the bubble while its base remains attached to the orifice. The second stage, or detachment stage, considers the interval while the bubble base moves away from the orifice but still continues its expansion due to indirect contact with the orifice through a gas stream protruding from the orifice. This second stage finishes when the bubble has drifted away of the orifice a distance equal to half of the diameter of the bubble obtained in the first stage. A sketch of these stages is given in Figure 5.1.

First Stage or Expansion Stage

Body Forces:

$$g V_b \Delta \rho / g_c \dots \dots \dots (5.1)$$

Surface Forces:

$$f_D \rho_l v_l^2 \pi d^2 / (8 g_c) \dots \dots \dots (5.2)$$

$$\pi d_N \sigma_1 \cos \theta \doteq \pi d_N \sigma_1 \dots \dots \dots (5.3)$$

Inertial Forces:

$$d/dt (m_{vb} v_l) = m_{vb} d/dt (v_l) + v_l d/dt (m_{vb}) \dots \dots \dots (5.4)$$

where the virtual mass of the bubble is given by

$$\begin{aligned} m_{vb} &= V_b (\rho_g + (11/16) \rho_l) \\ &= q_N t (\rho_g + (11/16) \rho_l) \dots \dots \dots (5.4a) \end{aligned}$$

The average velocity of the bubble, v_l is given by the velocity of the bubble center

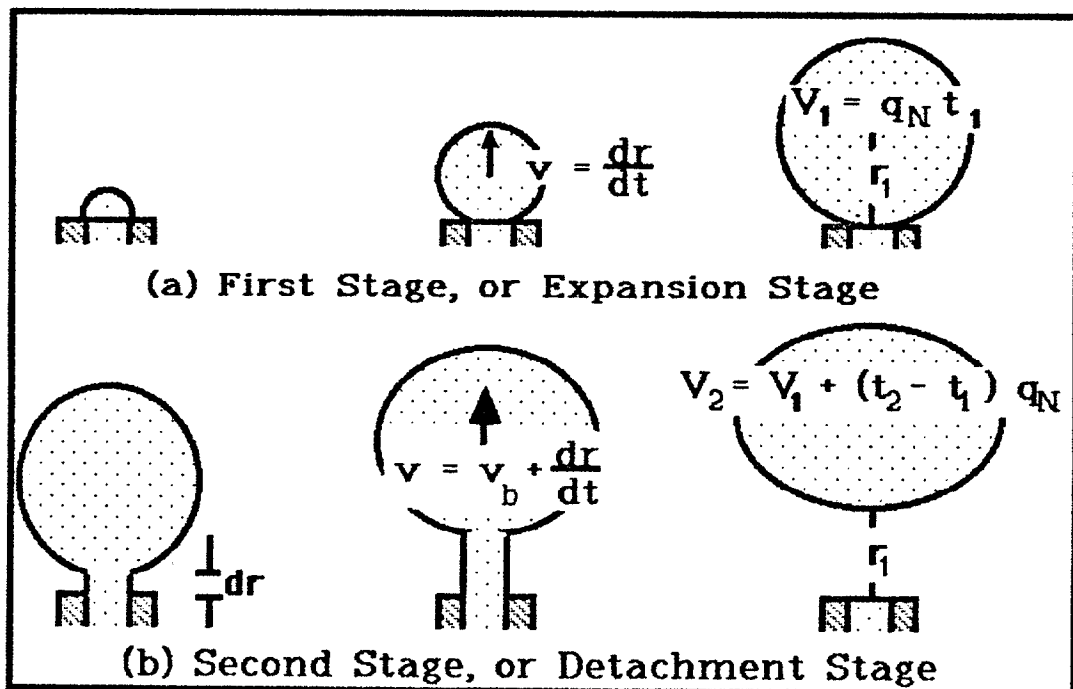


Figure 5.1 Two Stage Model of Bubble Formation

$$v_1 = \frac{1}{2} \frac{d}{dt} (d_e)$$

but $d(V_b) = d(1/6 \pi d_c^3) = q_N dt$

which implies $d/dt (d_e) = 2 q_N / (\pi d_e^2)$

and the average velocity becomes:

$$v_1 = q_N / (\pi d_e^2) \dots \dots \dots (5.4b)$$

Now we can evaluate the elements of the r.h.s. terms of Equation (5.4). From Equation (5.4b)

$$\begin{aligned} d/dt (v_1) &= [q_N / \pi] [- 2 d/dt (d_e) / d_e^3] \\ &= - 4 q_N^2 / (6^{5/3} \pi^{1/3} V_b^{5/3}) \dots \dots \dots (5.4c) \end{aligned}$$

Also,

$$d/dt (m_{vb}) = (\rho_g + 11 \rho_l / 16) q_N \dots \dots \dots (5.4d)$$

We can recast the inertial forces as:

$$\begin{aligned} d/dt (m_{vb} v_1) &= m_{vb} \{ - 4 q_N^2 / (6^{5/3} \pi^{1/3} V_b^{5/3}) \} \\ &\quad + (q_N / (\pi d_e^2)) (\rho_g + 11 \rho_l / 16) q_N \\ &= (\rho_g + 11 \rho_l / 16) q_N^2 / (3 \pi (6/\pi)^{2/3}) (1/V_1^{2/3}) \\ &\dots \dots \dots (5.5) \end{aligned}$$

From Newton Second Law, we can write from Equations (5.1), (5.2), (5.3) and (5.5):

$$V_1^{5/3} = (\rho_g + 11\rho_l/16) Q_N^2 / [3\pi g (6/\pi)^{2/3} \Delta\rho] + (\pi/6)^{2/3} \rho_l f_D Q_N^2 / (8\pi g \Delta\rho) + g_c \pi d_N \sigma_l V_1^{2/3} / (g \Delta\rho) \dots \dots \dots (5.6)$$

This equation satisfies the force momentum balance during the first stage of the bubble formation. V_1 represents the volume obtained by the bubble at the end of this stage. Clearly, a trial and error procedure is required to evaluate the volume of the bubble.

Second Stage

In this stage the base of the bubble drifts away from the tip of the orifice due to the dominant effect of the buoyancy.

Body Forces

$$g V_b \Delta\rho / g_c \dots \dots \dots (5.7)$$

Surface Forces

$$(1/g_c) [f_D \rho_l (v_2 + v_{2e})^2 / 2] (\pi d^2/4) \dots \dots \dots (5.8)$$

$$\pi d_N \sigma_l \cos \theta \doteq \pi d_N \sigma_l \dots \dots \dots (5.9)$$

Inertial Forces

$$d/dt [m_{vb} (v_2 + v_{2e})] = m_{vb} [d/dt v_2 + d/dt (v_{2e})] + (v_2 + v_{2e}) d/dt (m_{vb}) \dots \dots \dots (5.10)$$

where

v_2 = bubble velocity

v_{2e} = average bubble velocity due to expansion of the bubble as a result the gas injected to the rising bubble through its connecting "neck",

again, the expansion velocity is given by

$$v_{2e} = (1/2) \, d/dt \, (d_e) = q_N / (\pi d_e^2) \dots \dots \dots (5.10b)$$

Now we can evaluate the local acceleration due to gas injection:

$$\begin{aligned} d(v_{2e})/dt &= (q_N / \pi) (d/dt) (1 / d_e^2) \\ &= -4 q_N^2 / (6^{5/3} \pi^{1/3} v^{5/3}) \dots \dots \dots (5.10c) \end{aligned}$$

$$d/dt (m_{vb}) = (\rho_g + 11 \rho_l / 16) q_N \dots \dots \dots (5.10d)$$

The drag force given by Equation (5.8) can be expressed as follows:

$$\begin{aligned} &[6^{2/3} \pi^{1/3} f_D \rho_l V^{2/3} v_2^2] / (8 g_c) + [f_D \rho_l q_N v_2] / (4 g_c) \\ &+ [f_d \rho_l q_N^2] / [8 \cdot 6^{2/3} \pi^{1/3} V^{2/3}] \dots \dots \dots (5.11) \end{aligned}$$

From Newton Second Law, and upon grouping the terms containing v_2 and dividing by $(\rho_g + 11 \rho_l / 16) V$ we obtain:

$$\begin{aligned}
 & d/dt (v_2) + [q_N + (f_D \rho_1 q_N) / (4 (\rho_g + 11 \rho_1 / 16))] v_2 / V \\
 & + \{ (6^{2/3} \pi^{1/3} f_D \rho_1) / [8 (\rho_g + 11 \rho_1 / 16)] \} v_2^2 / V^{1/3} = g \Delta\rho / (\rho_g \\
 & + 11 \rho_1 / 16) - (f_D \rho_1 q_N^2) / [6^{2/3} \pi^{1/3} 8 (\rho_g + 11 \rho_1 / 16) V^{5/3}] \\
 & - (\pi d_N \sigma_1) / [(\rho_g + 11 \rho_1 / 16) V] + 4 q_N^2 / (6^{5/3} \pi^{1/3} V^{5/3}) \\
 & - q_N^2 / (6^{5/3} \pi^{1/3} V^{5/3}) (5.12)
 \end{aligned}$$

Since

$$V = q_N t$$

$$dV = q_N dt \Rightarrow dt = dV / q_N \dots\dots\dots (5.13)$$

We can recast Equation (5.12) in terms of the variation of velocity with respect to volume; i.e. the first term of the left hand side of Equation (5.12) can be expressed as

$$d/dt (v_2) = q_N [d/dV (v_2)] \dots\dots\dots (5.14)$$

Also, recasting Mendelson's²³ Equation (2.26) in terms of the bubble volume:

$$v_2^2 / V^{1/3} = (\pi / 6)^{1/3} (2 \rho_1 / V^{2/3}) + g (6 / \pi)^{1/3} / 2 \dots\dots\dots (5.15)$$

We are going to restrict our generalized solution to non-Stokes regime by using Equation (5.15) in the third term of the l.h.s. of Equation (5.13). Use of Equations (5.14) and (5.15) in Equation (5.13) gives:

$$\begin{aligned} d/dV (v_2) + A v_2 / V &= B + C V^{-5/3} - E V^{-1} - G V^{-2/3} - H \\ &= (B - H) + C V^{-5/3} - E V^{-1} - G V^{-2/3} \dots \dots \dots (5.16) \end{aligned}$$

where

$$\begin{aligned} A &= [1 + f_D \rho_1 / (4 (\rho_g + 11 \rho_1 / 16)] \\ B &= g \Delta \rho / [(\rho_g + 11 \rho_1 / 16) q_N] \\ C &= \{ 4 / (6^{5/3} \pi^{1/3}) - 1 / (6^{2/3} \pi^{1/3}) - (f_D \rho_1) \\ &\quad / [8 \cdot 6^{2/3} \pi^{1/3} (\rho_g + 11 \rho_1 / 16) q_N] \} \\ E &= (\pi d_N \sigma_1) / [(\rho_g + 11 \rho_1 / 16) q_N] \\ G &= (6^{2/3} \pi^{1/3} f_D \rho_1 \cdot 2 (\pi / 6)^{1/3} \sigma_1) / [8 (\rho_g + 11 \rho_1 / 16) q_N] \\ H &= (6^{2/3} \pi^{1/3} f_D \rho_1 (6 / \pi)^{1/3} g) / [8 (\rho_g + 11 \rho_1 / 16) q_N] \end{aligned}$$

where f_D is an average drag factor acting during the second stage.

Note:

$$\begin{aligned} d(v \cdot V^A) &= V^A dv + v A V^{A-1} dV \\ d/dV (v \cdot V^A) &= V^A d/dV (v) + v A V^{A-1} \\ &= V^A (d/dV (v) + A v/V) \end{aligned}$$

We can complete the differential in Equation (5.16)

$$\begin{aligned} d(v_2 V^A) &= [(B - H) V^A \\ &\quad + C V^{A-5/3} - E V^{A-1} - G V^{A-2/3}] dV \dots \dots \dots (5.17) \end{aligned}$$

Integrating between the appropriate limits:

$$v^A u \Big|_{u=0}^{u=v_2} = \left[\frac{B-H}{A+1} U^{A+1} + \frac{C}{A-2/3} U^{A-2/3} - \frac{E}{A} U^A - \frac{G}{A+1/3} U^{A+1/3} \right]_{U=V_1}^{U=V}$$

$$\Rightarrow v_2 = \frac{1}{V^A} \left[\frac{(B-H)}{A+1} (V^{A+1} - V_1^{A+1}) + \frac{C}{A-2/3} (V^{A-2/3} - V_1^{A-2/3}) \right]$$

$$- \frac{E}{A} (V^A - V_1^A) - \frac{G}{A+1/3} (V^{A+1/3} - V_1^{A+1/3}) \dots \dots \dots (5.18)$$

we can write the distance from the orifice as:

$$dz = v_2 \, dV / q_N$$

so that Equation (5.18) becomes:

$$dz = \frac{1}{q_N} \left[\left(\frac{B-H}{A+1} \right) V + \frac{C}{A-2/3} V^{-2/3} - \frac{E}{A} - \frac{G}{A+1/3} V^{1/3} \right] dV$$

$$= \frac{1}{q_N} \left[\left(\frac{B-H}{A+1} \right) V^{A+1} + \frac{C}{A-2/3} V^{A-2/3} - \frac{E}{A} V^A - \frac{G}{A+1/3} V^{A+1/3} \right] \frac{dV}{V^A}$$

but at $z = 0$, the volume of the bubble is V_1

$z = r_1$, the volume of the bubble is V_2

Upon integration between the appropriate limits, we obtain:

$$r_1 = \frac{1}{2q_N} \left(\frac{B-H}{A+1} \right) (V_2^2 - V_1^2) + \frac{3C}{q_N(A-2/5)} (V_2^{3/5} - V_1^{3/5}) - \frac{E}{q_N A} (V_2 - V_1)$$

$$- \frac{3G}{4q_N (A+1/5)} (V_2^{4/3} - V_1^{4/3}) - \left[\left(\frac{B-H}{A+1} \right) V_1^{A+1} + \frac{C}{(A-2/5)} V_1^{A-2/5} - \frac{E}{A} V_1 - \frac{G}{(A+1/5)} V_1^{A+1/5} \right] \frac{1}{q_N} \frac{V_2^{1-A} - V_1^{1-A}}{(1-A)} \dots \dots \dots (5.19)$$

This equation satisfies the force momentum balance during the second stage of the bubble formation. V_2 represents the final volume of the bubble. Again a trial and error procedure is required to evaluate the volume of the bubble because we obtained an implicit equation for the final volume of the bubble.

Procedure of Calculation:

1. The determination of the volume of the bubble at the first stage, V_1 , given by Equation (5.6) requires an iterative method. The second and third terms of the r.h.s. of Equation (5.6) depend on the volume of the bubble. In the second term the dependence on the

volume is hidden in the drag factor which is a function of the velocity of the bubble. (Recall that the velocity of the bubble is due to its expansion.) Therefore, we have to assume a volume in order to calculate these two r.h.s. terms of the equation to start a trial and error method of solution until Equation (5.6) is satisfied. Once this volume is determined, we proceed to the solution of the equation for the detachment stage of the bubble.

2. The determination of the volume of the bubble at the second stage, given by Equation (5.19) also requires an iterative method of solution. Once that V_1 is calculated from Equation (5.6), we have to assume a final bubble volume V_2 , to define the r.h.s. terms of Equation (5.19) and proceed with the trial and error method of solution.

Equations (5.6) and (5.19) describe the formation of bubbles at immersed nozzles or orifices. Equation (5.6) describes an expansion process where the body of the bubble is directly attached to the orifice and Equation (5.19) describes a detachment process where the bubble goes away from the orifices due to the buoyancy effects, but still it continues expanding due to an "umbilical cord-like" gas feeding line to the nozzle. When the gas flow rates injected through the nozzle approach zero, the volume of the bubble during the first stage becomes mainly a function of the buoyancy and interfacial tension. Note that in this case, the first two terms of Equation (5.6) will vanish due to the low gas flow rates. Also the vanishing gas flow rates will result in a neglectable volume added during the second stage so that the final volume of the bubble is practically that obtained in the expansion stage. On the other hand, for high gas flow rates, the volume of the bubble during the first stage becomes a strong function of both the inertia and drag terms, and they overshadow the effect of the surface tension term. The model

presented predicts that the volume of the bubble will increase with increasing gas flow rates. This model should describe the size of the bubbles as long as continuity is satisfied by the formation of single bubbles. To validate this model, it is required to obtain experimental data for moderate to high gas flow rates. To accomplish this task, the experimental equipment described in the following section was constructed.

5.2 EXPERIMENTAL APPARATUS

A set up as it is shown in Fig. 5.2a was used to measure the volume of the bubbles formed at the tip of the orifices. The next paragraph describes the main parts of such apparatus.

A compressed N_2 cylinder was the source (A) of gas. The pressure of the gas was reduced with the pressure regulator (B) to a desired working pressure indicated by the pressure gauge (C). The gas flow was regulated with a needle valve (D). The gas was discharged through a tubing (E) into the fluid (F). The fluid was contained in a transparent tank whose dimensions are also shown in Figure 5.2a.

The stream of bubbles was recorded with a video cassette recorder (G). The frequency of bubble formation was determined by the number of bubbles formed in a given time interval by replaying the tape at low velocity.

5.3 ACTUAL AND THEORETICAL VOLUME OF THE BUBBLES

A series of runs were formed in the apparatus described in section 5.2. The properties of the fluids used in the experimental runs are given in Table 5.2. The diameter of tubings used as gas

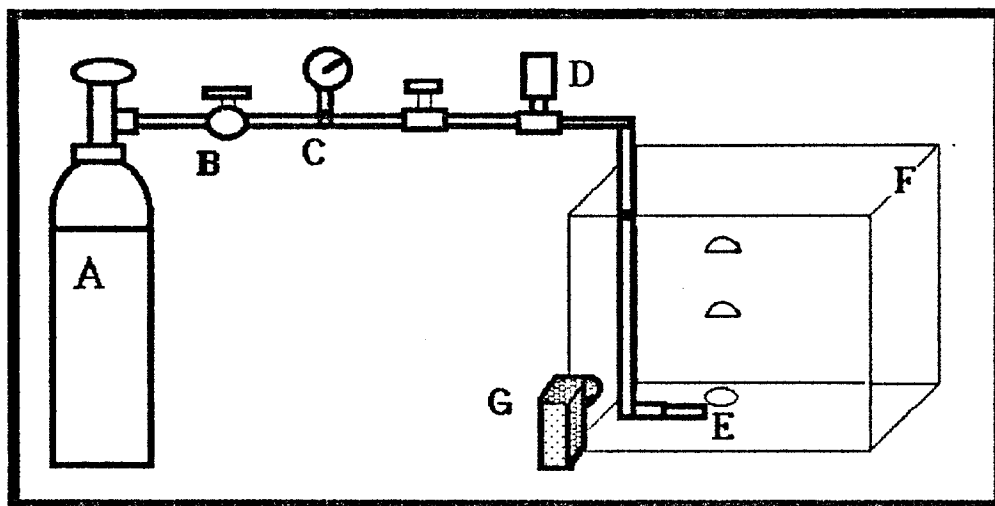


Figure 5.2a Experimental Apparatus to Generate Bubbles.

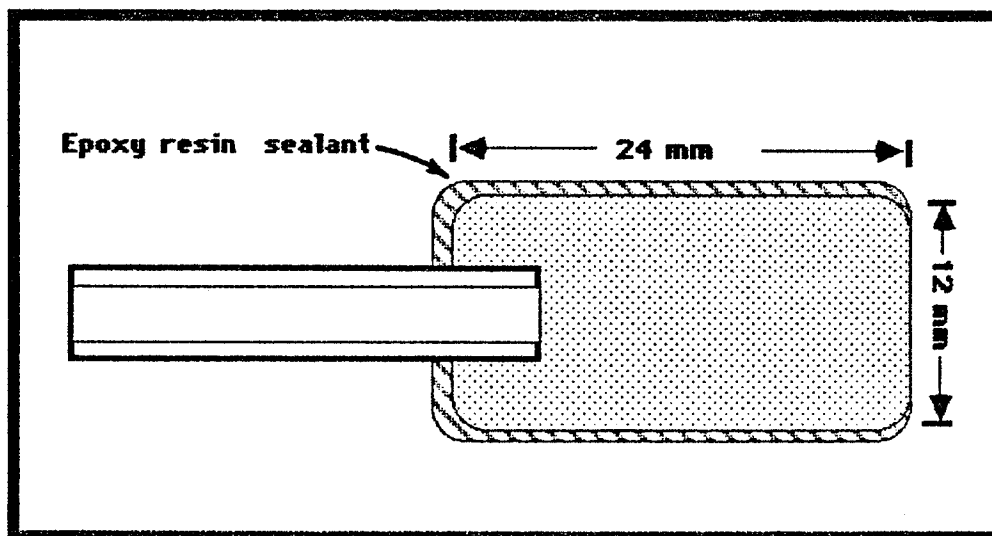


Figure 5.2b Schematic of Porous Media Used to Generate Bubbles.

TABLE 5.1 DIAMETER OF TUBINGS

O.D.[in]	1/8	1/4	3/8	1/2
I.D.[in]	0.055	0.1800	0.305	0.430
I.D.[cm]	0.1397	0.4572	0.7747	1.0922

TABLE 5.2 FLUID PROPERTIES

	Specific Gravity	Viscosity [cp]	Surface Tension [dyne/cm]
5% (wt) NaCl Solution	1.034	0.9639	77.52
Glycerine Solution	1.21	500.	66.4
Glycerine Solution	1.19	250.	67.6
Glycerine Solution	1.17	162.	68.3
Glycerine Solution	1.15	78.	69.5

spargers is shown in Table 5.1. The description of porous cylinders used to analyze the effects of gas dispersion in bubble formation are given in the following section.

Porous Cylinders

Two porous cylinders, made from bounded glass beads, were obtained for this work. These cylinders were acquired from Kordon, a division of Novalek, Inc. in Hayward, CA. The cylinders are available in three grades: 62501, 62502, and 62503. These grades correspond to coarse glass beads, medium glass beads and fine glass beads, respectively. The coarse and the fine grade cylinders were purchased. The dimensions of the cylinders are 12mm diameter by 24.4mm height. The porous cylinders are attached to a 22 cm glass tubing of 6mm external diameter. The cylindrical surface and the annular surface where the tubing is attached, were sealed with a thin film of epoxy resin so that gas injected into the porous material through the tubing is forced to exit through the remaining unsealed circular face, as it is shown in Figure 5.2b.

Before discussing the effect of the nozzles, porous media, and fluid properties on the size of the bubbles, some remarks on phenomena such as liquid backflow and formation of gas jets are presented.

Backflow

During calibration runs, circulation of liquid or backflow was noticed to occur due to density differences between the gas contaminated region and the rest of the fluid. No attempt was made to obtain a calm section near the gas spargers. It was felt that providing a calming section would lead to an unrealistic situation. The circulation phenomenon increased with the gas flow rates. At high flow rates, the liquid backflow becomes strong enough to trap small lenticular bubbles.

The former observation appears to point out that the size of the bubbles generated could be different from the size of the bubbles generated without the "circulation" or backflow effect.

The observed circulation provides an upward frictional drag on the bubbles; due to the velocity of the fluid. This could lead to the formation of smaller bubbles. On the other hand, the generated streams of fluid may also result in bubble coalescence.

Formation of Gas Jet

Also, during calibration runs, the formation of gas jet at high flow rates was noticed. Under this situation, bubble formation occurred at the tip of the gas jet. However, the bubble formation phenomenon appears to be the same regardless of the point where the bubbles are actually formed. In other words, apparently the gas jet has the effect of a translation of the point where bubble generation actually starts, as if it were a prolongation of the tubing or orifice. At some high flow rates issuing through small diameter tubing, an additional phenomenon was observed: secondary bubbles were generated along the jet stream. This situation was never reached for the range of flow rates used in actual data acquisition.

5.3.1. Discussion of Experimental Data.

Effect of porous media.

A series of tests were performed to analyze the effect of dispersion of the gas on the bubble formation. Some tests, for low gas flow rates, were done in order to check qualitatively if the grades of the porous media could duplicate some already reported effects on bubble size⁵³; among these effects are that: (1) bubble formation through gas diffusers gives smaller gas bubbles for finer porous media; and (2) bubble formation, under a given gas flow rate, produces smaller bubbles in solutions containing higher concentrations of inorganic electrolytes.

Qualitative observations

The coarse and fine porous media, already described, were used to bubble the gas into the liquid. A swarm of bubbles was obtained at flow rates lower than 900×10^{-6} SCF/s. Spherical bubbles were obtained at low gas flow rates and the size of the individual bubbles increased with the gas flow rates. The bubble geometry also changed when the gas flow rates increased beyond of a certain value. At low gas flow rates, the bubbles produced through the fine porous media, were smaller than those produced through the course porous media, as it has already been reported by some researchers⁵³; also, bubbles produced in solutions containing inorganic electrolytes appear to increase the range of gas flow rates where small spherical bubbles are produced. For gas flow rates higher than 900×10^{-6} SCF/s, the following quantitative data was obtained.

Quantitative observations

At flow rates above 1000×10^{-6} SCF/s, the porous media delivered the gas into the liquid as if it were a tubing of approximately $\frac{1}{4}$ " diameter. Figure 5.3 illustrates the fact that above of a level of gas flow rates, the bubble formation is independent from the porous media. Figure 5.11 shows the same effect mentioned above, but in viscous fluid. Also, runs of bubble formation in NaCl solutions were performed. The same observations mentioned above apply for this experiment. In fact, Figure 5.3 includes the results obtained by gas injection through porous media into both distilled water and 5% NaCl solution.

The conclusion is that bubbles formed using porous materials are not noticeably different from bubbles formed from a tube once a critical flow rate is exceeded. Moreover, for the range of flow rates studied, the bubble formation falls in the trend of that obtained by injecting the gas through a vertical tubing of $\frac{1}{4}$ " diameter, as it is

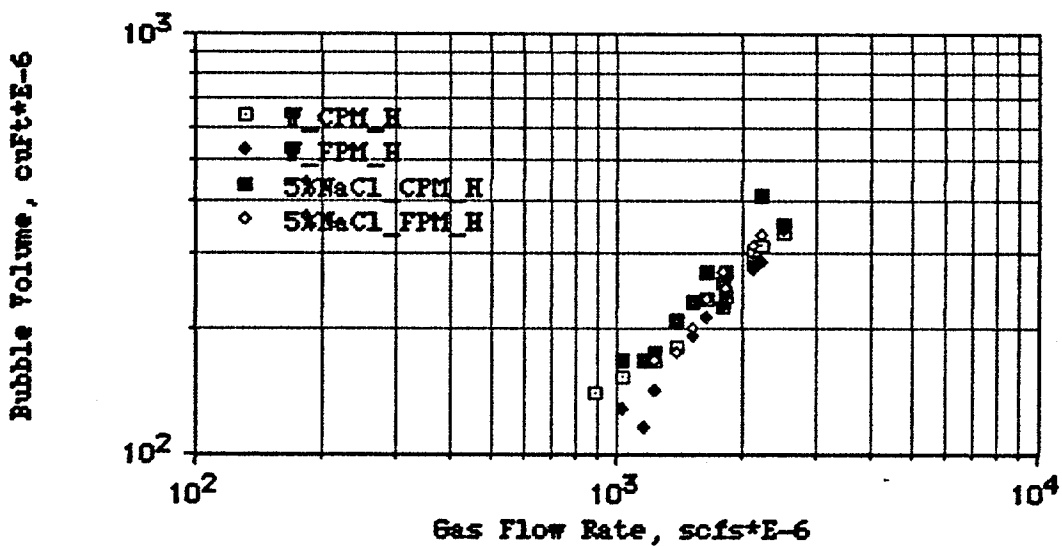


Figure 5.3 Volume of Bubble Formed as a Function of Gas Injection Rate When Gas is Injected through Porous Media

KEY OF THE LEGEND

FLUID	INJECTION DEVICE	INJECTION DEVICE ORIENTATION
-------	------------------	------------------------------

FLUID:

W = distilled water

5%NaCl = solution of 5% sodium chloride by weight

INJECTION DEVICE:

CPM = coarse porous media

FPM = fine porous media

INJECTION DEVICE ORIENTATION:

H = horizontal

shown in Figure 5.4.

Effect of Tubing Inclination

Figure 5.5 shows that the orientation of the orifice or tubing inclinations does not play an important role in bubble formation. As predicted by the theoretical derivations, the phenomenon is dominated by gas injection rate, buoyancy, and interfacial tension.

Effect of Gas

Nitrogen gas, and Methane gas were injected through orifices into both NaCl solution and distilled water. As it was expected, no effect of the type of gas was observed on the bubble formation phenomenon. Figure 5.6 displays the data obtained for distilled water only. For clarity purposes, the data obtained in salty water was not included, since they overlapped with the data exhibited in Figure 5.6.

Effect of Salt Content

As mentioned above, NaCl did not influence the size of the gas bubbles generated for the combination of orifice sizes and gas flow rates covered in our experiment, as it is displayed in Figure 5.7.

Effect of Tubing Diameter

Figures 5.8 and 5.10 show that the size of the bubbles increases with the size of the orifice for a given gas flow rate. However, this effect vanishes as the gas flow rate increases.

Effect of Viscosity

For the range of gas flow rates and orifices used in this experimental work, the size of the bubbles was not strongly affected by the viscosity of the fluid. Apparently, only at low gas flow rates, there is some increase of bubble size with viscosity. For the data of Figure 5.9, the glycerine allows bigger bubbles to be formed below approximately 300×10^{-6} SCF/s.

Effect of Surface Tension

No data was obtained to determine particularly the effect of

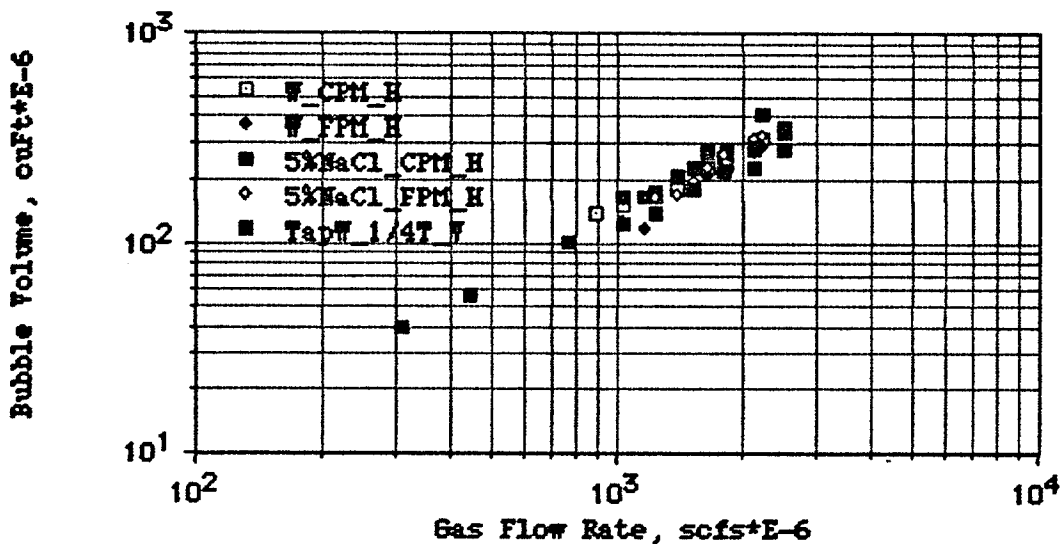


Figure 5.4 Comparison of Bubble Volumes Formed from Porous Media and from 0.25-in. Tubing as a Function of Gas Injection Rate. Data Obtained in Low Viscosity Fluids

KEY OF THE LEGEND

FLUID	INJECTION DEVICE	INJECTION DEVICE ORIENTATION
-------	------------------	------------------------------

FLUID:

W = distilled water
 5XNaCl = solution of 5% sodium chloride by weight
 TapW = tap water

INJECTION DEVICE:

CPM = coarse porous media
 FPM = fine porous media
 1/4T = tubing of 1/4" outer diameter

INJECTION DEVICE ORIENTATION:

H = horizontal
 V = vertical

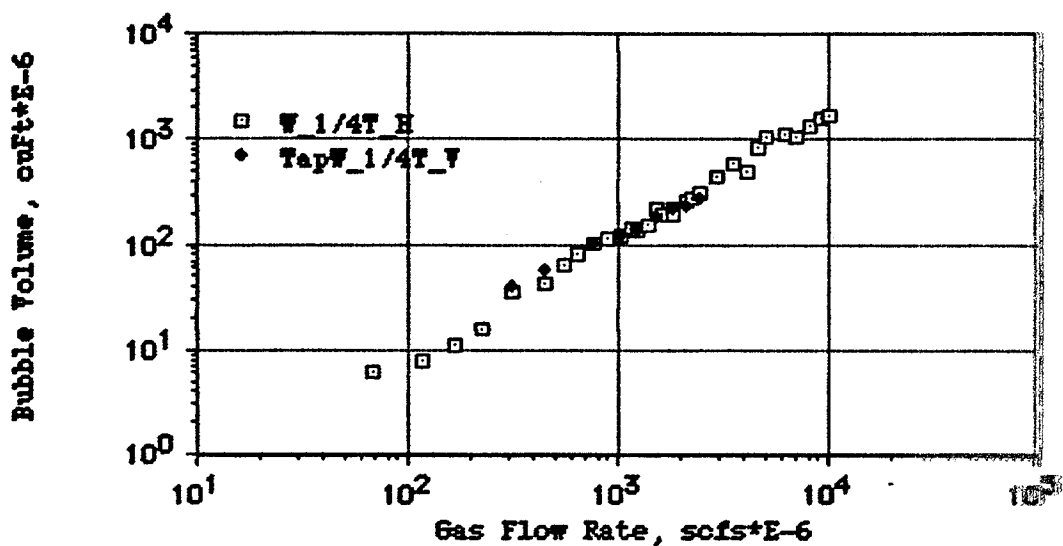


Figure 5.5 Comparison of Bubble Volumes Obtained from Horizontal and Vertical Tubings

KEY OF THE LEGEND

FLUID	_	INJECTION DEVICE	_	INJECTION DEVICE ORIENTATION
-------	---	------------------	---	------------------------------

FLUID:

W = distilled water
TapW = tap water

INJECTION DEVICE:

1/4T = tubing of 1/4" outer diameter

INJECTION DEVICE ORIENTATION:

H = horizontal
V = vertical

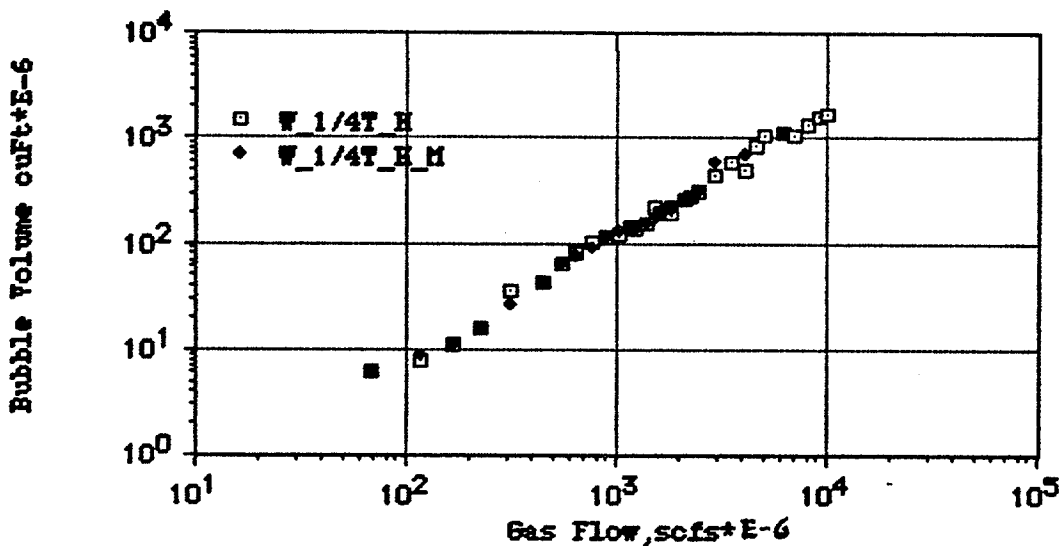


Figure 5.6 Comparison of Bubble Volumes Obtained by Injecting Nitrogen Gas and Methane Gas through a 0.25-in. Tubing

KEY OF THE LEGEND

FLUID	INJECTION DEVICE	INJECTION DEVICE ORIENTATION	GAS
-------	------------------	------------------------------	-----

FLUID:

W = distilled water

INJECTION DEVICE:

1/4T = tubing of 1/4" outer diameter

INJECTION DEVICE ORIENTATION:

H = horizontal

GAS

Default = Nitrogen gas

M = Methane gas

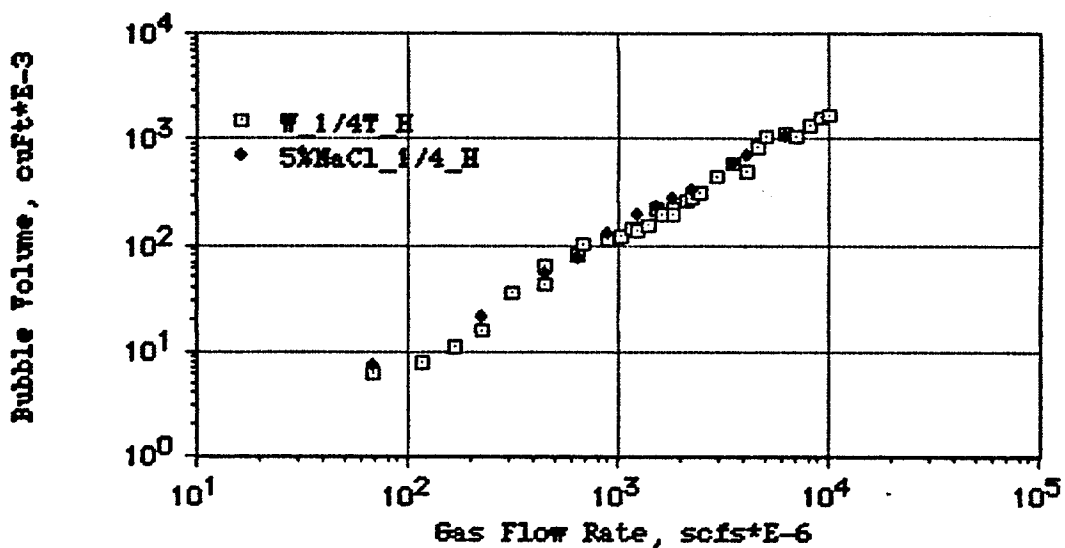


Figure 5.7 Comparison of Bubble Volumes Obtained in Water and in a Solution Containing 5% Sodium Chloride

KEY OF THE LEGEND

FLUID	_	INJECTION DEVICE	_	INJECTION DEVICE ORIENTATION
-------	---	------------------	---	------------------------------

FLUID:

W = distilled water
 5%NaCl = solution of 5% sodium chloride by weight

INJECTION DEVICE:

1/4T = tubing of 1/4" outer diameter

INJECTION DEVICE ORIENTATION:

H = horizontal

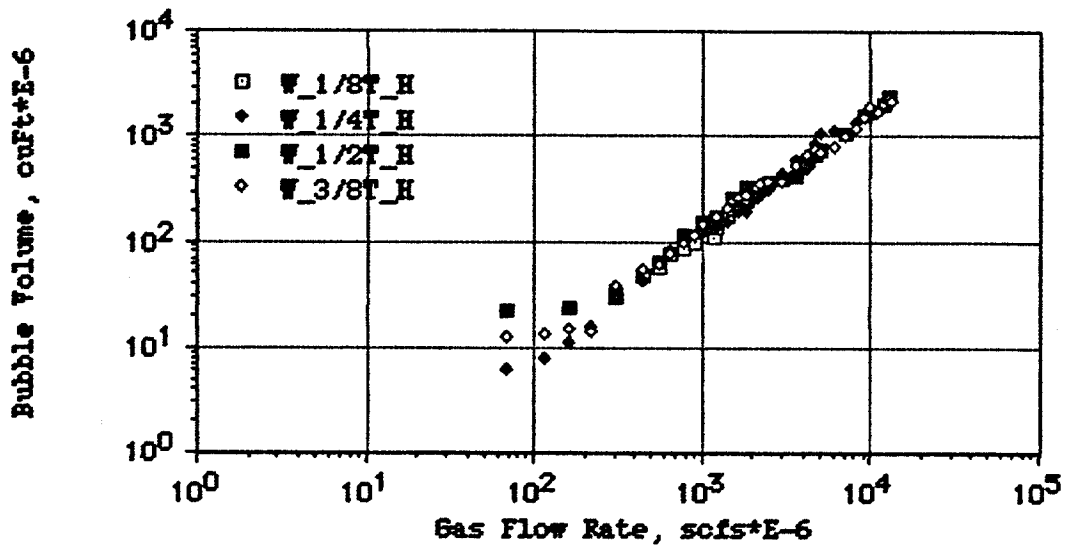


Figure 5.8 Comparison of Bubble Volumes Obtained in Water by Injecting Gas Through Tubings of Various Diameters

KEY OF THE LEGEND

FLUID	_	INJECTION DEVICE	_	INJECTION DEVICE ORIENTATION
-------	---	------------------	---	------------------------------

FLUID:

W = distilled water

INJECTION DEVICE:

1/8T = tubing of 1/8" outer diameter
 1/4T = tubing of 1/4" outer diameter
 3/8T = tubing of 3/8" outer diameter
 1/2T = tubing of 1/2" outer diameter

INJECTION DEVICE ORIENTATION:

H = horizontal

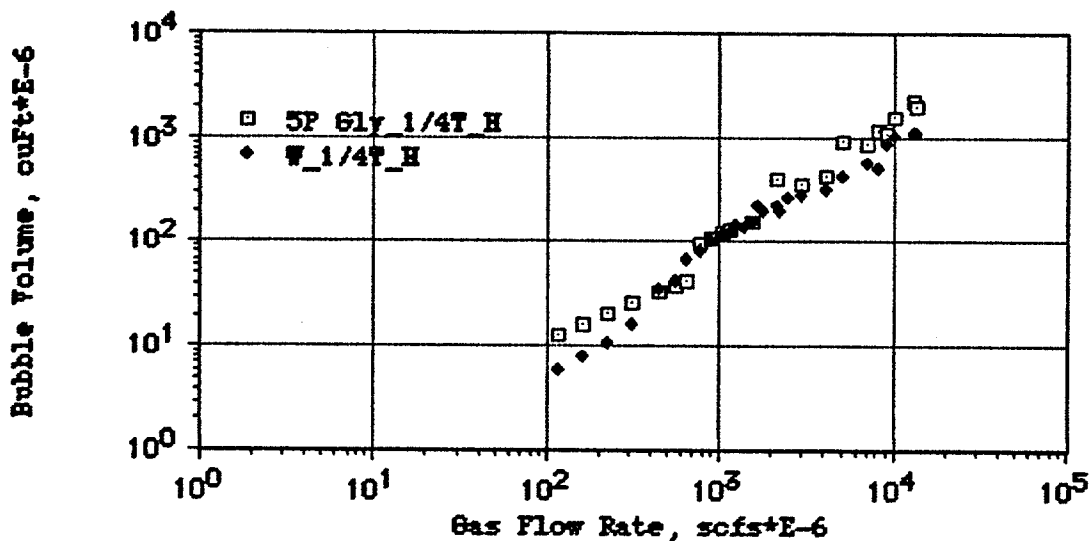


Figure 5.9 Comparison of Bubble Volumes Obtained in Water and in a 5 Poise Glycerine Solution by Injecting Gas through a 0.25-in. Tubing

KEY OF THE LEGEND

FLUID	INJECTION DEVICE	INJECTION DEVICE ORIENTATION
-------	------------------	------------------------------

FLUID:

W = distilled water
 5P Gly = Glycerine solution of 5 poise

INJECTION DEVICE:

1/4T = tubing of 1/4" outer diameter

INJECTION DEVICE ORIENTATION:

H = horizontal

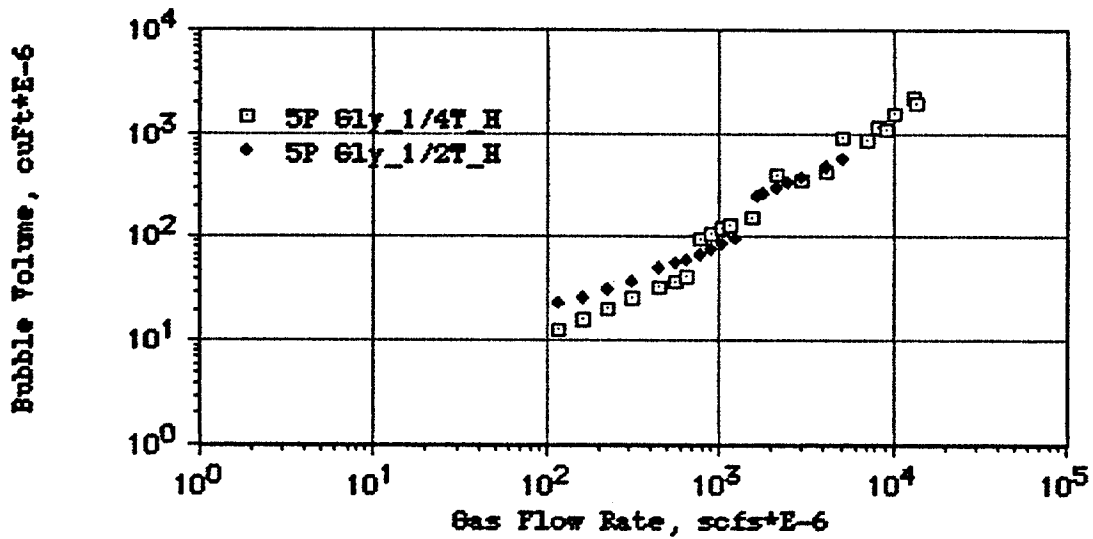


Figure 5.10 Comparison of Bubble Volumes Obtained in Glycerine by Injecting Gas through Tubings of Various Diameters

KEY OF THE LEGEND

FLUID	_	INJECTION DEVICE	_	INJECTION DEVICE ORIENTATION
-------	---	------------------	---	------------------------------

FLUID:

5P Gly = Glycerine solution of 5 poise

INJECTION DEVICE:

1/4T = tubing of 1/4" outer diameter

1/2T = tubing of 1/2" outer diameter

INJECTION DEVICE ORIENTATION:

H = horizontal

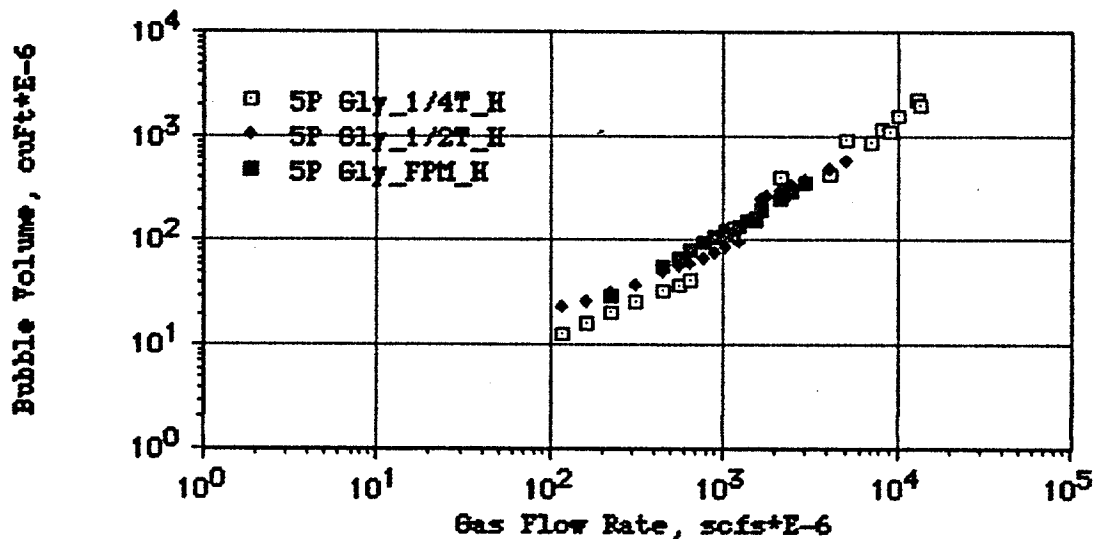


Figure 5.11 Comparison of Bubble Volumes Obtained in Glycerine by Injecting Gas Through a Porous Media, and Through Tubings of Various Diameters

KEY OF THE LEGEND

FLUID	_	INJECTION DEVICE	_	INJECTION DEVICE ORIENTATION
-------	---	------------------	---	------------------------------

FLUID:

5P Gly = Glycerine solution of 5 poise

INJECTION DEVICE:

1/4T = tubing of 1/4" outer diameter

1/2T = tubing of 1/2" outer diameter

FPM = fine porous media

INJECTION DEVICE ORIENTATION:

H = horizontal

this parameter. All the fluids used in this experimental work fall in the range of 70 cp.

Effect of Density

Table 5.2 shows that for the fluids used in this experimental work, an increase of the density of the fluid is associated with a much larger increase in fluid viscosity. The observed bubble size difference under similar conditions were attributed to viscosity effects rather than to density effects. However, from Equation (5.6), it is expected that an increase in density will reduce the size of the bubbles due to the increased buoyancy.

5.3.2 Discussion of Theoretical Data

Except for the porous media that was not considered in our theoretical runs, all the applicable remarks of the previous section were reproduced by the mathematical model. The model predicted: the effect of gas flow rate, the effect of the fluid properties, and the effect of tubing diameter on the formation of bubbles issuing through a tubing immersed in a given fluid. Particular examples on the effects on tubing diameter and viscosity are presented.

Effect of Tubing Diameter

Figure 5.12 shows the generation of bubbles through $\frac{1}{4}$ " and $\frac{1}{2}$ " tubings in water. The $\frac{1}{2}$ " diameter tubing produced larger bubbles than those produced by the $\frac{1}{4}$ " diameter tubing in the region of low gas rates; from 80 to 1000×10^{-6} SCF/s. Beyond of this point the data converges to a single exponential curve. Figure 5.13 exhibits the same trend for tubings in 500 cp glycerine.

Effect of Viscosity

Figure 5.14 displays theoretical points obtained to compare bubble formation in a low viscosity fluid (water) and a high viscosity fluid (500 cp glycerine). Larger bubbles were formed in the fluid with larger viscosity at all flow rates.

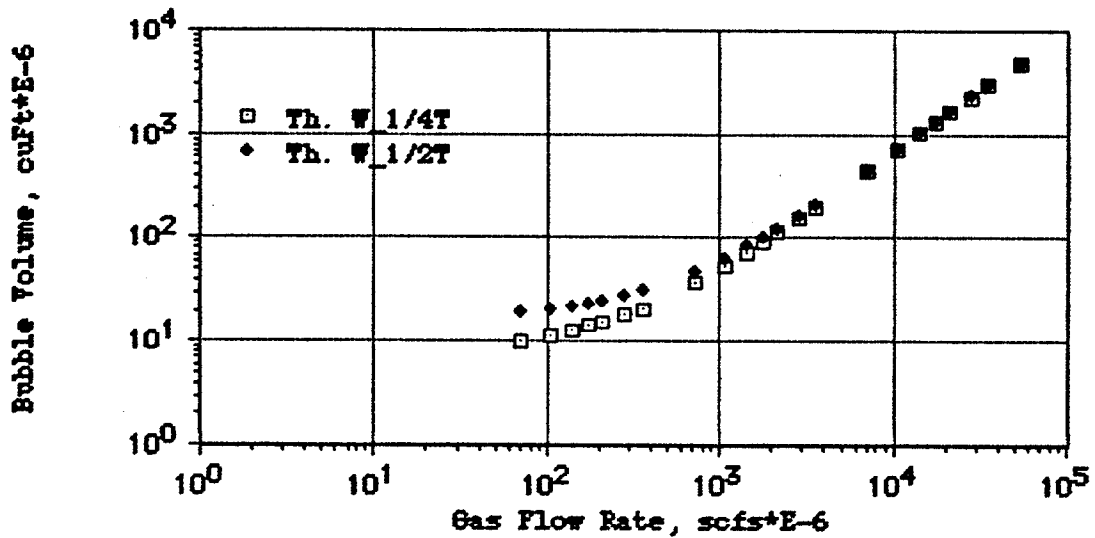


Figure 5.12 Theoretical Bubble Volumes Obtained for 0.25-in. , and 0.50-in. Diameter Tubings in Water

KEY OF THE LEGEND

Prefix. FLUID _ INJECTION DEVICE

Prefix:

Th. = theoretical data

Default = actual data

FLUID:

W = distilled water

INJECTION DEVICE:

1/4T = tubing of 1/4" outer diameter

1/2T = tubing of 1/2" outer diameter

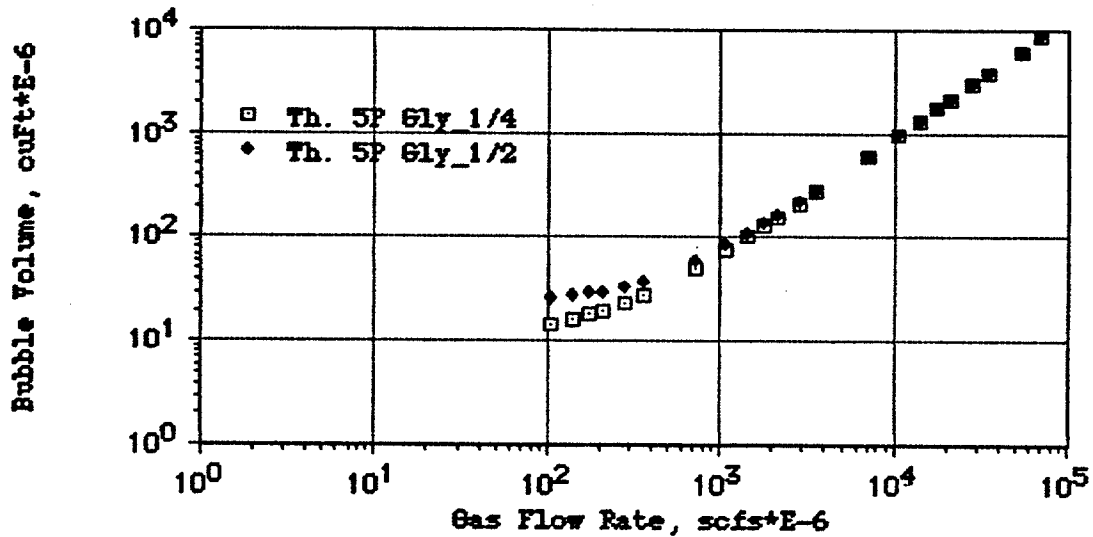


Figure 5.13 Theoretical Bubble Volumes Obtained for 0.25-in. and 0.50-in. Diameter Tubings in a 5 Poise Fluid

KEY OF THE LEGEND

Prefix. FLUID _ INJECTION DEVICE

Prefix:

Th. = theoretical data

Default = actual data

FLUID:

5P Gly = Glycerine solution of 5 poise

INJECTION DEVICE:

1/4T = tubing of 1/4" outer diameter

1/2T = tubing of 1/2" outer diameter

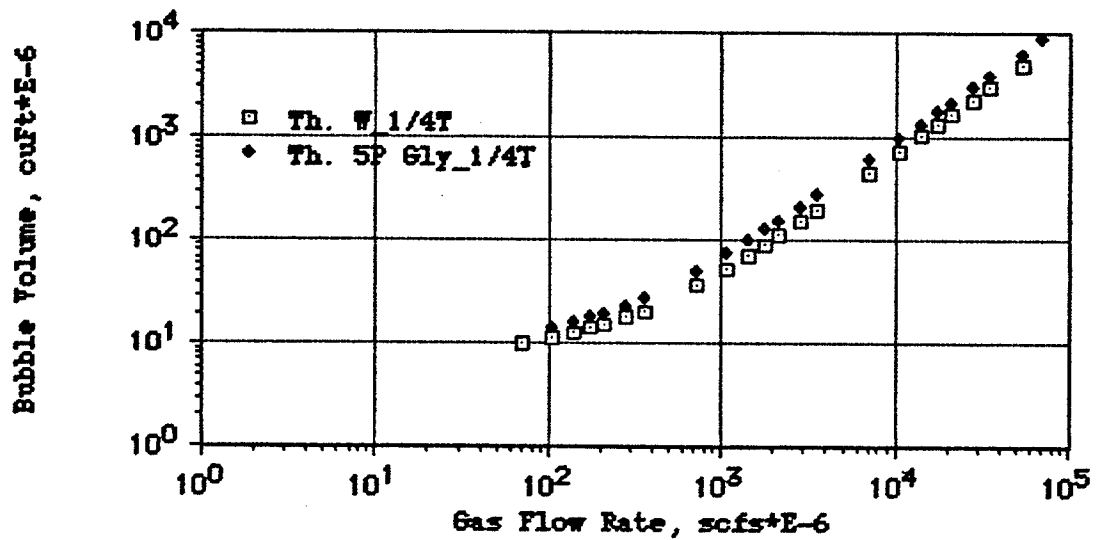


Figure 5.14 Theoretical Bubble Volumes Obtained for Water and for a 5 Poise Fluid . Tubing of 0.25-in. Diameter

KEY OF THE LEGEND

Prefix. FLUID _ INJECTION DEVICE

Prefix:

Th. = theoretical data

Default = actual data

FLUID:

W = distilled water

5P Gly = Glycerine solution of 5 poise

INJECTION DEVICE:

1/4T = tubing of 1/4" outer diameter

5.3.3 Comparison of Actual and Theoretical Bubble Size

Bubble formation through $\frac{1}{4}$ " diameter tubing in water was chosen as representative of the theoretical versus actual trends, in both low viscosity and high viscosity liquids.

Low Viscosity

The model predicts a slightly high bubble volume for low gas flow rates and underpredicts the bubble volume for high flow rates (Fig. 5.15). The drag factor was taken as a constant for all the formed bubble sizes, so that the model does not follow the shift that results in the form drag imprinted in the individual bubble diagram of f_D vs. size of the bubble.

High Viscosity

The fit between the experimental and computed bubble size was better for the high viscosity liquid (Figure 5.16). However, Figure 5.16 shows again the effects of the shift in drag due to changes in the shape of the bubble. Recall (See Chapter IV), that the change of drag is less severe for a high viscosity number of fluid than that of a low viscosity fluid.

Discussion of the Theoretical vs Actual Data

As was mentioned in section 5.3.3, the friction factor was assumed to be a constant for all the gas flow rates for a given fluid. Since the model gave an acceptable description of the bubble formation phenomena, no attempt was made to obtain the drag factor that corresponds to each specific bubble size. To do this will result in three nested iterative procedures needed (1) to calculate the initial volume of the bubble, (2) to calculate the final volume of the bubble, and (3) to determine the drag factor of the bubble.

The bubble volume data also supports the bubble shape map developed in Chapter IV. Clearly, the actual data for water shown in Figure 5.15 changes its trend at around 1.5×10^{-6} ft³ of bubble

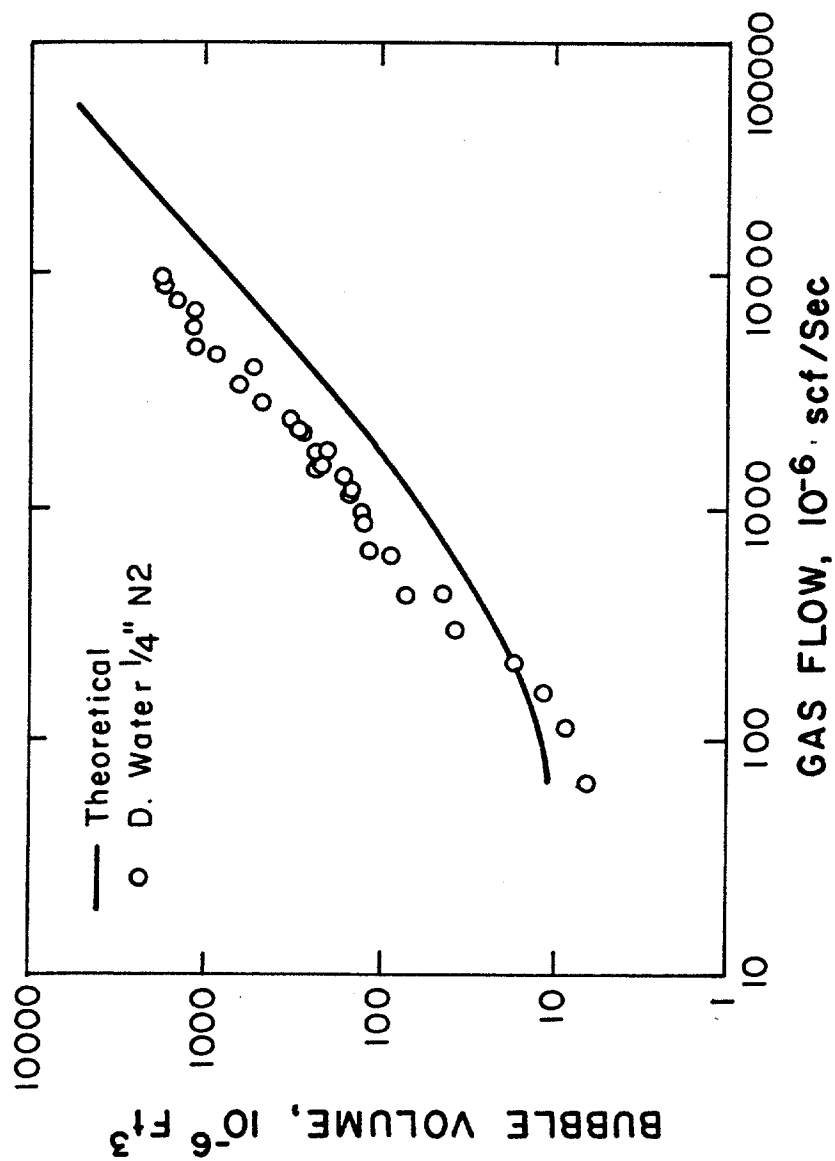


FIGURE 5.15 . COMPARISON OF THEORETICAL VS. ACTUAL BUBBLE VOLUMES FORMED IN WATER BY INJECTING N₂ GAS THROUGH A 0.25--IN DIAMETER TUBING

volume. This bubble has a Reynolds number of around 1100 which is in the neighborhood of the critical Reynolds number for spherical bubbles. At higher gas flow rates the volume of the bubbles start to fall in the oblate spheroid bubble region (as defined by Figure 4.2) and the drag factor increases due to its change of shape. According to Equation (5.6), an increased drag factor results in a larger bubble volume, especially due to the increased influence of the second term of the r.h.s. of Equation (5.6). The steeper slope from gas flow rates from 150×10^{-6} to 800×10^{-6} SCF/s is the result of such increasing drag factor. At 800×10^{-6} SCF/s the measured bubble volume is 85×10^{-6} . This gives a Reynolds number of around 4700 which is in the neighborhood of the critical Reynolds number for oblate spheroid bubbles. At higher gas flow rates the volume of the bubbles start to fall in the lenticular bubble region (Figure 4.2) and the drag factor becomes 2.6, the characteristic drag factor for lenticular bubbles. A less steep slope above of gas flow rates of 800×10^{-6} SCF/s is the result of such a constant drag factor.

A similar explanation applies to the data obtained in the 500 cp fluid (Figure 5.16) except that now the changes discussed above should happen at bubble Reynolds numbers of 4.1 and 25.5. This indicates that the theoretical prediction can be improved to forecast this discussed change in slope.

As a first approximation, it can be assumed that the initial size of individual bubbles is predicted by the analytical model discussed in this chapter. Furthermore, a lower upper bound and a tentative upper lower bound can be set for the predicted initial size. However, a remaining problem to be solved is how the bubble size and concentration will change to reflect the existing fluid environment in the well.

Before pursuing the subject on bubble size, the relationships

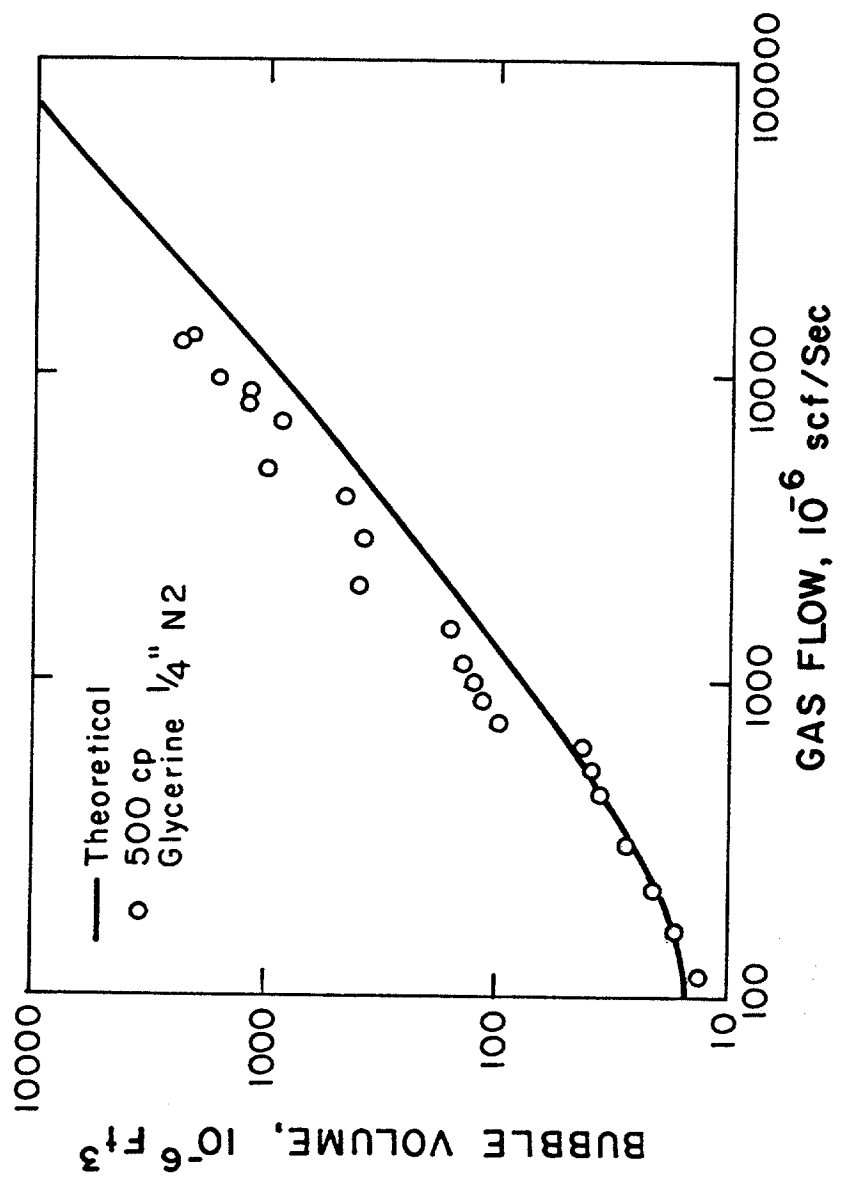


FIGURE 5.16. COMPARISON OF THEORETICAL VS. ACTUAL BUBBLE VOLUMES FORMED IN 500CP GLYCERINE SOLUTION BY INJECTING N₂ GAS THROUGH A 0.25-IN. DIAMETER TUBING

between the parameters ruling the rising of a swarm of bubbles with the parameters ruling the rising of a representative bubble of the swarm, will be presented in the following chapter. Also, an overview of the conventional solution for the pressure losses in two phase flow through vertical pipes will be presented.

CHAPTER VI

ON THE VELOCITY OF A SWARM OF BUBBLES

A correlation and a model were developed to predict the shape and size of an individual bubble. Once that the shape and size of a bubble are known, it is possible to find the rising velocity of the bubble. It is required to predict the rising velocity of a swarm of bubbles and this can be accomplished by applying an analysis of forces acting on an individual particle of a swarm of bubbles. Figure 6.1 shows such a bubble in dark color, surrounded by similar bubbles represented by white bubbles. The effective buoyancy force, F_{eB} , and the drag force, F_D , are given by Equations (6.1) and (6.2), respectively. The relationship between gas and liquid concentration is given by Equation (6.3).

Assume that constant flow rates are entering and leaving the control volume shown in Figure 6.1. Mass conservation allows us to write Equation (6.4).

$$F_{eB} = (g / g_c) (\rho_m - \rho_g) (\pi d^3 / 6) \dots \dots \dots (6.1)$$

$$F_D = (1 / g_c) (f_D \rho_l v_R^2 / 2) (\pi d_e^2 / 4) \dots \dots \dots (6.2)$$

$$1 = \alpha + H_l \dots \dots \dots (6.3)$$

$$v_{sm} = v_{sg} + v_{sl} = \alpha v_g + (1 - \alpha) v_l \dots \dots \dots (6.4)$$

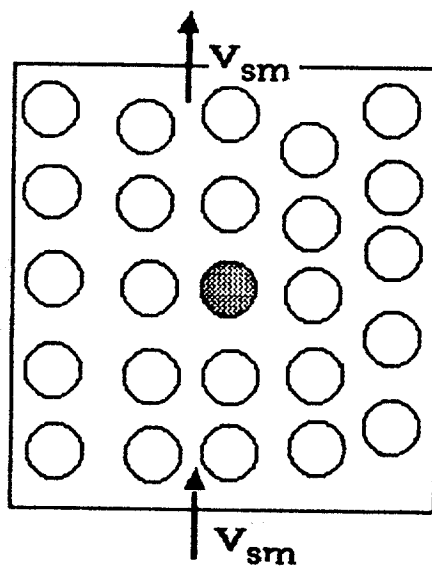


Figure 6.1 Individual Bubble Rising in a Swarm of Bubbles.

where

ρ_m = mixture density

ρ_g = gas density

ρ_l = liquid density

d_e = bubble diameter

f_D = drag factor

v_g = effective gas velocity

v_l = effective liquid velocity

$v_R = v_g - v_l$

v_{sm} = volumetric superficial mixture velocity

μ_m = mixture viscosity

v_{sg} = volumetric superficial gas velocity

v_{sl} = volumetric superficial liquid velocity

α = gas fraction

H_l = liquid fraction

A_D = projected area of the bubble in a plane normal to the
velocity direction

v_D = volume of the bubble

t = time

From Equations (6.1), (6.2), and (6.3) we can write:

$$f_D = [(4/3) (g \Delta\rho d_e) / (v_R^2 \rho_l)] (H_l) \dots \dots \dots (6.5)$$

where

$$\Delta\rho = \rho_l - \rho_g$$

and f_D is a drag that takes into account the effect of the ensemble of bubbles.

For a single bubble in an extended liquid we can write

$$f_{D\infty} = [(4/3) (g \Delta\rho d_e) / (v_\infty^2 \rho_l)] \dots \dots \dots (6.6)$$

Where $f_{D\infty}$ and v_∞ are the drag factor and the relative velocity single sphere rising in an extended liquid. From Equations (6.5) and (6.6) we can write:

$$(f_D / f_{D\infty}) = (v_\infty / v_R)^2 H_1 \dots \dots \dots (6.7)$$

Equation (6.7) allows us to use theoretical relationships⁽²⁷⁾ between f_D and $f_{D\infty}$. In this way we can solve for the relative velocity of an individual particle. Furthermore, the Karman number, N_K for an element of a swarm of bubbles is

$$N_K = \{ 4/3 g (\rho_l \Delta\rho d^3) / \mu_m^2 (1 - \alpha) \}^{0.5} \dots \dots \dots (6.8)$$

Again we can express N_K of the swarm in terms of the Karman number for a single bubble rising in an infinite, $N_{K\infty}$, i.e.

$$N_K / N_{K\infty} = \mu_l / \mu_m (1 - \alpha)^{0.5} \dots \dots \dots (6.9)$$

where μ_m is the apparent mixture viscosity as defined by rheologists

to account for the increased resistance of the mixture to flow due to the presence of the dispersed phase.

6.1 RELATIONSHIPS BETWEEN PARAMETER OF SINGLE BUBBLES AND SWARM OF BUBBLES

Richardson and Zaki⁵⁷ determined the following correlation between the velocity of a single solid sphere in an infinite liquid and the velocity of a swarm of spheres:

$$v_{sl} = v_{\infty} (1 - \alpha)^{n(R)} \dots \dots \dots (6.10)$$

where

v_{sl} = superficial liquid velocity needed to balance the velocity of the swarm of spherical particles

v_{∞} = velocity of a single element of the swarm of particles

$n(R)$ = exponent whose values are in the range of 2.39 to 4.65 approximately for Newton region and Stokes region, respectively

We can write

$$v_R / v_{\infty} = (1 - \alpha)^{n(R)-1} \dots \dots \dots (6.10a)$$

$$f_D / f_{D\infty} = (1 - \alpha)^{-2n(R) + 3} \dots \dots \dots (6.10b)$$

Different functions of voidage for the drag ratio can be obtained from theoretical analysis and correlations. These analyses and correlations have been carried out by various researchers^{44,45}.

Pressure gradient correlations for bubble flow in a vertical pipe have been published in two-phase flow papers. Recall that bubble flow is one of the flow patterns included in the typical correlations that use transitional boundary lines on a so called flow pattern map. These correlations are used to solve the total pressure gradient, and they have been reviewed in Chapter II. An overview of the total pressure gradient is presented in the next section.

6.2 THEORY OF TWO-PHASE BUBBLE FLOW

It is well known that the mechanical energy balance for two-phase flow in vertical pipes can be obtained either from Newton's second law, or from an energy balance¹⁹. In this way, an equation for the total pressure gradient is obtained.

Momentum Balance.— Suppose a homogeneous dispersion of bubbles, as it is shown in Figure 6.1, flows upwards in a vertical pipe. From a force momentum balance, and assuming that the fluids can be treated as incompressible fluids, we can write

$$dp/dz = g / g_c \rho_m + dp_f / dz \dots \dots \dots (6.11)$$

where

ρ_m is the mixture density given by

$$\rho_m = (1 - \alpha) \rho_l + \alpha \rho_g \dots \dots \dots (6.12)$$

Equations (6.11) and (6.12) show that the pressure gradient is composed by the hydrostatic gradient, $(g / g_c) \rho_m$, plus the pressure gradient, dp_f / dz , due to shear stresses on the interphases and on the vertical surface of the control volume.

Energy Balance.- It is well known⁵⁹ that an energy balance will yield the following expression for the total pressure gradient of a single phase flowing in a vertical pipe:

$$dp / dz = (g / g_c) \rho + \rho v dv / g_c + dp_f / dz \dots \dots \dots (6.13)$$

If this equation is applied to Figure 6.1, and it is assumed that the fluid is an incompressible fluid, we can write:

$$dp / dz = (g / g_c) \rho_m + dp_f / dz \dots \dots \dots (6.14)$$

which shows the same dependence of the total pressure gradient on the gas concentration given by the momentum balance analysis.

The energy equations and the momentum equation show that the gradient of pressure is a function of the voidage. To solve any of these equations for the pressure losses information on the voidage is needed.

Prediction of Gas Concentration

Equation (6.14) in the above section, requires the knowledge of the gas concentration and the average bubble size. Traditionally, the solution of the pressure gradient equation for two-phase flow is based on correlations. A review of this subject is presented by Beggs and Brill⁵⁸. The correlations are obtained for steady state conditions as it was discussed in previous chapter. Recall that it is needed to find the length and position of the gas contaminated zone for a series of processes in which there is not gas throughout the well. There are two ways to attack the task of the prediction of length and position of a gas contaminated zone: (a) to develop a correlation based in experimental data, or (b) to develop a theoretical model. The second

alternative was chosen because a correlation on the drag coefficients of bubbles rising in any liquid has already been developed in Chapter IV. A model based on the already known relationships between drag, volume and shape of a single bubble will be developed.

Minimum Energy Dissipation Principle

Equation (6.14) alone does not provide a solution for the problem encountered in well control operations, so the theorem on minimum energy dissipation will be used to develop an equilibrium bubble diameter correlation. Also, the theorem will be applied to obtain the gas concentration associated with a given bubble diameter.

CHAPTER VII

PRINCIPLE OF MINIMUM ENERGY DISSIPATION

H. Lamb⁵⁹ presents a short discussion of general theorems and Helmholtz and Korteweg theorems on the dissipation of energy in the steady state motion of viscous liquids under the action of external forces. In a simplified way the principle of minimum energy dissipation states that in any viscous, incompressible liquid moving under steady state conditions, the velocity distribution is such that a minimum of dissipative energy is obtained.

The principle has been extended and applied successfully to systems with free interfaces such as intensive bubbling in liquids for vessels of small length.

Appendix A gives more detail about this principle. It will be applied recursively to obtain an equation for two-phase flow mixtures encountered during well control operations.

7.1 SPECIFIC ENERGY OF A SWARM OF BUBBLES

An equation of the energy of a swarm of bubbles, as a function of the characteristics of an individual bubble is required to apply the theorem of minimum energy dissipation. The required expression can be obtained by applying a momentum balance on an individual bubble of a swarm of bubbles rising in a vertical vessel. With reference to Figure 6.1, we can write:

Body Forces

$$(g / g_c) (\rho_m - \rho_g) V_b \dots \dots \dots (7.1)$$

Surface Forces

$$(f_D \rho_l v_R A_b) / (2 g_c) \dots \dots \dots (7.2a)$$

$$3/g_c \pi d v_R \mu_m \dots \dots \dots (7.2b)$$

Inertia Forces

$$d/dt (m_{vb} v_R) \dots \dots \dots (7.3)$$

Also, from material balance and from mass conservation, we can write:

$$1 = \alpha + H_l \dots \dots \dots (7.4)$$

$$v_{sm} = v_{sg} + v_{sl} \dots \dots \dots (7.5)$$

where:

ρ_m = mixture density

ρ_g = gas density

ρ_l = liquid density

d_e = bubble diameter

f_D = drag factor

v_g = effective gas velocity

v_l = effective liquid velocity

$v_R = v_g - v_l$

v_{sm} = volumetric superficial mixture velocity

μ_m = mixture viscosity

v_{sg} = volumetric superficial gas velocity

v_{sl} = volumetric superficial liquid velocity

α = gas fraction

H_l = liquid fraction

A_b = projected area of the bubble in a plane normal to the velocity of the bubble

V_b = volume of the bubble

$m_{vb} = V_b (\rho_g + \rho_l / 2)$ = virtual mass of the bubble

t = time

From Newton's second law:

$$\begin{aligned} & (g/g_c) (\rho_m - \rho_g) V_b - (1/2 g_c) f_D \rho_l v_R^2 A_b - (m_{vb} / g_c) \\ & \dot{v}_R = 0 \dots \dots \dots (7.6) \end{aligned}$$

where m_{vb} is the virtual mass of the bubble and the upper dot means derivative w.r. to time.

From Equations (7.4) and (7.5)

$$\rho_m - \rho_g = (1 - \alpha) \Delta p \dots \dots \dots (7.7)$$

where

$$\Delta p = \rho_l - \rho_g$$

Inserting this value in Equation (7.6) and multiplying by the velocity v_R , we obtain the change in bubble energy, E_b , to be:

$$\begin{aligned}
\dot{E}_b &= (g/g_c) \Delta \rho V_b (1 - \alpha) \dot{z} \\
&- (\frac{1}{2} g_c) f_D \rho_l A_b v_R^2 \dot{z} - (\rho_{vb} / g_c) V_b v_R \dot{v}_R \\
&= (g / g_c) \Delta \rho V_b (1 - \alpha) \dot{z} - (\frac{1}{2} g_c) f_D \rho_l A_b v_R^2 \dot{z} \\
&- (\rho_{vb} / 2 g_c) V_b (\dot{v}_R^2) \dots \dots \dots (7.8)
\end{aligned}$$

where

$$\begin{aligned}
(\dot{v}_R^2) &= d/dt (v_R^2) \\
\dot{z} &= v
\end{aligned}$$

Then the total energy of an individual bubble, E_b , in a swarm of bubbles can be written as

$$\begin{aligned}
E_b &= (g/g_c) \Delta \rho V_b (1 - \alpha) z_c - (\frac{1}{2} g_c) f_D \rho_l A_b v_R^2 z_c \\
&- (\rho_{vb} / (2 g_c)) V_b v_R^2 + (4 \sigma_l / g_c) A_b \dots \dots \dots (7.9)
\end{aligned}$$

where σ_l is the interfacial tension.

Now, we can recast this equation as

$$\begin{aligned}
E_b &= (g / g_c) \Delta \rho V_b (1 - \alpha) z_c - (\frac{1}{2} g_c) f_D \rho_l (3/2) (V_b / d_e) v_R^2 z_c \\
&- (\rho_{vb} / (2 g_c)) V_b v_R^2 + (6 \sigma_l / g_c d_e) V_b \dots \dots \dots (7.10)
\end{aligned}$$

where d_e is the diameter of a sphere having the same volume of the bubble.

For a unitary area, dV is numerically equal to dz_c , and we can define the energy dE of this volume as

$$dE = (g / g_c) \Delta \rho \propto (1-\alpha) z_c dz_c - (3/(4 g_c)) f_D \rho_l v_R^2 \propto z_c dz_c / d_e$$

$$- (\rho_{vb} / (2 g_c)) v_R^2 \propto dz_c + (6 / g_c) \sigma_l / d_e \propto dz_c \dots \dots (7.11)$$

The energy per unit of height, E, will be given by

$$E = (g/2 g_c) \Delta \rho (1 - \alpha) d_e + (6/g_c) (\sigma_l/d_e) \propto$$

$$- [\rho_{vb} / (2g_c)] \propto v_R^2 - (3/ 8g_c) f_D \rho_l v_R^2 \dots \dots \dots (7.12)$$

where we approximate the product of the dimension of the cell, z_c , times the fraction of gas with the characteristic dimension of the bubble, d_e .

If we use Equation (6.10b) into the above equation, we get

$$E = (g/ (2 g_c)) \Delta \rho (1 - \alpha) d_e + (6/g_c) (\sigma_l/d_e) \propto$$

$$- [\rho_{vb} / (2g_c)] \propto v_R^2 - (3/ (8g_c)) (f_{D\infty} / (1-\alpha)^m) \rho_l v_R^2 \dots (7.13)$$

where

$$m = 2n - 3$$

and n is defined as in Equation (6.10b)

$$\text{Let } B = (g/2 g_c) \Delta \rho d_e$$

$$T = (6/g_c) (\sigma_l/d_e)$$

$$S = (3/ 8g_c) f_{D\infty} \rho_l$$

$$I = \rho_{vb} / (2g_c)$$

$$\dots \dots \dots (7.14)$$

Equation (7.13) can be written in terms of these coefficients as

$$E = B (1-\alpha) + T \alpha - S (1-\alpha)^{-m} v_R^2 - I \alpha v_R^2 \dots \dots \dots (7.15)$$

This equation shows that E is a function of the fraction of the dispersed phase, α . Recall that v_R , the relative velocity between the dispersed and the continuous phase, depends also on the voidage.

The swarm of bubbles will tend to a concentration or voidage such that the dissipated energy due to the movement of the bubbles is at a minimum. Therefore, the more probable gas concentration will be the one that provides an extreme for the Equation (7.15).

For a cocurrent two-phase flow process, the gas concentration will be given by the root of

$$\begin{aligned} E_\alpha = & (-B + T) \alpha^3 (1-\alpha)^{m+3} + S \{ [2 - (m + 2) \alpha] (1 - \alpha)^2 v_{sg}^2 \\ & - [2 - 2 (m + 2) \alpha] \alpha (1-\alpha) v_{sg} v_{sl} - \alpha^3 (m + 2) v_{sl}^2 \} \\ & + I \{ \alpha (1-\alpha)^{m+3} v_{sg}^2 + 2\alpha^3 (1-\alpha)^{m+1} v_{sg} v_{sl} \\ & - (1+\alpha) \alpha^3 (1-\alpha)^n v_{sl}^2 \} = 0 \dots \dots \dots (7.16) \end{aligned}$$

and for migration of a gas contaminated region, the gas concentration will be given by the root of

$$E_\alpha = (-B + T) \alpha^3 (1-\alpha)^{m+3} - S (m+2) v_g^2 - I v_g^2 (1+\alpha) (1-\alpha)^m = 0 \dots (7.17)$$

where

v_g = the average, absolute gas velocity, or bubble velocity with respect to the tube

$E_{\alpha} = d/d\alpha =$ derivative of E with respect to α

For the circulation of a gas contaminated region, the gas concentration will be given by the root of

$$E_{\alpha} = (-B + T) (1-\alpha)^{m+3} - S (m + 2) (v_g^2 + v_{sl}^2 - 2 v_g v_{sl}) \\ + I (v_g^2 + v_{sl}^2 - 2 v_g v_{sl}) (1 + \alpha) (1 - \alpha)^m = 0 \dots \dots \dots (7.18)$$

which includes the particular case of gas migration.

Equations (7.17) and (7.18) can be solved if the characteristics of the bubbles and the exponent m are known.

7.2 EQUILIBRIUM BUBBLE SIZE

It has been seen in Chapter V, that the size of the bubbles generated throughout orifices depends on inertia, drag forces and surface tension. The equation developed and the experimental work show that large initial sizes of bubbles in the range of 4 cm of equivalent diameter can be obtained. On the other hand, small initial sizes of bubbles in the range of 0.5 cm of equivalent diameter can also be obtained. Smaller sizes are reported elsewhere in the literature.

Most of the work on bubbles has been carried out in vessel with relatively short dimensions. The question that arises is what would be, if any, the equilibrium size of the bubbles if they were far away of the end effects of a vertical vessel.

From experimental work, Hinze⁵¹ proposed a correlation to obtain a critical size for drops dispersed in a liquid under forced convection. For gas in water systems, his formula gives an

equivalent diameter of 0.45 to 0.54 cm. The terminal velocity of such a bubble in water is 24 cm/sec (7.9 ft/sec) approximately. Also, a survey of bubbly flow, shows this to be the diameter-velocity reported more frequently in experimental works with a number of different devices (sinterized plates, spargers) to generate bubbles in water^{53,60,61}. Larger bubbles in cocurrent two-phase flow has been observed to occur at the gas distributor or at some distance above it⁶⁰ and Lockett and Kirkpatrick say: "Little is known about the formation of large bubbles in the main part of the bubble column, well away from the distributor, and indeed it is not clear whether they form there at all." These researchers also found the above mentioned diameter and velocity of the bubbles in water for a countercurrent process.

This ubiquitous equivalent diameter for bubbles in water, has been explained to be the size where the bubble balances the mechanisms of fragmentation and coalescence. Some authors⁵⁶ use the minimum energy dissipation theorem to justify this "equilibrium" bubble diameter, as it follows.

The energy dissipation of a single bubble rising in an infinite liquid is expressed by

$$dE_D = F_D v_\infty \dots \dots \dots (7.19)$$

for a bubble rising at its terminal velocity, v_∞ , under the action of a constant force F_D . The velocity of the bubbles in pure water is given by Equation (2.26), and from this equation we can write

$$d v_\infty / d r_e = (\sigma_1 \rho_1^{-1} r_e^{-2} + g) / \{2 (\sigma_1 \rho_1^{-1} r_e^{-1} + g r_e)^{0.5}\} \dots \dots (7.20)$$

which shows that we will have a minimum velocity at an equivalent bubble radius

$$r_e = \{ (g \rho_l)^{-1} \sigma_l \}^{0.5} \dots \dots \dots (7.21)$$

It follows that the energy dissipation of the bubble will be minimum at an equivalent diameter of 0.54 cm.

Unfortunately, there is not such a minimum in the velocity-diameter diagram for bubbles in liquids with a high liquid viscosity number.

To make some progress, we will assume that a specific equilibrium diameter exists for any gas-liquid system. Moreover, we will assume as a first approximation that a relationship exists between the viscosity number and the Reynolds number of the equilibrium bubble, $(N_{Reb})_e$, following the trend of the transitional lines given in Chapter III. i.e.

$$(N_{Reb})_e = C (N_{Reb})_s \dots \dots \dots (7.22)$$

where $(N_{Reb})_s$ is the transitional boundary line between spherical bubbles and oblate spheroid bubbles as given in Equation (4.8). From the water data, the constant C is calculated to be 1.468 approximately.

This correlation is expected to work at least for bubbles in liquids with liquid viscosity number, raised to the fourth power, less than or equal to 10^{-6} . As we already mentioned, the velocity-diameter relationship of the bubbles do not show a minimum in the deformed bubble region, but rather a transition

between the curve characteristic of bubbles in laminar flow and the curve characteristic of deformed bubbles at high viscosity numbers².

We will extend Equation (7.22) for liquids with any viscosity number. In other words, it is proposed that, even when there is not a minimum in the relationship between velocity and bubble radius for the deformed bubbles for some liquids, physically an equilibrium bubble size exists, and it is approximately the size given by the intersection between bubbles following deformed bubble drag law and bubbles following spherical drag law.

With this correlation, the size of the bubble can be estimated, and the drag associated to these bubbles is obtained with the method proposed in Chapter IV. All of the coefficients of Equations (7.16) - (7.18) can now be evaluated.

7.3 DRAG LAW FOR A SWARM OF BUBBLES

We will adapt the correlation between the velocity of a single sphere and the velocity of a set of spheres found by Richardson and Zaki⁵⁷ and given by Equation (6.10b). They determined the value of n to be a function of the sphere Reynolds number from a series of experiments on fluidization and sedimentation of spherical particles.

This empirical equation has been already applied in bubbly flow by Lockett and Kirkpatrick⁶⁰. They compared various equations with their experimental data on countercurrent bubbly flow. Richardson and Zaki's equation gave a good fit of the data of Lockett and Kirkpatrick. These authors proposed a correction factor to improve the fit of the empirical equation with their data in the region of high voidages (30% to 65%). The deviation of the correlation, in the high voidage range, was attributed to bubble deformation and mobility of the bubble interface.

From the Richardson and Zaki's correlation⁵⁷, the exponent m of Equation (7.16) and (7.18), lies in the range

$$1.78 \leq m \leq 6.3$$

where m is a function of the bubble Reynolds number, N_{Reb} , given by

$$N_{Reb} = d_e v_\infty \rho_l / \mu_l \dots \dots \dots (7.23)$$

where

d_e = equivalent bubble diameter

v_∞ = velocity of a single bubble in an extended liquid

ρ_l = liquid density

μ_l = viscosity of the liquid

The left side limit is for spheres in the Newton flow region, and the right side limit is for spheres in Stokes flow region⁵⁷.

Equations (7.17) and (7.18) can now be evaluated to find the more probable gas concentration for a given process.

7.4 THEORETICAL GAS CONCENTRATION

Gas Injection

Figure 7.1 displays the results obtained with the use of Equation (7.22) and Equation (7.16). The predicted gas concentration for a high viscosity fluid is lower than that predicted for a low viscosity fluid. At high superficial gas velocities, both of them converge to a limiting value, in the range of 35% and 53%, respectively.

The same results as displayed in Figure 7.2 with the axis interchanged. This plot can be directly compared with a typical curve

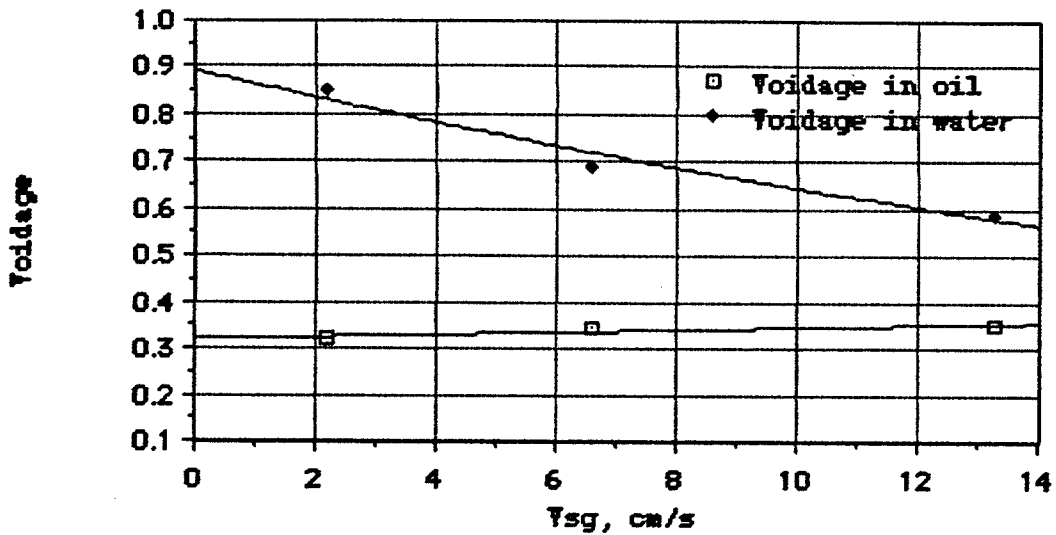


Figure 7.1 Voidage vs Superficial Gas Velocity
as Predicted by Equation 7.16

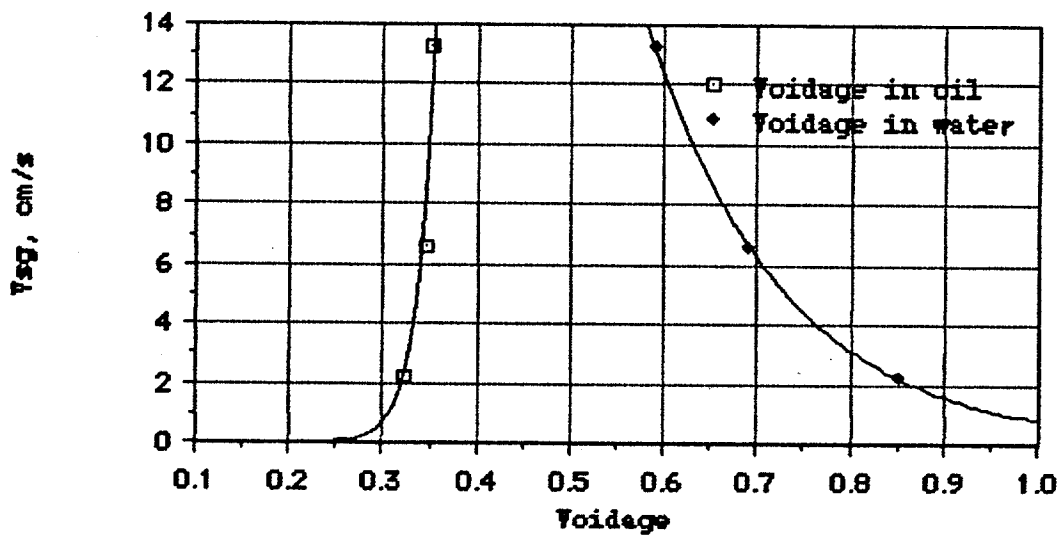


Figure 7.2 Voidage vs Superficial Gas Velocity
as Predicted by Equation 7.16

obtained with Richardson and Zaki's correlation⁵⁷ (Figure 7.3) and with representative vertical two-phase flow experimental data, (Figure 7.4).

The high viscosity fluid follows a path of increasing gas concentration with increasing superficial gas velocity and reaches a maximum value of gas concentration (Figure 7.2). This is in agreement with the low velocity trend seen in Figure 7.4. On the other hand, the low viscosity fluid follows a path of decreasing gas concentration with increasing superficial gas velocity and reaches a maximum value of gas concentration (Figure 7.2). This is in agreement with the path from left to right of Figure 7.3. Exhibit 7.3 shows that continuity can be satisfied in a steady state bubbly process by two points: one at low gas concentration, and another at high gas concentration. This is true until a maximum flow rate is reached, known as the flooding point. In experimental work, this flooding point has not been achieved when a path of increasing gas flow rate is followed (Figure 7.4). The departure from the theoretical concentration curve at points below of the flooding point is attributed to entrance phenomenon in the experimental apparatus.

The previous theoretical results should apply to the process of taking a gas kick under zero liquid circulation. The case of taking a kick under liquid circulation is also covered by Equation (7.18), but the gas concentration predicted converges to the non-slip voidage. Once a gas kick from the formation has entered the well, the process changes to either gas migration or gas circulation.

Gas Migration

Equation (7.18) predicts the theoretical relation between gas concentration and the average upward swarm velocity obtained during the migration of a gas contaminated zone. Figure 7.5 exhibits an example gas concentration-superficial gas velocity relationship

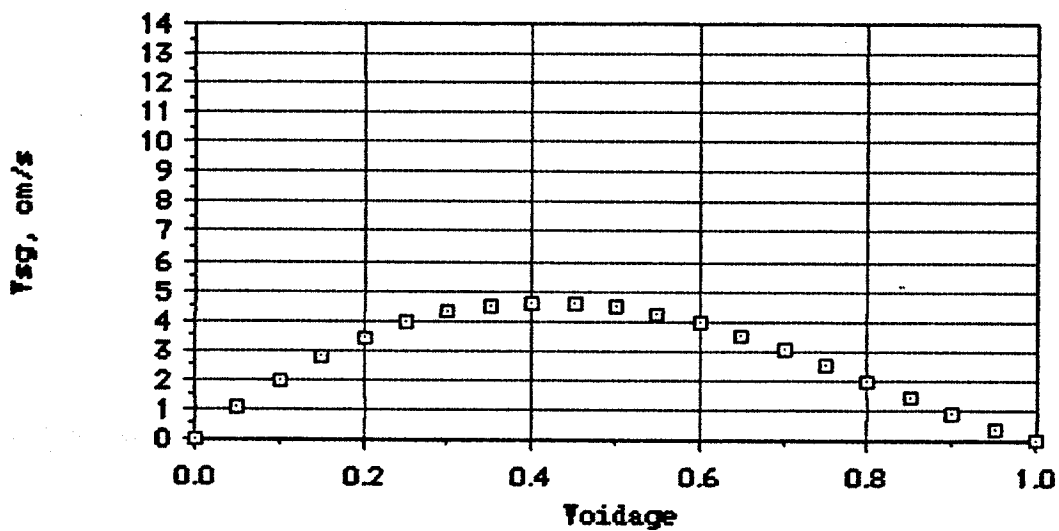


Figure 7.3 Typical Superficial Gas Velocity vs Voidage Obtained with Richardson and Zaki's Correlation. Exponent 2.39

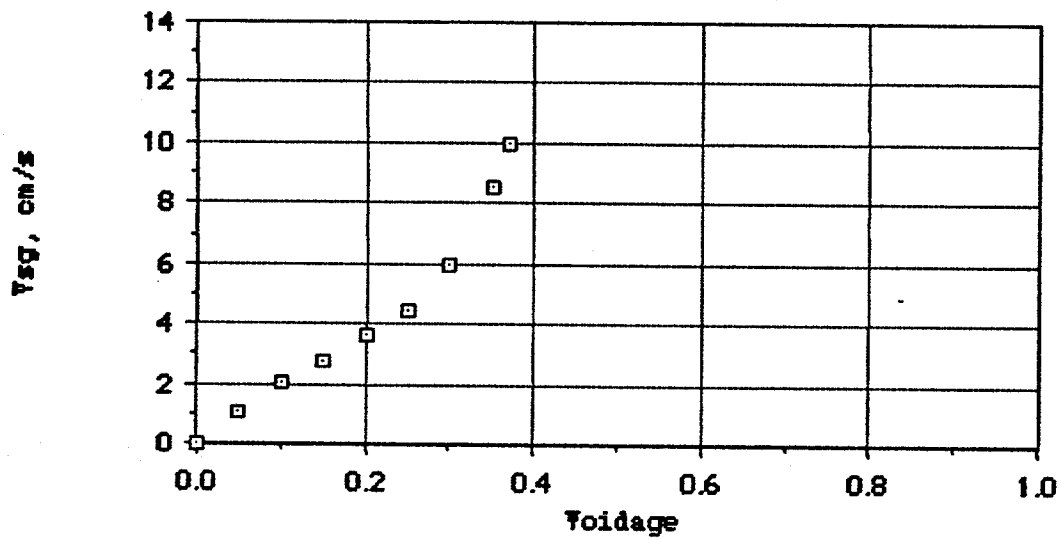


Figure 7.4 Superficial Gas Velocity vs Voidage from Experimental Data.

obtained for a typical well geometry and drilling fluid. Since gas velocity increases with decreasing gas concentration, this will cause dispersion of the leading edge of the gas contaminated region.

Circulation of a Gas Contaminated Zone

The theoretical results for circulation of a gas kick are also represented by Figure 7.5. However, in the actual flow in a pipe, there is going to be a velocity distribution. In laminar and transitional liquid flow regime, the gas will tend to concentrate towards the central core of the flow area. This difference in concentration may, in turn, cause bubble coalescence and liquid circulation. In developed turbulent flow, the theory of Hinze⁵¹ applies and the average size of the bubbles would be known. However, there is not an agreement in regard to the effect of turbulence of the liquid on the bubble swarm velocity.

The previous explanations can be enlightened by the Rietema and Ottengraf⁶² analysis of their experimental results in a liquid-solid system. They feed a cylindrical reservoir with spheres falling at the liquid free surface with a constant frequency. They observed that the spheres remained dispersed homogeneously in the column and therefore, no overall liquid circulation occurred. They explained this phenomenon to be in accordance with the principle of minimum energy dissipation as follows:

Let the energy dissipation rate be expressed by

$$E = g/g_c v_{sd} A Z | \rho_d - \rho_{app} | \dots \dots \dots (7.24)$$

where

v_{sd} = superficial dispersed phase velocity

A = flow area

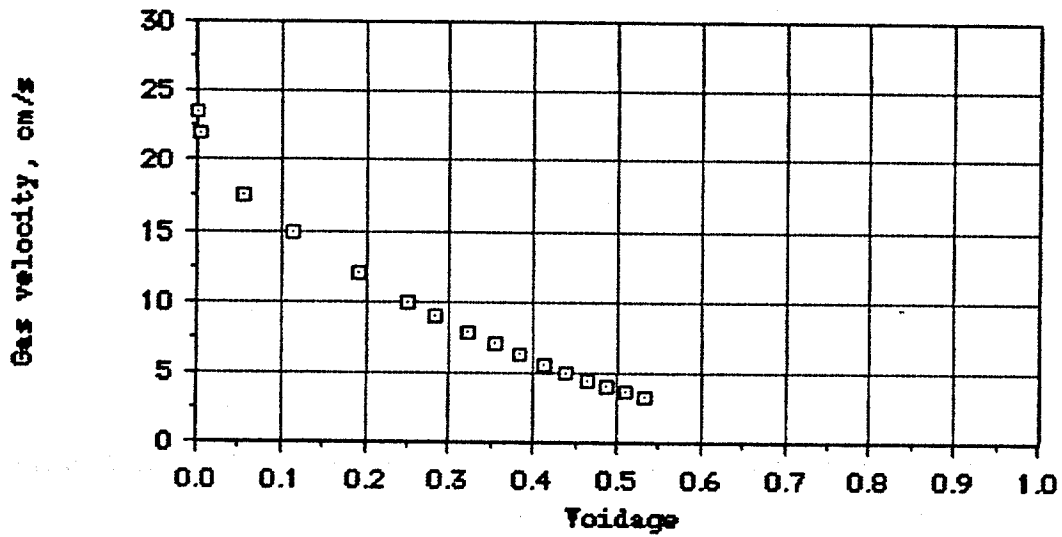


Figure 7.5 Gas Velocity vs Voidage as Predicted by Equation 7.18 for an Unweighted, Water Base Mud

ρ_d = dispersed phase density

ρ_{app} = apparent density of the fluid column

Z = height of the fluid column

For the energy dissipation rate to be minimum, it is required ρ_{app} to tend towards a maximum. This is achieved in a homogeneous dispersion, where no liquid circulation will occur. The same argument should hold for uniformed size bubbles, since this will be a mirror image of this experiment. In this case, the upper part of the pipe is closed. Note, however, that if there is a velocity profile, or if the column departs from the vertical, the former statement ceases to apply. Then there can be liquid circulation.

Restrictions of the Equations

The assumptions done in the development of our equations are that:

- (1) there is an average or representative bubble diameter
- (2) there is a homogeneous dispersion of bubbles
- (3) the empirical drag law for an ensemble of spherical particles⁵⁷ applies for a swarm of bubbles
- (4) the velocity profile corresponds to that of an ideal liquid

The rheology of the fluid is taken into account in calculating the drag of a single bubble, regardless of the bubble Reynolds number, or the flow pattern of the liquid around the bubble. Also, the deformation of the bubble is taken into account into our correlation.

Use of Developed Equations and Correlations

Equations and correlations developed in this work, were programmed as subroutines which in turn were used by a subroutine called ABSVEL. This subroutine requires: mud properties

(density, plastic viscosity, yield point and surface tension), gas density and gas flow rates at operating conditions, liquid flow rate, flow area, pipe Reynolds Number, fanning friction factor associated with the pipe Reynolds Number and a flag to select the output of the subroutine. The output can be either the gas fraction or the gas velocity with respect to the pipe. The ABSVEL subroutine was programmed to be integrated in a numerical model to simulate well control operations

CHAPTER VIII

MODELLING OF WELL CONTROL OPERATIONS

Previous work by Bourgoyne, Holden and Langlinais⁶⁴ has demonstrated the inaccuracies of existing well control simulators. Shown in Figure 8.1 is a typical comparison of computed and observed results for a training exercise conducted using an actual well. Note that the increase in casing pressure due to arrival of gas at the sea floor occurred much earlier than predicted and was less severe than predicted. Such inaccuracies limit the usefulness of these simulators.

The correlations given by Equations (4.7), (4.8), (4.9), (7.22) together with theoretical Equations (7.16), (7.17) and (7.18) were programmed and integrated to create the subroutine ABSVEL, described at the end of the previous chapter. The subroutine was incorporated in a numerical model to simulate well control operations. This numerical model was developed as part of the ongoing research effort towards the development of improved pressure control procedures for floating drilling operations. The ABSVEL subroutine is called by the numerical model for predicting the initial gas concentration and the velocity of the gas contaminated regions. When the gas concentration is calculated by the model, the subroutine returns the velocity of the gas with respect to the pipe, otherwise it returns the gas concentration associated to liquid and gas flow rates.

The numerical model was applied to simulate three experimental runs performed in the LSU-Goldking No.1 well. Two

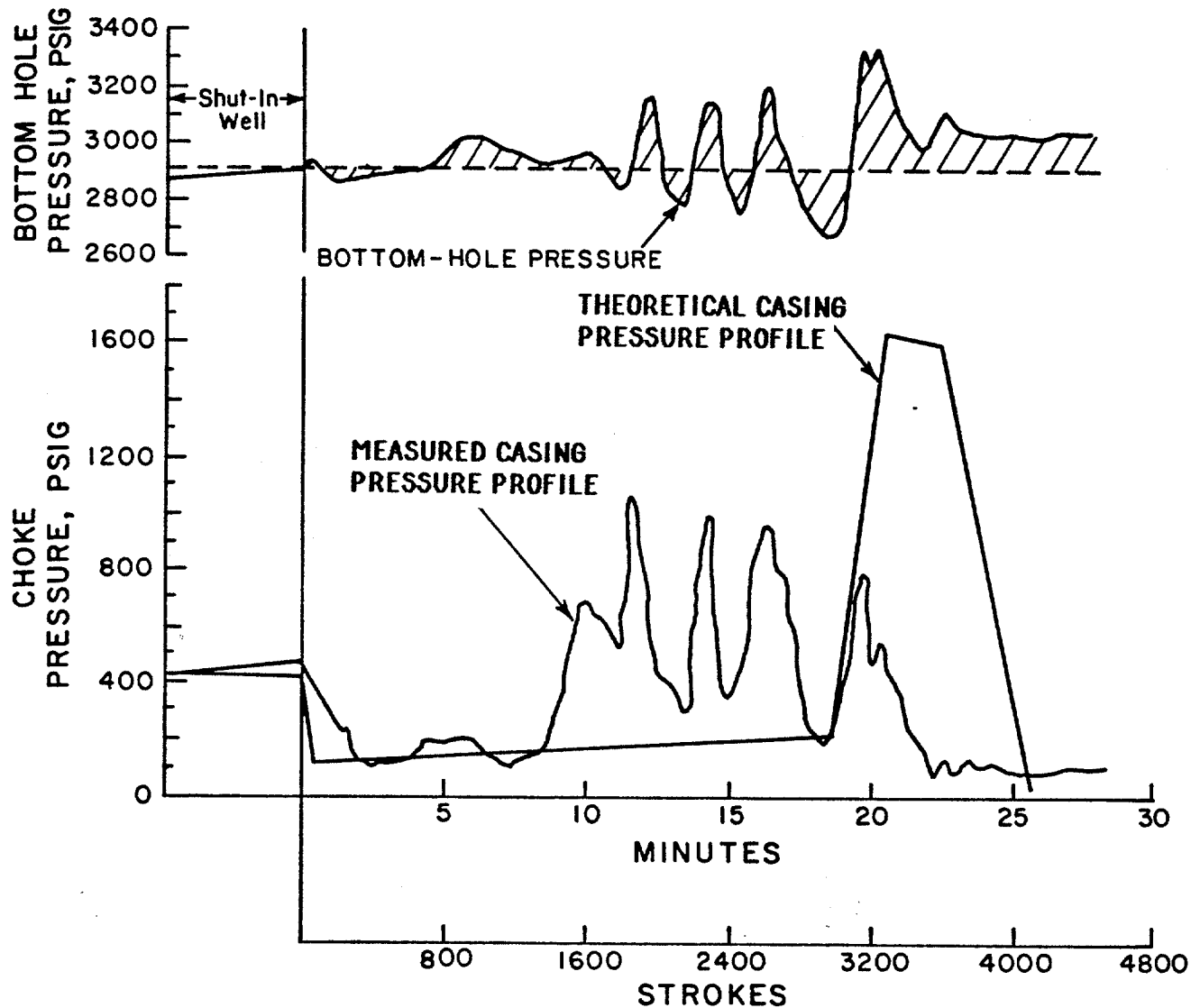


Figure 8.1 Comparison of Theoretical Casing Pressure Profile as Obtained by Existing Well Control Simulators and Measured Casing Pressure Profile for 15 bbl Gas Kick.

(After Bourgoyne, Holden, and Langlinais)

types of experiments were conducted: gas migration in a shut-in well and gas kick circulations.

8.1 EXPERIMENTAL APPARATUS AND PROCEDURE

The LSU-Goldking No.1, (schematic presented in Figure 8.2), is a 6000-ft research well modelling the well-control flow geometry present on a floating drilling vessel operating in 3000 ft of water⁶⁴. The gas kicks were simulated by the injection of nitrogen gas into the bottom of the well. The gas was compressed to a predetermined pressure in the gas storage and compression wells, and then injected through the valve shown as "Formation and productivity simulator control" in Figure 8.2.

The bottom hole pressure was monitored with a pressure sensor located at the bottom of the nitrogen-injection line and transmitted to the surface either through a 0.125-in. capillary tubing strapped to the 1.315 tubing or through the gas injection line once that the formation productivity simulator control valve was closed. This last procedure was used in the gas circulation runs. Mud to circulate the gas kicks was pumped to the bottom of the well through the annular space formed between the gas injection line and the 2-7/8" tubing. The mud circulated towards the surface through the annular space formed between the 2-7/8" tubing and the 7-5/8" casing and then through the 2-3/8" tubings.

The bottom hole pressure, casing (choke line) pressure, drill pipe pressure, strokes per minute of the pump, choke position and gas production rate were recorded for the gas kick circulation exercises. For the gas migration run, the mud gain was also measured. The gas flow rate was determined as follows:

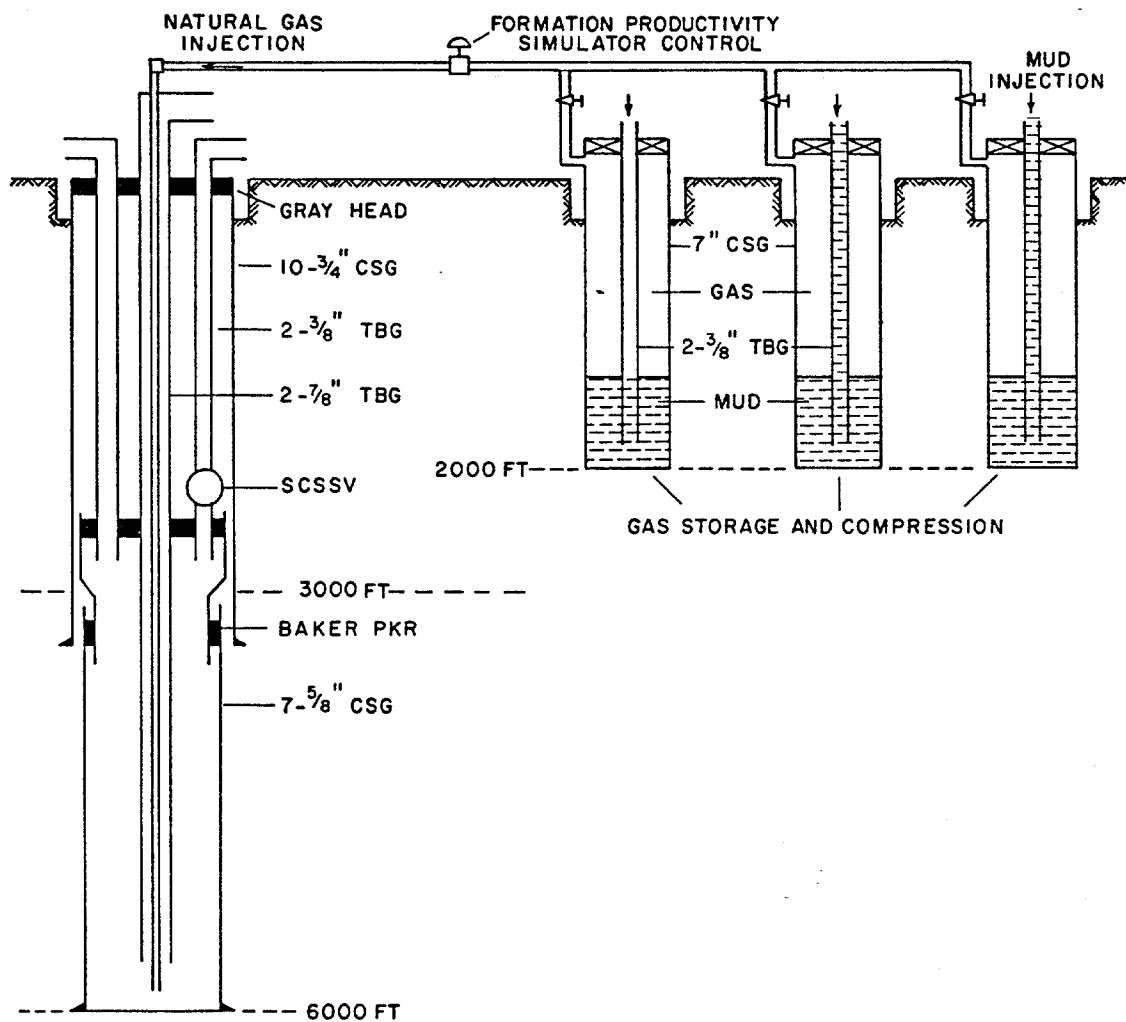


Figure 8.2 Schematic of the LSU-Goldking No.1 Research Well, and the Gas Storage and Compression Wells.

(After Bourgoyne, Holden, and Langlinais)

a) Gas Migration Run.- For this run, the gas flow rate was obtained by recording mud gain against time. The total recorded mud gain was 14.8 bbl in approximately 20 minutes of gas injection.

b) Gas Kick Circulation Runs.- For these runs, the gas injected was determined by material balance. The total gas injected was around 11.18 bbl at bottom hole conditions during an interval of 6 minutes for the first run, and around 11.16 bbl at BHC during an interval of 7.6 minutes for the second run.

The bottom hole pressure monitored in the above described runs was given as data and the casing pressure was calculated with the numerical well control simulator. The input data used in the numerical program is given in Appendix B.

8.2 COMPARISON OF ACTUAL AND THEORETICAL CASING PRESSURE

The theoretical casing pressure as a function of time predicted by the numerical model was plotted together with the actual data for each of the experimental runs. Figures 8.3, 8.4 and 8.5 display the actual data on the theoretical casing pressure.

Figure 8.3 shows that for the gas migration experiment the actual casing pressure is closely predicted by the numerical model. The maximum difference between the actual and the predicted casing pressure is 150 psi. This represents a maximum error of 7%. This plot exhibits five intervals that are characterized by different slopes of the casing pressure versus time plots. These slopes represent (a) gas migration in the annulus until a time of around 60 minutes is reached, (b) gas migration in both the annular space and the choke line until a time of around 150 minutes is reached, (c) gas migration dominated by the choke line until a time of around 220 minutes is reached, (at this point the slope decreases continuously

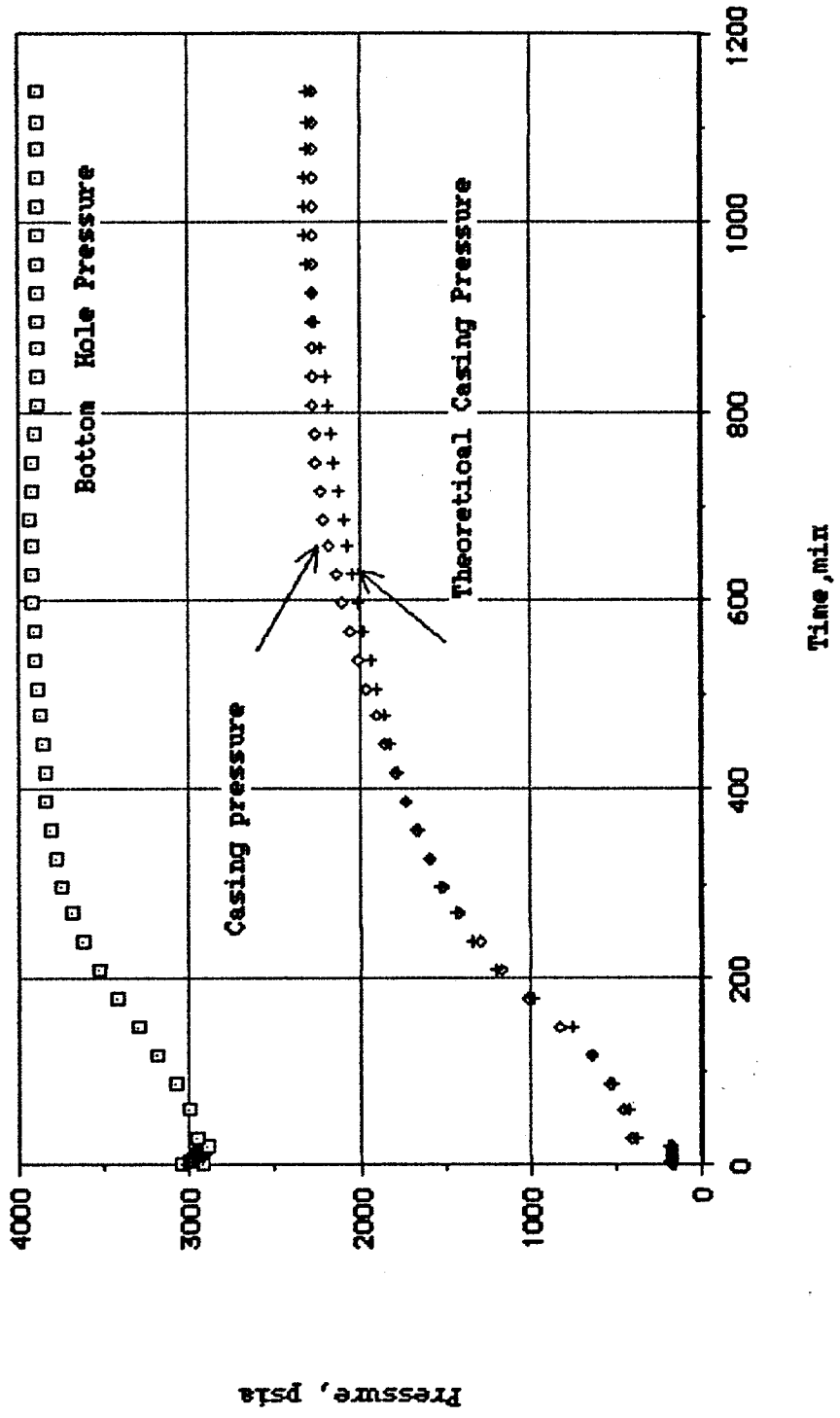


Figure 8.3 Comparison of Theoretical and Measured Casing Pressure Profiles for Gas Migration of a 14.8 bbl Gas kick

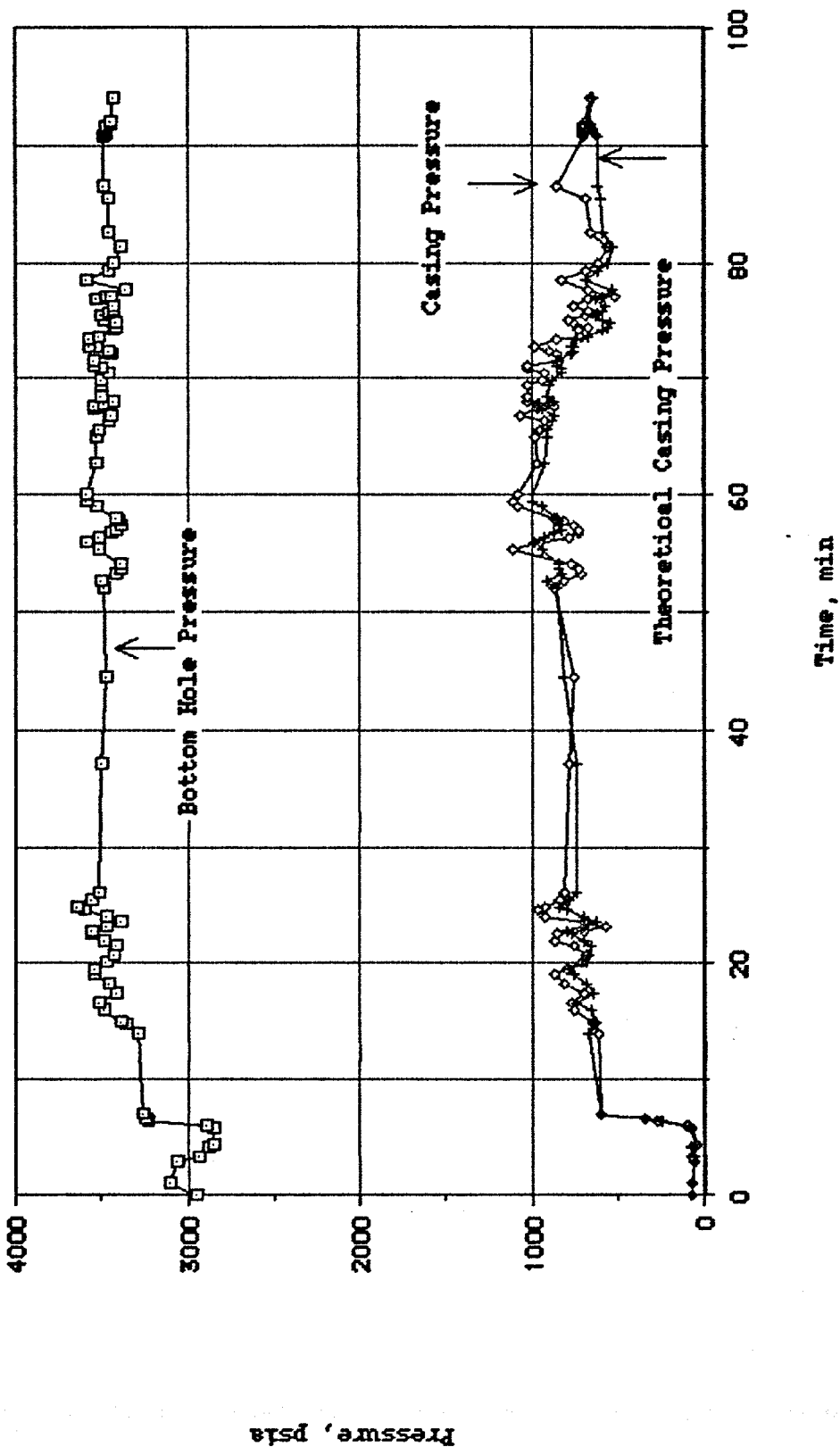


Figure 8.4 Comparison of Theoretical and Measured Casing Pressure Profiles for the 11.18 bbl Gas Kick Circulation Run

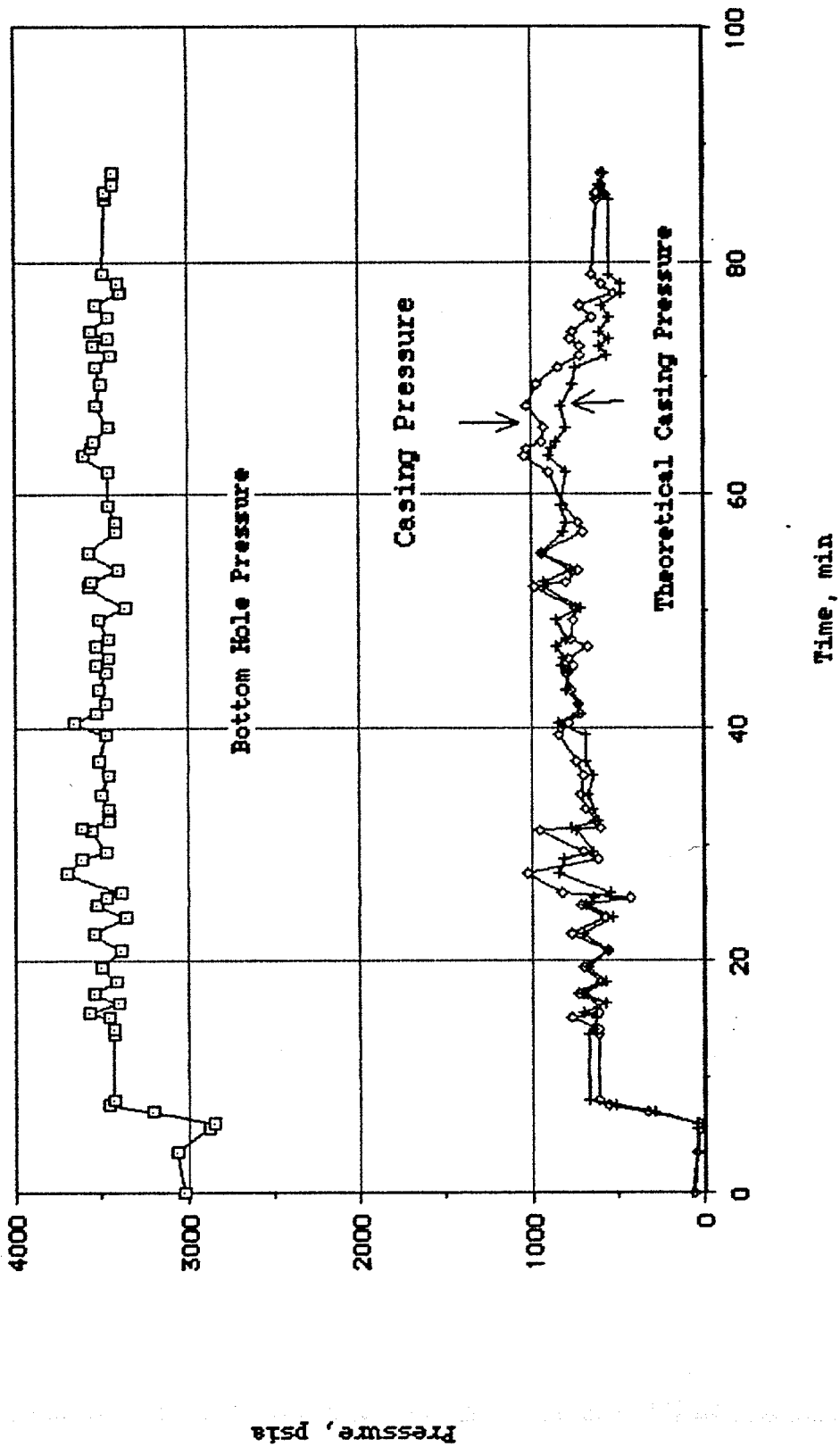


Figure 8.5 Comparison of Theoretical and Measured Casing Pressure

Profiles for the 11.16 bbl Gas Kick Circulation Run

due to the formation of a gas cap), (d) after the gas reaches the surface the formation of a gas cap occurs and the slope decreases continuously until a time of around 800 minutes is reached, (e) the fluids are essentially gravitationally segregated and the slope tends to zero.

Figure 8.4 shows that for the 11.18 bbl gas kick, the actual casing pressure is closely predicted by the numerical model during the first stages, and then the casing pressures are slightly underpredicted. The maximum difference between theoretical and measured casing pressure is 200 psi. This value represents a maximum error of 23%. Due to the adjustments made in the choke size by the operator, there are not clear regions as those described in the migration experiment. However, it appears that gas migration occurred in the annulus until a time of 37 minutes was reached. Then the gas migration took place in both the annulus and the choke line until a time of 47 minutes was obtained. At around this time the gas reaches the surface and the casing pressure peaks and remains relatively constant due to the fact that the choke line is continuously filled by gas contaminated mud. At around 70 minutes the tail of the main body of the gas contaminated mud reaches the seafloor and the casing pressure tends to decrease as a result of the increased weight of the mud displacing the gas contaminated region. In the interval from 80 to 90 minutes apparently more gas invades the choke line which is reflected by an increase in the casing pressure. The numerical model does not show this increase in casing pressure. This was probably caused by an inability to model the expansion of gas from the gas injection string during the well control operation. It was not felt to be important to model this phenomenon since it would not apply in an actual field situation.

Figure 8.5 shows the 11.16 bbl gas kick circulation pressures as a

function of time. This figure exhibits practically the same trends described in the previous paragraph. As in the former case, the model slightly underpredicts the casing pressure during the last stages. In this case the maximum pressure difference between predicted and actual casing pressure is 300 psi which represents a maximum error of 20%.

The numerical model using the ABSVEL subroutine closely predicts the casing pressure which indicates that the model correctly forecasts the migration of gas. This points out that the assumption of an equilibrium bubble size may be indeed true for pipes of large length to area ratio. Moreover, the observed dispersion of the gas contaminated zones are predicted as a consequence of the computed dependence of the gas velocity on the gas concentration. This dependence of the velocity of the gas on the concentration of bubbles is in agreement with both the theoretical and experimental evidence found in the literature review. The prediction of pressure of the circulation of gas kicks also shows an agreement with the actual data which confirms the validity of the approach used to predict the concentration of gas and the velocity of the gas contaminated zones.

CHAPTER IX

SUMMARY AND CONCLUSIONS

Our understanding of the behavior of mixtures of gas and drilling fluid in wellbores have been increased in the following areas:

- (1) Stability of the bubbles.
- (2) Generation of bubbles through orifices.
- (3) Drag factors of oblate spheroid bubbles.
- (4) Equilibrium or critical bubble size of bubbles under dynamic conditions.
- (5) Generation of gas contaminated zones under forced convection.
- (6) Bubble migration in vertical geometries.

The knowledge of the drag factor of deformed bubbles and the stability of the bubbles allow the prediction of the size of bubbles generated in a typical borehole. The knowledge of the equilibrium bubble size under dynamic conditions allow the prediction of the properties and migration rates of gas contaminated zones under forced convection.

The models and the correlations developed in this work can be applied in the solution of other practical problems, in addition to improved modelling of gas kick behavior. For example, the correlations would apply to the development of a model for:

- (a) Design of a subsea gas diverter in deep water off-shore wells
- (b) The prediction of a "gas plume" generated by a blow-out in off-shore wells
- (c) Design of gas risers

As a result of the work presented on this dissertation, the following conclusions are drawn:

1. The condition for which the bubble shape changes from spherical to oblate spheroids, then to lenticular bubbles can be predicted. In addition, the condition under which bubble fragmentation occurs can be estimated.
2. The friction drag of oblate spheroid bubbles can be obtained from the developed correlations.
3. The size of bubbles generated at the discharge of orifices, under constant gas injection, is predicted by the generalized model developed in this work.
4. The mathematical model and the correlations mentioned above were successfully used in the estimation of the size of bubbles generated in the experimental apparatus described in section 5.2.
5. A model for predicting the concentration of a gas contaminated zone was developed.
6. A correlation to estimate the equilibrium bubble size was developed.
7. An improved computer program for modelling of generation, migration and transportation of gas kicks has been developed.

As a result of this study, it is recommended that additional work should be done to:

1. Study the effect of the velocity distribution on the size and distribution of the bubbles.
2. Study the effect of tube inclination on the liquid velocity and on the gas velocity.
3. Design laboratory equipment to study if the formation of large bubbles is possible in regions not influenced by end

effects in vertical gas migration and circulation.

4. Evaluate dispersion coefficients, for bubble migration and bubble transportation.
5. Develop a theoretical model for predicting bubble dispersion in the processes encountered in well control operations.

NOMENCLATURE

English Upper Case

A	Transversal area of a tube, or projected area of a body in a plane normal to its velocity
A_B	Projected area of a bubble in a plane normal to its velocity
C	Constant
D	Internal tube diameter
E	Specific energy of a swarm of bubbles
E_α	Derivative of E with respect to α
E_I	Energy input
E_K	Kinetic energy
E_{IV}	Specific energy input
E_O	Energy dissipation associated to M_O
E_I	Energy dissipation associated to M_I
F_B	Buoyancy force
F_D	Drag force
F_{eB}	Effective buoyancy force, given by Equation (6.1)
$F_f(n)$	Function of the pseudoplasticity index for fluid spheres
$F_{f,sw}(n)$	Function of the pseudoplasticity index for a swarm of fluid sphere
$F_f(N_B)$	Function of the Bingham number
$F_s(n)$	Function of the pseudoplasticity index for rigid spheres

$F_{s,sw}(n)$	Function of the pseudoplasticity index for a swarm of rigid spheres
H_l	Liquid fraction, or liquid hold-up
K	Factor that depends on pipe Reynolds number
K_{lv}	Factor defined by Equation (2.48)
L_B	Parameter defined by Equation (2.2a)
L_{el}	Equivalent liquid length defined by Equation (2.78)
L_s	Gas slug length
L_x	Parameter defined by Equation (2.2c)
L_1, L_2	Parameters defined by Figure 2.5
M_0	Mode of liquid flow in a bubble column in steady state
M_1	Mode of liquid flow such that $M_1 \neq M_0$
N	Dimensional property parameter defined by Equation (2.50)
N_B	Bingham number defined by Equation (2.35)
N_D	Diameter number defined by Equation (2.1b)
N_{ch}	Chamber number
N_{Fr}	Froude number defined by Equation (2.48)
N_{Frm}	Modified Froude number defined in Equation (2.96)
N_{FrN}	Froude number at the discharge of a nozzle
N_{gv}	Gas velocity number defined by Equation (2.1a)
N_K	Karman number of the bubble defined as $f_D^{1/2}$ times N_{Reb}
$N_{K\infty}$	Karman number for a bubble rising in an infinite liquid
N_{lv}	Liquid velocity number defined by Equation (2.1d)
N_{RB}	Bubble Reynolds number defined by Equation (2.65)

N_{Reb}	Bubble Reynolds number
$(N_{Reb})_e$	Equilibrium bubble Reynolds number, Equation (7.22)
$(N_{Reb})_l$	Critical bubble Reynolds number up to which lenticular bubbles can exist, defined by Equation (4.9)
$(N_{Reb})_o$	Critical bubble Reynolds number up to which oblate spheroid bubbles can exist, defined by Equation (4.8)
$(N_{Reb})_s$	Critical bubble Reynolds number up to which spherical bubbles can exist, defined by Equation (4.7)
N_{RN}	Modified Reynolds number at the discharge of a nozzle
N_{RPL}	Generalized bubble Reynolds number
N_{Rzk}	Reynolds number defined by Equation (2.52)
N_s	Slip velocity number defined by Equation (2.76)
N_x	Parameter defined by Equation (2.3b)
N_y	Parameter defined by Equation (2.3d)
N_j	Parameter defined by Equation (2.3c)
N_μ	Fluid viscosity number defined by Equation (2.52)
V	Volume
V_b	Bubble volume
V_{b1}	Bubble volume defined either by Equation (2.86) or by Equation (2.89)
V_{b2}	Bubble volume defined by Equation (2.90)
V_{bf}	Final bubble volume
V_{ch}	Chamber volume
V_1	Volume of the bubble at the end of its first stage of formation

V_2	Volume of the bubble at the end of its second stage of formation
W_b	Bubble weight
Z	Height of fluid column

English Lower Case

b	Number defined in Figure 2.9, Bubble
c	Concentration of transported mass
c_1, c_2	Numbers defined in Figure 2.10
d_b	Bubble diameter
d_{bi}	Initial bubble diameter
d_e	Equivalent spherical diameter of a bubble
d_{ei}	Bubble diameter defined by Equation (2.90)
d_{eav}	Average bubble diameter defined by Equation (2.84)
d_N	Nozzle diameter
d_1, d_2	Diameters defining a concentric, annular area
d_{95g}	Bubble diameter defined by Equation (2.92a)
e	Dissipation per unit of volume
f_D	Drag factor
$f_{D\infty}$	Drag factor for a bubble rising in an extended liquid
f_{Dsw}	Drag factor for a swarm of bubbles rising in an extended liquid
f_M	Moody friction factor
g	Acceleration due to gravity
g_c	Conversion factor between mass and force units

k	Equivalent poise of a Power law fluid
k_{lv}	Coefficient defined by Equation (2.44)
l	Channel length
l_E	Length defined by Equation (2.4)
m	Exponent
m_{vb}	Virtual mass of a bubble
n	Pseudoplasticity index
$n(R)$	Exponent defined in Equations (6.10)
p	Pressure
P_f	Pressure loss
q_g	Volumetric gas flow rate
q_{gN}	Volumetric gas flow rate per nozzle
q_l	Volumetric liquid flow rate
q_N	Volumetric rate per nozzle
r_c	Curvature radius of the leading edge of the bubble
r_e	Equivalent spherical radius of a bubble
r_{el}	Equivalent bubble radius defined by Equation (2.87)
r_t	Internal radius of a pipe
r_l	Equivalent bubble radius defined by Equation (5.19)
v	Average velocity with respect to the tube
v_b	Bubble velocity with respect to the tube
v_{bo}	Bubble velocity in a stagnant liquid
$v_{bo\Box}$	Bubble velocity in a stagnant liquid contained in a vessel of rectangular cross section

$v_{b\infty}$	Velocity of a lenticular plane bubble rising in infinitely wide parallel plates
v_{b+}	Velocity of a bubble with respect to the velocity of the fluid ahead of the bubble
v_g	Average gas velocity with respect to the tube
v_l	Average liquid velocity with respect to the tube
v_{l+}	Average velocity of the liquid ahead of the leading edge of a bubble
v_{gN}	Gas velocity through a nozzle
v_{sd}	Superficial dispersed phase velocity
v_{sg}	Superficial gas velocity
v_{sl}	Superficial liquid velocity
v_{sm}	Superficial velocity of the mixture
v_{sw}	Velocity of a swarm of bubbles in a stagnant liquid
v_{∞}	Velocity of a bubble rising in an extended liquid
v_R	Relative velocity between gas and liquid
v_{zk}	Velocity defined by Equation (2.51)
$v(o)$	Fluid velocity at the axis of a pipe
v_1	Expansion velocity of the bubble during its first stage of formation
v_2	Bubble velocity during its second stage of formation
v_{2e}	Expansion velocity of the bubble during its second stage of formation
t	Time
w	Width of a channel

z	Vertical coordinate
z_c	Thickness of a layer of bubbles, or vertical dimension of a two-phase cell

Greek Upper Case

$\Delta\rho$	Density of the liquid minus density of the gas
Σ	Number defined by Equation (2.53)

Greek Lower case

α	Average volumetric gas fraction
δ	Total dispersion coefficient
θ	Contact angle
μ_l	Liquid viscosity
μ_p	Plastic viscosity
μ_m	Apparent viscosity of the mixture
ρ	Density
ρ_{app}	Apparent or equivalent density of the fluid column
ρ_d	Dispersed phase density
ρ_g	Gas density
ρ_m	Mixture density
ρ_{vb}	Density that corresponds to the virtual mass of the bubble
σ_l	Interfacial tension of the liquid
τ	Shear stress
τ_y	Yield stress of a Bingham fluid

SUBSCRIPTS**English Upper Case**

B	Buoyancy, Bingham
D	Drag
E	Equivalent
Fr	Froude
K	Kinetic, Karman
M	Moody
N	Nozzle
R	Relative
Re	Reynolds
RPL	Reynolds for a power law

English Lower Case

av	Average
b	Bubble
c	Curvature
ch	Chamber
d	Dispersed phase
e	Equivalent, effective, equilibrium
f	Fluid, final
g	Gas
i	Initial
l	Liquid
m	Modified
o	Stagnant media, oblate spheroid
s	Solid, slug, slip, spherical
sw	Swarm
t	Tubing or pipe

v Virtual
 zk As defined by Zukosky

Greek Lower case

α Derivative with respect to gas concentration
 ∞ In infinite media

Other Symbols

1 First
2 Second
 2_e Expansion in second
+ Ahead of the leading edge
 \square Rectangular cross section geometry

Vectors

U Velocity field
 U_0 Velocity field that characterizes M_0
 U_1 Velocity field that characterizes M_1

REFERENCES

1. Harris, L.M.: "Design for Reliability in Deepwater Floating Drilling Operations", The Petroleum Publishing Company. Tulsa, Oklahoma.
2. Haberman, W.L. and Morton, R.K.: "An Experimental Study of Bubbles Moving in Liquids", Trans. ASCE (1954) 227.
3. Levich, V.L., "Physicochemical Hydrodynamics", p. 395 (1962), Prentice-Hall, N. Y.
4. Taitel, Y., Bornea, D., and Dukler, A.E.: "Modeling Flow Pattern Transitions for Upward Gas-Liquid Flow in Vertical Tubes", A.I.Ch.E. Journal (May, 1980) Vol.26, No.3, 345.
5. Davies, R.M. and Taylor, G.: "The Mechanics of Large Bubbles Rising Through Extended Liquids and Through Liquids in Tubes", Proc. Royal Society, London (1950) 200, series A, 375-390.
6. Griffith, P., and Wallis, G.B.: "Two Phase Slug Flow", J. Heat Trans., (1961) 83, 307.
7. Duns, Jr. H., and Ross, N.C.: "Vertical Flow of Gas and Liquid Mixtures from Boreholes", Proc. 6th. World Petroleum Congress. Frankfurt (June, 1963).
8. Sternling, V.C. "Two Phase Flow Theory and Engineering Decisions", A.I.Ch.E. Annual Meeting (December 1965).
9. Wallis, G.B.: "One Dimensional Two-Phase Flow", McGraw Hill (1969).
10. Hewitt, G.F. and Roberts, D.N.: "Studies of Two-Phase Flow Patterns by Simultaneous X-Ray and Flash Photography", UK Atomic Energy Authority Report AERE-M 2159 (1969).
11. Govier, G.W. and Aziz, K.: "The Flow of Complex Mixtures in Pipes", Van Nostrand Reinhold Co. (1972).

12. Gould, T.L. "Vertical Two-Phase Steam-Water Flow in Geothermal Wells", *Journal of Petroleum Technology* (1974) 26, 833.
13. Oshinawa, T. and Charles, M.E. "Vertical Two-Phase Flow Part II", *Can. J. Chem. Eng.* (1974) 56, 438.
14. Chierici, G.L., Clucci, G.M., Schloechl, G.: "Two-Phase Vertical Flow in Oil Wells-Prediction of Pressure Drop", *Journal of Petroleum Technology* (August, 1974) 927.
15. Bailey, R.V., Zmola, P.C., Taylor, F.M., and Planchet, R.J.: "Transport of Gases Through Liquid-Gas Mixtures", Available from P.C. Zmola, Combustion Engineering, Windsor, Conn.
16. Orkiszewski, J. "Predicting Two-Phase Pressure Drops in Vertical Pipes", *Journal of Petroleum Technology* (June, 1967) 829-838.
17. Zukoski, E.E. "Influence of Viscosity, Surface Tension, and Inclination Angle on Motion of Long Bubbles in Closed Tubes", *Fluid Mech.* (1966), Vol. 25, Part 4 pp. 821-837.
18. Rader, D.W., Bourgoyne, Jr. A.T., and Ward, R.H.: "Factors Affecting Bubble-Rise Velocity of Gas Kicks", *Journal of Petroleum Technology* (May, 1975) 571-584.
19. Nicklin, D.J.: "Two-Phase Bubble Flow", *Chemical Engineering Science*, (1962) Vol. 17, 693-702.
20. Hadamard, J.S.: *Compt. Rend. Acad. Sci. Paris*, Vol.152, (1911), 1735-1738.
21. Rybezynski, W.: *Bull. Acad. Sci. Cracovie*, Vol.A, (1911) p.40-46.
22. Peebles, F.N., and Garber, H.J.: "Studies on the Motion of Gas Bubbles in Liquids", *Chemical Engineering Progress* (February, 1953), 88-97.
23. Mendelson, H.D.: "The Prediction of Bubble Terminal Velocities from Wave Theory", *A.I.Ch.E. Journal* (March, 1967), 250-252.
24. Acharya, A., Mashelkar, R.A., Ulbrecht, J.: "Mechanics of Bubble Motion and Deformation in Non-Newtonian Media", *Chemical Engineering Science* (1977) 863-872.

25. Ishii, T., and Pei, C.T.: "Drag Coefficient of Relatively Contaminated Gas Bubbles", *The Canadian Journal of Chemical Engineering*, (February, 1980), Vol. 58, 25-32.
26. Wasserman, M.L. and Slattery, J.C.: "Upper and Lower Bounds on the Drag Coefficient of a Sphere in a Power-Model Fluid", *A.I.Ch.E. Journal*, Vol. 10, No. 3, 383.
27. Acharya, A., Mashelkar, R.A., Ulbrecht, J.: "Bubble Formation in Non-Newtonian Liquids", *Industrial Engineering Chemical Fundamentals* (1978) Vol. 17, No. 3. 230-232.
28. Hirose, T. and Moo-Young, M.: "Bubble Drag and Mass Transfer in Non-Newtonian Fluids: Creeping Flow with Power Law Fluids", *The Canadian Journal of Chemical Engineering*, June, 1969, Vol. 47, 265.
29. Bhavaraju, S.M., Mashelkar, R.A. and Blanchi, H.W.: "Part I. Single Bubble in Power Law and Bingham Fluids", *A.I.Ch.E. Journal* Vol.24 No. 6, 1063-1070.
30. O'Brien, M.P., and Gosline, J.E.: "Velocity of Large Bubbles in Vertical Tubes", *Industrial and Engineering Chemistry* (December 1935) Vol.27, No.12, 1436-1440.
31. Dumitrescu, D.T., "Stromungan einer Luftblase imsenkrechten Rohr", *Z.Agnew Math. Mech.* (June 1943) Vol. 23, 139-149.
32. Laird, A.D.K., and Chisholm, D.: "Pressure and Forces Along Cylindrical Bubbles in a Vertical Tube", *Industrial and Engineering Chemistry* (August, 1956) Vol. 48, No.8, 1361-1364.
33. Uno, S., and Kintner, R.C.: "Effect of Wall Proximity on the Rate of Rise of Single Air Bubbles in a Quiescent Liquid", *A.I.Ch.E. Journal* (September, 1956) Vol.2, No.3, 420-425.
34. Nicklin, D.J., Wilkes, J.O., and Davidson, J.F.: "Two-Phase Flow in Vertical Tubes", *Trans. Inst. Chem. Engrs.* (1962) Vol.40, 61-68.
35. White, E.T., Beardmore, R.H.: "The Velocity of Rise of Single Cylindrical Air Bubbles Through Liquids Contained in Vertical Tubes", *Chem. Eng. Sc.* (1962) Vol.17, 351-361.

36. Brown, R.A.S.: "The Mechanics of Large Gas Bubbles in Tubes", The Canadian Journal of Chemical Eng. (October, 1965) 217-223.
37. Collins, R.: "The Effect of a Containing Cylindrical Boundary on The Velocity of a Large Gas Bubble in a Liquid", J. Fluid Mech. (1967) Vol. 28, Part 1, 97-112.
38. Casariego, V.: "Experimental Study of Two Phase Flow Patterns Occurring in a Well During Pressure Control Operations", M.S. Thesis, Louisiana State University, Baton Rouge, LA April, 1981.
39. Griffith, P.: American Society of Mechanical Engineers, Paper No. 63-HT-20.
40. Collins, R.: "A Simple Model of the Plane Gas Bubble in a Finite Liquid", J. Fluid Mech. (1965) Vol.22, Part 4, 763-771.
41. Maneri and Mendelson: "The Rise Velocity of Bubbles in Tubes and Rectangular Channels as Predicted by Wave Theory", A.I.Ch.E. Journal (March, 1968) Vol.14, No. 2, 295-300.
42. Nickens, H.V.: "The Velocity and Shape of Gas Slugs Rising in Vertical Tubes and Rectangular Slots", Ph.D. Thesis, Louisiana State University, Baton Rouge, LA, 1984.
43. Hagedorn, A. R. and Brown, K. E.: "Experimental Study of Pressure Gradients Occurring During Continuous Two-Phase Flow in Small-Diameter Vertical Conduits", Journal of Petroleum Technology. (April, 1965) 475-484.
44. Marrucci, G.: "Rising Velocity of a Swarm of Spherical Bubbles", Industrial Engineering Chemical Fundamentals (May, 1965), Vol.4, No.2, 224-225.
45. Bhatia, V.K.: "Gas Hold-Up of a Bubble Swarm in Two-Phase Vertical Flow", A.I.Ch.E. Journal (May, 1969) Vol.15, No. 3, 466-469.
46. Bhavaraju, S.M., Mashelkar, R.A. and Blanch, H.W.: "Part II. Swarm of Bubbles in a Power Law Fluid", A.I.Ch.E. Journal Vol.24 No. 6, 1070.

47. Ramakrishnan, S., Kumar, R. and Kuloor, N.R.: "Studies in Bubble Formation I. Bubble Formation Under Constant Flow Conditions", Ch.E.Science, 1969, Vol.24, 731-747.
48. Tsuge, H. and Hibino, S.: "Effect of Column Diameter on the Volume of a Bubble Formed from a Single Submerged Orifice", International Chemical Engineering, January, 1981, Vol.21, No.1, 66.
49. Takahashi, T. and Miyahara, T.: "Volume of a Bubble Formed at a Single, Circular, Submerged Orifice. Effect of the Volume of the Gas Chamber", International Chemical Engineering, April, 1981, Vol.21, No.2, 224-228.
50. Pinczewski, W.V.: "The Formation and Growth of Bubbles at a Submerged Orifice", Chemical Engineering Science, 1981, Vol.36, 405-411.
51. Hinze, J.O.: "Fundamentals of the Hydrodynamic Mechanism of Splitting in Dispersion Processes", A.I.Ch.E. Journal, 1985, Vol.1, 289-295.
52. Sada, E., Yasinishi, A., Kato, S., and Nishioka, M.: "Bubble Formation in Flowing Liquid", The Canadian Journal of Chemical Engineering. (December, 1978) Vol.56, 669-672.
53. Marrucci, G. and Nicodemo, L.: "Coalescence of Gas Bubbles in Aqueous Solutions of Inorganic Electrolytes", Ch.E.Sc. Vol.22, 1257-1265. (1967)
54. Kashnikov, A.M. Candidate's Dissertation, D.I. Mendeleev Moscow Inst. of Chemical Tech., 1965.
55. Azbel, D.: "Two-Phase Flows in Chemical Engineering", Cambridge University Press, (1981).
56. Mathews, J.L. and Bourgoyne, Jr. A.T.: "How to Handle a Gas Kick Moving Up in a Shut-in Well", World Oil, December 1983, 51.
57. Richardson, J.F. and Zaki, W.N.: "Sedimentation and Fluidisation: Part I", Trans. Instn. Chem. Engrs., Vol. 32, 1954.
58. Brill, J.P. and Beggs, H.D.: "Two-Phase Flow in Pipes", University of Tulsa.

59. Lamb, H.: "Hydrodynamics", 6th Edition, Dover Publication, Inc. New York, N.Y. 10014.
60. Lockett, M.J. and Kirkpatrick, R.D.: "Ideal Bubbly Flow and Actual Flow in Bubble Columns", Trans. Instn. Chem. Engrs. Vol.53, 267, 1975.
61. Zuber, N. and Hench, J.: "Steady State and Transient Void Fraction of Bubbling Systems and Their Operating Limits", General Engineering Laboratory Report 62GL100, July 1, 1962.
62. Rietema, K. and Ottengraf, S.P.P.: "Laminar Liquid Circulation and Bubble Street Formation in a Gas-Liquid System", Trans. Instn. Chem. Engrs. Vol.48, T-54-62, 1970.
63. Bennett, C.O. and Myers, J.E: "Momentum, Heat and Mass Transfer", Third Edition. McGraw Hill Chem. Eng. 1982.
64. Bourgoyne, A. T. Jr., Holden, W. R., and Langlinais, J. P.: "Development of Improved Blowout Prevention Procedures for Deep Water Drilling Operation", Final Report. Contract No. 14-08-0001-17225, Mod. 5, USMAS, Reston, VA.
65. Bourgoyne, A. T. Jr., Holden, W. R.: "An Experimental Study of Well Control Procedures for Deepwater Drilling Operations", JPT, July 1985, 1239-1250.
66. Bourgoyne, A. T. Jr., Hise, B. R., Holden, W. R., and Sullins, R. S.: "Well Control Procedures for Deepwater Initiation of Well Control Operations", Ocean Resources Engineering, December 1978.

BIBLIOGRAPHY

- Acharya, A., Mashelkar, R.A., Ulbrecht, J.: "Bubble Formation in Non-Newtonian Liquids", *Industrial Engineering Chemical Fundamentals* (1978) Vol. 17, No. 3. 230-232.
- Acharya, A., Mashelkar, R.A., Ulbrecht, J.: "Mechanics of Bubble Motion and Deformation in Non-Newtonian Media", *Chemical Engineering Science* (1977) 863-872.
- Azbel, D.: "Two-Phase Flows in Chemical Engineering", Cambridge University Press, (1981).
- Bailey, R.V., Zmola, P.C., Taylor, F.M., and Planchet, R.J.: "Transport of Gases Through Liquid-Gas Mixtures", Available from P.C. Zmola, Combustion Engineering, Windsor, Conn.
- Bennett, C.O. and Myers, J.E: "Momentum, Heat and Mass Transfer", Third Edition. McGraw Hill Chem. Eng. 1982.
- Bhatia, V.K.: "Gas Hold-Up of a Bubble Swarm in Two-Phase Vertical Flow", *A.I.Ch.E. Journal* (May, 1969) Vol.15, No. 3, 466-469.
- Bhavaraju, S.M., Mashelkar, R.A. and Blanch, H.W.: "Part I. Single Bubble in Power Law and Bingham Fluids", *A.I.Ch.E. Journal* Vol.24 No. 6, 1063-1070.
- Bhavaraju, S.M., Mashelkar, R.A. and Blanch, H.W.: "Part II. Swarm of Bubbles in a Power Law Fluid", *A.I.Ch.E. Journal* Vol.24 No. 6, 1070.
- Bourgoyne, A. T. Jr., Hise, B. R., Holden, W. R., and Sullins, R. S.: "Well Control Procedures for Deepwater Initiation of Well Control Operations", *Ocean Resources Engineering*, December 1978.
- Bourgoyne, A. T. Jr., Holden, W. R.: "An Experimental Study of Well Control Procedures for Deepwater Drilling Operations", *JPT*, July 1985, 1239-1250.

- Bourgoyne, A. T. Jr., Holden, W. R., and Langlinais, J. P.: "Development of Improved Blowout Prevention Procedures for Deep Water Drilling Operation", Final Report. Contract No. 14-08-0001-17225, Mod. 5, USMAS, Reston, VA.
- Brill, J.P. and Beggs, H.D.: "Two-Phase Flow in Pipes", University of Tulsa.
- Brown, R.A.S.: "The Mechanics of Large Gas Bubbles in Tubes", The Canadian Journal of Chemical Eng. (October, 1965) 217-223.
- Casariogo, V.: "Experimental Study of Two Phase Flow Patterns Occurring in a Well During Pressure Control Operations", M.S. Thesis, Louisiana State University, Baton Rouge, LA April, 1981.
- Chierici, G.L., Ciucci, G.M., Schloechi, G.: "Two-Phase Vertical Flow in Oil Wells-Prediction of Pressure Drop", Journal of Petroleum Technology (August, 1974) 927.
- Collins, R.: "A Simple Model of the Plane Gas Bubble in a Finite Liquid", J. Fluid Mech. (1965) Vol.22, Part 4, 763-771.
- Collins, R.: "The Effect of a Containing Cylindrical Boundary on The Velocity of a Large Gas Bubble in a Liquid", J. Fluid Mech. (1967) Vol. 28, Part 1, 97-112.
- Davies, R.M. and Taylor, G.: "The Mechanics of Large Bubbles Rising Through Extended Liquids and Through Liquids in Tubes", Proc. Royal Society, London (1950) 200, series A, 375-390.
- Dumitrescu, D.T.: "Stromungan einer Luftblase imsenkrechten Rohr". Z. Agnew Math. Mech. (June 1943) Vol. 23, 139-149.
- Duns, Jr. H., and Ross, N.C.: "Vertical Flow of Gas and Liquid Mixtures from Boreholes", Proc. 6th. World Petroleum Congress. Frankfurt (June, 1963).
- Govier, G.W. and Aziz, K.: "The Flow of Complex Mixtures in Pipes", Van Nostrand Reinhold Co. (1972)

- Gould, T.L.: "Vertical Two-Phase Steam-Water Flow in Geothermal Wells", *Journal of Petroleum Technology* (1974) 26, 833.
- Griffith, P.: American Society of Mechanical Engineers, Paper No. 63-HT-20.
- Griffith, P., and Wallis, G.B.: "Two Phase Slug Flow", *J. Heat Trans.*, (1961) 83, 307.
- Haberman, W.L. and Morton, R.K.: "An Experimental Study of Bubbles Moving in Liquids", *Trans. ASCE* (1954) 227.
- Hadamard, J.S.: *Compt. Rend. Acad. Sci. Paris*, Vol.152, (1911), 1735-1738.
- Hagedorn, A. R. and Brown, K. E.: "Experimental Study of Pressure Gradients Occurring During Continuous Two-Phase Flow in Small-Diameter Vertical Conduits", *Journal of Petroleum Technology*. (April, 1965) 475-484.
- Harris, L.M.: "Design for Reliability in Deepwater Floating Drilling Operations", The Petroleum Publishing Company. Tulsa, Oklahoma.
- Hewitt, G.F. and Roberts, D.N.: "Studies of Two-Phase Flow Patterns by Simultaneous X-Ray and Flash Photography", UK Atomic Energy Authority Report AERE-M 2159 (1969).
- Hinze, J.O.: "Fundamentals of the Hydrodynamic Mechanism of Splitting in Dispersion Processes", *A.I.Ch.E. Journal*, 1985, Vol.1, No. 3, 289-295.
- Hirose, T. and Moo-Young, M.: "Bubble Drag and Mass Transfer in Non-Newtonian Fluids: Creeping Flow with Power Law Fluids", *The Canadian Journal of Chemical Engineering*. June, 1969, Vol. 47, 265.
- Ishii, T., and Pei, C.T.: "Drag Coefficient of Relatively Contaminated Gas Bubbles", *The Canadian Journal of Chemical Engineering*, (February, 1980), Vol. 58, 25-32.
- Kashnikov, A.M. Candidate's Dissertation, D.I. Mendeleev Moscow Inst. of Chemical Tech., 1965.

- Laird, A.D.K., and Chisholm, D.: "Pressure and Forces Along Cylindrical Bubbles in a Vertical Tube", *Industrial and Engineering Chemistry* (August, 1956) Vol. 48, No.8, 1361-1364.
- Lamb, H.: "Hydrodynamics" 6th Edition, Dover Publication, Inc. New York, N.Y. 10014.
- Levich, V.L.: "Physicochemical Hydrodynamics", p. 395 (1962), Prentice-Hall, N. Y.
- Lockett, M.J. and Kirkpatrick, R.D.: "Ideal Bubbly Flow and Actual Flow in Bubble Columns", *Trans. Instn. Chem. Engrs.* Vol.53, 267, 1975.
- Maneri and Mendelson: "The Rise Velocity of Bubbles in Tubes and Rectangular Channels as Predicted by Wave Theory", *A.I.Ch.E. Journal* (March, 1968) Vol.14, No. 2, 295-300.
- Marrucci, G.: "Rising Velocity of a Swarm of Spherical Bubbles", *Industrial Engineering Chemical Fundamentals* (May, 1965), Vol.4, No.2, 224-225.
- Marrucci, G. and Nicodemo, L.: "Coalescence of Gas Bubbles in Aqueous Solutions of Inorganic Electrolytes", *Ch.E.Sc.* Vol.22, 1257-1265. (1967).
- Mathews, J.L. and Bourgoyne, Jr. A.T.: "How to Handle a Gas Kick Moving Up in a Shut-in Well", *World Oil*, December 1983, 51.
- Mendelson, H.D.: "The Prediction of Bubble Terminal Velocities from Wave Theory", *A.I.Ch.E. Journal* (March, 1967), 250-252.
- Nickens, H.V.: "The Velocity and Shape of Gas Slugs Rising in Vertical Tubes and Rectangular Slots", Ph.D. Thesis, Louisiana State University, Baton Rouge, LA, 1984.
- Nicklin, D.J.: "Two-Phase Bubble Flow", *Chemical Engineering Science*, (1962) Vol. 17, 693-702.
- Nicklin, D.J., Wilkes, J.O., and Davidson, J.F.: "Two-Phase Flow in Vertical Tubes", *Trans. Inst. Chem. Engrs.* (1962) Vol.40, 61-68.

- O'Brien, M.P., and Gosline, J.E.: "Velocity of Large Bubbles in Vertical Tubes", *Industrial and Engineering Chemistry* (December 1935) Vol.27, No.12, 1436-1440.
- Orkiszewski, J.: "Predicting Two-Phase Pressure Drops in Vertical Pipes", *Journal of Petroleum Technology* (June, 1967) 829-838.
- Oshinawa, T. and Charles, M.E.: "Vertical Two-Phase Flow Part II", *Can. J. Chem. Eng.* (1974) 56, 438.
- Peebles, F.N., and Garber, H.J.: "Studies on the Motion of Gas Bubbles in Liquids", *Chemical Engineering Progress* (February, 1953), 88-97.
- Pinczewski, W.V.: "The Formation and Growth of Bubbles at a Submerged Orifice", *Chemical Engineering Science*, 1981, Vol.36, 405-411.
- Rader, D.W., Bourgoyne, Jr. A.T., and Ward, R.H.: "Factors Affecting Bubble-Rise Velocity of Gas Kicks", *Journal of Petroleum Technology* (May, 1975) 571-584.
- Ramakrishnan, S., Kumar, R. and Kuloor, N.R.: "Studies in Bubble Formation I. Bubble Formation Under Constant Flow Conditions", *Ch.E.Science*, 1969, Vol.24, 731-747.
- Richardson, J.F. and Zaki, W.N.: "Sedimentation and Fluidisation: Part I", *Trans. Instn. Chem. Engrs.*, Vol. 32, 1954.
- Rietema, K. and Ottengraf, S.P.P.: "Laminar Liquid Circulation and Bubble Street Formation in a Gas-Liquid System", *Trans. Instn. Chem. Engrs.* Vol.48, T-54-62, 1970.
- Rybezynski, W.: *Bull. Acad. Sci. Cracovie*, Vol.A, (1911) p.40-46.
- Sada, E., Yasinishi, A., Katoh, S., and Nishioka, M.: "Bubble Formation in Flowing Liquid", *The Canadian Journal of Chemical Engineering*. (December, 1978) Vol.56, 669-672.
- Sternling, V.C.: "Two Phase Flow Theory and Engineering Decisions", *A.I.Ch.E. Annual Meeting* (December 1965).

- Taitel, Y., Bornea, D., and Dukler, A.E.: "Modeling Flow Pattern Transitions for Upward Gas-Liquid Flow in Vertical Tubes", A.I.Ch.E. Journal (May, 1980) Vol.26, No.3, 345.
- Takahashi, T. and Miyahara, T.: "Volume of a Bubble Formed at a Single, Circular, Submerged Orifice. Effect of the Volume of the Gas Chamber", International Chemical Engineering, Vol.21, No. 2, 224-228.
- Tsuge, H. and Hibino, S.: "Effect of Column Diameter on the Volume of a Bubble Formed from a Single Submerged Orifice", International Chemical Engineering, January, 1981, Vol.21, No.1, 66.
- Uno, S., and Kintner, R.C.: "Effect of Wall Proximity on the Rate of Rise of Single Air Bubbles in a Quiescent Liquid", A.I.Ch.E. Journal (September, 1956) Vol.2, No.3, 420-425.
- Wallis, G.B.: "One Dimensional Two-Phase Flow", McGraw Hill (1969).
- Wasserman, M.L. and Slattery, J.C.: "Upper and Lower Bounds on the Drag Coefficient of a Sphere in a Power-Model Fluid", A.I.Ch.E. Journal, Vol. 10, No. 3, 383.
- White, E.T., Beardmore, R.H.: "The Velocity of Rise of Single Cylindrical Air Bubbles Through Liquids Contained in Vertical Tubes", Chem. Eng. Sc. (1962) Vol.17, 351-361.
- Zuber, N. and Hench, J.: "Steady State and Transient Void Fraction of Bubbling Systems and Their Operating Limits", General Engineering Laboratory Report 62GL100, July 1, 1962.
- Zukoski, E.E. "Influence of Viscosity, Surface Tension, and Inclination Angle on Motion of Long Bubbles in Closed Tubes", Fluid Mech. (1966), Vol. 25, Part 4 pp. 821-837.

APPENDIX A

APPENDIX A

RIETEMA AND OTTENGRAF'S PROOF OF THE THEOREM OF MINIMUM ENERGY DISSIPATION FOR CIRCULATING BUBBLE COLUMNS

Let: M_0 be the mode of liquid flow in a bubble column in steady state.

E_0 be the total energy dissipation associated to M_0 .

U_0 liquid velocity field that characterizes the mode M_0 .

M_1 be another mode of liquid flow such that M_1 is different from M_0 .

E_1 be the total energy dissipation associated to M_1 .

U_1 velocity field that characterizes the mode M_1 .

e dissipation per unit of volume.

g gravitational constant.

τ shear stress.

ρ density.

(a). Suppose that $U_D = U_1 - U_0 = 0$ at all fixed boundaries and at the surfaces where the energy is introduced.

(b). Define:

$$\tau_D = \tau_1 - \tau_0$$

$$U_D = U_1 - U_0$$

For E_0 to be the minimum energy dissipation of the system, it has

to be proved that $E_1 > E_0$.

We can write:

$$E_0 = \iiint e_0 dV = - \iiint \{ (\nabla \cdot [\tau_0 - U_0]) - (U_0 \cdot [\nabla \cdot \tau_0]) \} dV \dots \dots \dots (A-1)$$

$$E_1 = \iiint e_1 dV = - \iiint \{ (\nabla \cdot [\tau_1 - U_1]) - (U_1 \cdot [\nabla \cdot \tau_1]) \} dV \dots \dots \dots (A-2)$$

$$E_D = \iiint e_D dV = - \iiint \{ (\nabla \cdot [\tau_D - U_D]) - (U_D \cdot [\nabla \cdot \tau_D]) \} dV \dots \dots \dots (A-3)$$

From (b), we can write:

$$\tau_1 = \tau_D + \tau_0 \text{ and } U_1 = U_D + U_0 \dots \dots \dots (A-4)$$

Taking in account Equations (A-4), the total energy dissipation associated to M_1 is

$$E_1 = - \iiint \{ (\nabla \cdot [(\tau_D + \tau_0) \cdot (U_D + U_0)]) - (U_D + U_0) \cdot [\nabla \cdot (\tau_D + \tau_0)] \} dV \dots \dots \dots (A-5)$$

Recall that dot multiplication is distributive over addition:

$$E_1 = - \iiint \{ (\nabla \cdot [(\tau_D \cdot U_D) + (\tau_0 \cdot U_0) + (\tau_D \cdot U_0) + (\tau_0 \cdot U_D)]) - U_0 \cdot [\nabla \cdot \tau_0] - U_D \cdot [\nabla \cdot \tau_D] \}$$

$$- U_D \cdot [\nabla \cdot \tau_D] - U_D \cdot [\nabla \cdot \tau_0] \} dV \dots \dots \dots (A-6)$$

and from Equations (A-2) and (A-3), we can write

$$E_1 = E_D + E_0 - \iiint \{ (\nabla \cdot [\tau_D \cdot U_0]) - (U_0 \cdot [\nabla \cdot \tau_D]) \} dV \\ - \iiint \{ (\nabla \cdot [\tau_0 \cdot U_D]) - (U_D \cdot [\nabla \cdot \tau_0]) \} dV \dots \dots (A-7)$$

$$E_1 = E_D + E_0 - 2 \iiint \{ (\nabla \cdot [\tau_0 \cdot U_D]) - (U_D \cdot [\nabla \cdot \tau_0]) \} dV \dots (A-8)$$

Now,

$$\iiint \{ (\nabla \cdot [\tau_0 \cdot U_D]) - (U_D \cdot [\nabla \cdot \tau_0]) \} dV \\ = \iiint (\nabla \cdot [\tau_0 \cdot U_D]) dV - \iiint (U_D \cdot [\nabla \cdot \tau_0]) dV \dots (A-9)$$

Applying the Gauss theorem to the left integral of the r.h.s of Equation (A.9) we obtain

$$\iiint (\nabla \cdot [\tau_0 \cdot U_D]) dV = \iint [\tau_0 \cdot U_D] \cdot ds = 0 \dots (A-10)$$

where (a) has been applied, and also the fact that $\tau_0 = 0$ at the free surface and at the free surfaces of the bubbles.

$$E_1 = E_0 + E_D + 2 \iiint (U_D \cdot [\nabla \cdot \tau_0]) dV \dots \dots \dots (A-11)$$

In vector notation, the momentum Equation⁶³ for a steady state process is

$$(\nabla \cdot \tau_o) = - \nabla P + \rho g/g_c \dots \dots \dots (A-12)$$

Equation (A-11) becomes

$$E_1 = E_o + E_D + 2 \left\{ \iint U_D (P - \rho gh / g_c) \cdot ds - \iiint [(P - \rho gh / g_c) \nabla \cdot U_D] dV \right\} \dots \dots \dots (A-13)$$

But $U_D = 0$ perpendicular to the normal of the surface, and for an incompressible fluid $\nabla \cdot U_D = 0$. So, the energy dissipation associated to M_1 is:

$$E_1 = E_o + E_D \dots \dots \dots (A-14)$$

As E_o and E_D are positive:

$$E_1 > E_o$$

Rietema and Ottengraff⁶² also proved the theorem for the case that the inertia term cannot be neglected. Also, they said: "When the column is long enough it might be expected that the volume integral in equation A-7 can be neglected also, and so for columns long enough the principle of minimum energy dissipation would hold under any condition." Note that this is the case encountered in well control operations.

APPENDIX B

```

*-----*
*           N2 GAS MIGRATION IN W.B. MUD; OFFSHORE GEOM. LSU 0.48
*-----*
***** WELL GEOMETRY *****
*           DRILL STRING GEOMETRY (TOP TO BOTTOM)
*
* ENTER NO OF SECTIONS ( UP TO A MAXIMUM OF 10 ):
*-----*
*           1
*-----*
* COMPLETE TABLE BELOW FOR EACH SECTION OF PIPE HAVING A DIFFERENT ID:
* (START AT TOP OF DRILL STRING AND USE A MAXIMUM OF 10 SECTIONS)
*
* INJ STRING OD          DRILL STRING ID          LENGTH
* (INCHES)              (INCHES)                (FEET)
*-----*
*           1.315              2.441                6000.0
*-----*
*
* NO OF CHOKE LINES     CHOKE LINE DIAMETER     VERTICAL LENGTH
* (INTEGER NUMBER)     (INCHES)                (FT)
*-----*
*           1                  1.995                3000.0
*-----*
*
*           ANNULAR GEOMETRY (TOP TO BOTTOM)
*
* ENTER NUMBER OF SECTIONS HAVING DIFFERENT SIZE:
*-----*
*           1
*-----*
*
* COMPLETE THE TABLE BELOW STARTING AT TOP OF ANNULUS AND USING A
* MAXIMUM OF 10 SECTIONS:
*
* PIPE OD              CASING OR HOLE ID          LENGTH
* (INCHES)            (INCHES)                (FEET)
*-----*
*           2.875              6.875                3000.0
*-----*
*
* ENTER TOTAL FLOW AREA OF BIT:
* (SQ INCHES )
*-----*
*           1.914
*-----*

```


***** NUMERICAL MODEL PARAMETERS *****

* NUMBER OF CELLS (50 TO 500) *

* ----- *

300

* ----- *

* ENTER: 1 TO PRINTOUT THE DESCRIBED PARAMETER; 0 OTHERWISE *

* PRESSURE OIL WATER GAS SOLIDS *

* ----- *

* 1 0 0 0 0 *

* ----- *

***** WELL CONTROL OPERATING CONDITIONS *****

* * *

* SPECIFY THE WELL CONTROL OPERATING CONDITIONS BY COMPLETING THE *

* TABLES BELOW: *

* * *

* ENTER LOCATION OF SPECIFIED PRESSURE (1= PUMP, 2=BH, 3= CHOKE) *

* * *

* LOCATION *

* ----- *

2

* ----- *

* * *

* ENTER NUMBER OF TIME PERIODS NEEDED (MAXIMUM OF 120): *

* ----- *

32

* ----- *

* COMPLETE THE TABLE BELOW FOR THE SPECIFIED NUMBER OF TIME PERIODS: *

* * *

* GAS RATE SPECIFIED MUD SNAPSHOT

* TIME PUMP RATE ON BOTTOM PRESSURE 1=OLD DESIRED? *

* (MIN) (BBL/MIN) (BBL/MIN) (PSIA) 2=NEW (1= YES) *

* ----- *

0.0 0.3748 0.7400 2924.0 1 0

1.0 0.3748 0.7400 3047.0 1 0

2.0 0.3748 0.7400 2998.0 1 0

3.0 0.3748 0.7400 3001.0 1 0

4.0 0.3748 0.7400 2994.0 1 0

5.0 0.3748 0.7400 2988.0 1 0

6.0 0.3748 0.7400 2981.0 1 0

7.0 0.3748 0.7400 2975.0 1 0

8.0 0.3748 0.7400 2968.0 1 0

9.0 0.3748 0.7400 2962.0 1 0

10.0 0.3748 0.7400 2955.0 1 0

11.0 0.3748 0.7400 2948.0 1 0

12.0 0.3748 0.7400 2942.0 1 0

13.0 0.3748 0.7400 2935.0 1 0

14.0 0.3748 0.7400 2928.0 1 0

15.0 0.3748 0.7400 2920.0 1 0

16.0 0.3748 0.7400 2914.0 1 0

* * * *	TIME (MIN)	PUMP RATE (BBL/MIN)	GAS RATE ON BOTTOM (BBL/MIN)	SPECIFIED PRESSURE (PSIA)	MUD 1=OLD 2=NEW	SNAPSHOT DESIRED? (1= YES)	* * * *
	-----	-----	-----	-----	-----	-----	
	17.0	0.3748	0.7400	2906.0	1	0	
	18.0	0.3748	0.7380	2900.0	1	0	
	18.1	0.0	0.0	2900.0	1	0	
	27.0	0.0	0.0	2955.0	1	0	
	57.0	0.0	0.0	3010.0	1	0	
	147.0	0.0	0.0	3290.0	1	0	
	237.0	0.0	0.0	3615.0	1	0	
	297.0	0.0	0.0	3745.0	1	0	
	387.0	0.0	0.0	3840.0	1	0	
	477.0	0.0	0.0	3880.0	1	0	
	567.0	0.0	0.0	3910.0	1	0	
	657.0	0.0	0.0	3925.0	1	0	
	747.0	0.0	0.0	3915.0	1	0	
	837.0	0.0	0.0	3895.0	1	0	
	1140.0	0.0	0.0	3875.0	1	0	
* *	-----	-----	-----	-----	-----	-----	* *

***** END OF DATA *****

```

*-----*
      N2 KICK IN W.B. MUD; OFFSH GEOM. LSU 8.95PPG 11BBL 0.5.1
*-----*
***** DRILL STRING GEOMETRY (TOP TO BOTTOM) *****
*
* ENTER NO OF SECTIONS ( UP TO A MAXIMUM OF 10 ):
*-----
      1
*-----
* COMPLETE TABLE BELOW FOR EACH SECTION OF PIPE HAVING A DIFFERENT ID:
* (START AT TOP OF DRILL STRING AND USE A MAXIMUM OF 10 SECTIONS)
*
* INJ STRING OD          DRILL STRING ID          LENGTH
* (INCHES)              (INCHES)                 (FEET)
*-----
      1.315              2.441                    6000.0
*-----
*
* NO OF CHOKE LINES     CHOKE LINE DIAMETER     VERTICAL LENGTH
* (INTEGER NUMBER)     (INCHES)                (FT)
*-----
      2                  1.995                    3000.0
*-----
*
*
* ANNULAR GEOMETRY (TOP TO BOTTOM)
*
* ENTER NUMBER OF SECTIONS HAVING DIFFERENT SIZE:
*-----
      1
*-----
*
* COMPLETE THE TABLE BELOW STARTING AT TOP OF ANNULUS AND USING A
* MAXIMUM OF 10 SECTIONS:
*
* PIPE OD              CASING OR HOLE ID          LENGTH
* (INCHES)            (INCHES)                 (FEET)
*-----
      2.875              6.875                    3000.0
*-----
*
*
* ENTER TOTAL FLOW AREA OF BIT:
* (SQ INCHES )
*-----
      1.914
*-----

```


***** NUMERICAL MODEL PARAMETERS *****

*
* ENTER NUMERICAL MODEL PARAMETERS CONTROLLING ACCURACY, RUN-TIME,
* AND PRINTER PAPER CONSUMPTION BY COMPLETING TABLE BELOW:
*

NUMBER OF CELLS (50 TO 500)

300

* ENTER: 1 TO PRINTOUT THE DESCRIBED PARAMETER; 0 OTHERWISE
*

PRESSURE	OIL	WATER	GAS	SOLIDS
-----	-----	-----	-----	-----
1	0	0	0	0
-----	-----	-----	-----	-----

***** WELL CONTROL OPERATING CONDITIONS *****

* SPECIFY THE WELL CONTROL OPERATING CONDITIONS BY COMPLETING THE
* TABLES BELOW:
*

* ENTER LOCATION OF SPECIFIED PRESSURE (1= PUMP, 2=BH, 3= CHOKE)
*

LOCATION

2

* ENTER NUMBER OF TIME PERIODS NEEDED (MAXIMUM OF 140):
*

100

* COMPLETE THE TABLE BELOW FOR THE SPECIFIED NUMBER OF TIME PERIODS:
*

TIME	PUMP RATE	GAS RATE	SPECIFIED	MUD	SNAPSHOT
(MIN)	(BBL/MIN)	ON BOTTOM	PRESSURE	1=OLD	DESIRED?
-----	-----	(BBL/MIN)	(PSIA)	2=NEW	(1= YES)
-----	-----	-----	-----	-----	-----
0.00	2.166	0.0	2953.0	1	0
1.00	2.166	1.998	3104.0	1	0
2.90	2.1512	2.091	3067.0	1	0
3.20	0.0000	2.103	2941.0	1	0
4.00	0.2244	2.139	2878.0	1	0
4.40	0.0	2.160	2850.0	1	0
5.80	0.0	2.250	2849.0	1	0
6.00	0.0	2.250	2889.0	1	0
6.40	0.0	0.000	3233.0	1	0
6.50	0.0	0.000	3248.0	1	0
7.00	0.0	0.000	3368.0	1	0

* * * *	TIME (MIN)	PUMP RATE (BBL/MIN)	GAS RATE ON BOTTOM (BBL/MIN)	SPECIFIED PRESSURE (PSIA)	MUD 1=OLD 2=NEW	SNAPSHOT DESIRED? (1= YES)	* * * *
	14.00	0.0	0.000	3383.0	1	0	
	14.75	1.6	0.00	3383.0	1	0	
	15.00	1.77	0.00	3393.0	1	0	
	16.00	1.818	0.00	3428.0	1	0	
	16.65	1.897	0.00	3533.0	1	0	
	17.50	1.854	0.00	3423.0	1	0	
	18.30	1.814	0.00	3457.0	1	0	
	19.00	1.854	0.00	3548.0	1	0	
	19.50	1.888	0.00	3548.0	1	0	
	20.10	2.068	0.00	3473.0	1	0	
	20.65	1.888	0.00	3438.0	1	0	
	21.60	1.841	0.00	3423.0	1	0	
	22.00	1.814	0.00	3493.0	1	0	
	22.50	1.881	0.00	3563.0	1	0	
	22.70	1.910	0.00	3563.0	1	0	
	23.10	1.919	0.00	3473.0	1	0	
	23.50	1.842	0.00	3393.0	1	0	
	24.00	1.780	0.00	3478.0	1	0	
	24.60	1.848	0.00	3608.0	1	0	
	24.85	1.863	0.00	3618.0	1	0	
	25.40	1.888	0.00	3558.0	1	0	
	26.00	1.888	0.00	3518.0	1	0	
	37.00	1.888	0.0	3498.0	1	0	
	44.50	1.888	0.0	3473.0	1	1	
	52.00	1.873	0.0	3493.0	1	0	
	52.60	1.910	0.0	3498.0	1	0	
	53.30	1.941	0.0	3418.0	1	0	
	53.70	1.941	0.0	3388.0	1	0	
	54.00	1.926	0.0	3388.0	1	0	
	55.40	1.805	0.0	3518.0	1	1	
	56.00	1.879	0.0	3583.0	1	0	
	56.40	1.913	0.0	3523.0	1	0	
	56.80	1.931	0.0	3448.0	1	0	
	57.00	1.935	0.0	3416.0	1	0	
	57.40	1.925	0.0	3393.0	1	0	
	57.80	1.897	0.0	3398.0	1	0	
	58.00	1.882	0.0	3413.0	1	0	
	59.00	1.795	0.0	3528.0	1	0	
	59.50	1.795	0.0	3593.0	1	0	
	59.95	1.805	0.0	3593.0	1	0	
	62.70	1.842	0.0	3533.0	1	0	
	65.00	1.846	0.0	3528.0	1	0	
	65.60	1.873	0.0	3518.0	1	0	
	66.40	1.888	0.0	3468.0	1	0	
	66.90	1.832	0.0	3448.0	1	0	
	67.4	1.897	0.0	3553.0	1	0	

* * * *	TIME (MIN)	PUMP RATE (BBL/MIN)	GAS RATE ON BOTTOM (BBL/MIN)	SPECIFIED PRESSURE (PSIA)	MUD 1=OLD 2=NEW	SNAPSHOT DESIRED? (1= YES)	* * * *
	67.6	1.888	0.0	3548.0	1	0	
	67.8	1.857	0.0	3483.0	1	0	
	68.00	1.857	0.0	3433.0	1	0	
	68.5	1.857	0.0	3508.0	1	0	
	69.4	1.857	0.0	3508.0	1	0	
	69.9	1.882	0.0	3508.0	1	0	
	70.5	1.847	0.0	3458.0	1	0	
	71.0	1.826	0.0	3508.0	1	0	
	71.2	1.851	0.0	3548.0	1	0	
	71.6	1.894	0.0	3548.0	1	0	
	72.1	1.835	0.0	3448.0	1	0	
	72.3	1.814	0.0	3458.0	1	0	
	72.7	1.804	0.0	3538.0	1	0	
	72.8	1.814	0.0	3573.0	1	0	
	73.3	1.872	0.0	3578.0	1	0	
	73.6	1.903	0.0	3513.0	1	0	
	74.1	1.913	0.0	3433.0	1	0	
	74.3	1.914	0.0	3418.0	1	0	
	74.8	1.857	0.0	3413.0	1	0	
	75.1	1.872	0.0	3488.0	1	1	
	75.5	1.897	0.0	3508.0	1	0	
	75.7	1.909	0.0	3468.0	1	0	
	75.9	1.873	0.0	3438.0	1	0	
	76.2	1.847	0.0	3433.0	1	0	
	76.8	1.919	0.0	3528.0	1	0	
	77.0	1.938	0.0	3473.0	1	0	
	77.15	1.938	0.0	3448.0	1	0	
	77.6	1.786	0.0	3368.0	1	0	
	78.4	1.848	0.0	3583.0	1	0	
	79.3	1.891	0.0	3468.0	1	0	
	80.0	1.910	0.0	3428.0	1	0	
	81.3	1.919	0.0	3393.0	1	0	
	82.5	1.882	0.0	3458.0	1	0	
	85.4	1.866	0.0	3468.0	1	0	
	86.5	1.860	0.0	3488.0	1	1	
	90.8	1.854	0.0	3488.0	1	0	
	91.0	0.464	0.0	3478.0	1	0	
	91.2	0.390	0.0	3478.0	1	0	
	91.3	0.0	0.0	3478.0	1	0	
	91.6	0.0	0.0	3478.0	1	0	
	91.8	0.0	0.0	3450.0	1	0	
	92.0	0.0	0.0	3448.0	1	0	
	94.00	0.0	0.0	3438.0	1	0	

*
*
***** END OF DATA *****
*

```

*-----*
RUN 2  N2 GAS KICK IN W.B. MUD; OFFSH GEOM. LSU 9.15PPG 11 BBL 0.5.1
*-----*
*                DRILL STRING GEOMETRY (TOP TO BOTTOM)                *
*-----*
* ENTER NO OF SECTIONS ( UP TO A MAXIMUM OF 10 ):                      *
*-----*
*                1                *
*-----*
* COMPLETE TABLE BELOW FOR EACH SECTION OF PIPE HAVING A DIFFERENT ID: *
* (START AT TOP OF DRILL STRING AND USE A MAXIMUM OF 10 SECTIONS)      *
*-----*
* INJ STRING OD          DRILL STRING ID          LENGTH          *
* (INCHES)              (INCHES)              (FEET)            *
*-----*
*                1.315                2.441                6000.0            *
*-----*
*-----*
* NO OF CHOKE LINES     CHOKE LINE DIAMETER     VERTICAL LENGTH     *
* (INTEGER NUMBER)     (INCHES)              (FT)                *
*-----*
*                2                1.995                3000.0            *
*-----*
*-----*
*                ANNULAR GEOMETRY (TOP TO BOTTOM)                *
*-----*
* ENTER NUMBER OF SECTIONS HAVING DIFFERENT SIZE:                      *
*-----*
*                1                *
*-----*
* COMPLETE THE TABLE BELOW STARTING AT TOP OF ANNULUS AND USING A     *
* MAXIMUM OF 10 SECTIONS:                                              *
*-----*
* PIPE OD              CASING OR HOLE ID              LENGTH              *
* (INCHES)            (INCHES)              (FEET)              *
*-----*
*                2.875                6.875                3000.0              *
*-----*
*-----*
* ENTER TOTAL FLOW AREA OF BIT:                                         *
* (SQ INCHES )                                                    *
*-----*
*                1.914                *
*-----*

```


***** NUMERICAL MODEL PARAMETERS *****

*
* ENTER NUMERICAL MODEL PARAMETERS CONTROLLING ACCURACY, RUN-TIME,
* AND PRINTER PAPER CONSUMPTION BY COMPLETING TABLE BELOW:
*

NUMBER OF CELLS (50 TO 500)

300

* ENTER: 1 TO PRINTOUT THE DESCRIBED PARAMETER; 0 OTHERWISE
*

PRESSURE	OIL	WATER	GAS	SOLIDS
-----	-----	-----	-----	-----
1	0	0	0	0
-----	-----	-----	-----	-----

***** WELL CONTROL OPERATING CONDITIONS *****

* SPECIFY THE WELL CONTROL OPERATING CONDITIONS BY COMPLETING THE
* TABLES BELOW:
*

* ENTER LOCATION OF SPECIFIED PRESSURE (1= PUMP, 2=BH, 3= CHOKE)
*

LOCATION

2

* ENTER NUMBER OF TIME PERIODS NEEDED (MAXIMUM OF 140):
*

80

* COMPLETE THE TABLE BELOW FOR THE SPECIFIED NUMBER OF TIME PERIODS:
*

TIME	PUMP RATE	GAS RATE	SPECIFIED	MUD	SNAPSHOT
(MIN)	(BBL/MIN)	ON BOTTOM	PRESSURE	1=OLD	DESIRED?
-----	-----	(BBL/MIN)	(PSIA)	2=NEW	(1= YES)
-----	-----	-----	-----	-----	-----
0.00	2.1666	0.7553	3016.0	1	0
1.00	2.1666	1.5106	3121.0	1	0
2.00	2.1666	1.5106	3092.0	1	0
3.00	2.1666	1.5106	3074.0	1	0
3.50	2.1666	1.5106	3062.0	1	0
3.60	0.0	1.5106	2978.0	1	0
3.80	0.0	2.2659	2922.0	1	0
3.90	0.526	1.5106	3148.0	1	0
5.40	0.526	1.5106	2901.0	1	0
5.60	0.0	1.5106	2885.0	1	0
6.00	0.0	1.5106	2850.0	1	0

* * * *	TIME (MIN)	PUMP RATE (BBL/MIN)	GAS RATE ON BOTTOM (BBL/MIN)	SPECIFIED PRESSURE (PSIA)	MUD 1=OLD 2=NEW	SNAPSHOT DESIRED? (1= YES)	* * * *
	-----	-----	-----	-----	-----	-----	
	7.00	0.0	1.5106	3205.0	1	0	
	7.60	0.0	1.5106	3455.0	1	0	
	7.70	0.0	0.0	3495.0	1	0	
	8.00	0.0	0.0	3435.0	1	0	
	13.70	0.0	0.0	3435.0	1	0	
	14.10	1.764	0.0	3435.0	1	0	
	15.10	1.764	0.0	3465.0	1	0	
	15.60	1.888	0.0	3575.0	1	0	
	16.40	1.826	0.0	3405.0	1	0	
	17.30	1.906	0.0	3545.0	1	0	
	18.30	1.888	0.0	3415.0	1	0	
	19.50	1.907	0.0	3505.0	1	0	
	20.90	1.857	0.0	3395.0	1	0	
	22.40	1.857	0.00	3545.0	1	0	
	23.80	1.857	0.00	3365.0	1	0	
	24.80	1.876	0.00	3525.0	1	0	
	25.50	1.919	0.00	3475.0	1	0	
	25.80	1.870	0.00	3390.0	1	0	
	27.40	1.869	0.00	3705.0	1	0	
	28.70	1.931	0.00	3615.0	1	0	
	29.40	1.894	0.00	3480.0	1	0	
	31.10	1.888	0.00	3565.0	1	0	
	31.40	1.925	0.00	3615.0	1	0	
	32.0	1.919	0.0	3465.0	1	0	
	33.00	1.910	0.0	3465.0	1	0	
	34.20	1.897	0.0	3500.0	1	0	
	35.90	1.897	0.0	3460.0	1	0	
	37.00	1.888	0.0	3515.0	1	0	
	39.40	1.826	0.0	3480.0	1	0	
	40.40	1.857	0.0	3665.0	1	0	
	41.10	1.894	0.0	3525.0	1	0	
	42.00	1.894	0.0	3480.0	1	0	
	43.30	1.894	0.0	3520.0	1	0	
	44.70	1.876	0.0	3475.0	1	0	
	45.30	1.909	0.0	3530.0	1	0	
	46.00	1.888	0.0	3465.0	1	0	
	46.90	1.919	0.0	3530.0	1	0	
	47.60	1.910	0.0	3455.0	1	0	
	49.20	1.925	0.0	3515.0	1	0	
	50.20	1.934	0.0	3365.0	1	0	
	52.00	1.857	0.0	3575.0	1	0	
	52.40	1.910	0.0	3565.0	1	0	
	53.40	1.928	0.0	3405.0	1	0	
	54.90	1.872	0.0	3575.0	1	0	
	56.80	1.941	0.0	3415.0	1	0	
	57.60	1.928	0.0	3415.0	1	0	

* * * *	TIME (MIN)	PUMP RATE (BBL/MIN)	GAS RATE ON BOTTOM (BBL/MIN)	SPECIFIED PRESSURE (PSIA)	MUD 1=OLD 2=NEW	SNAPSHOT DESIRED? (1= YES)	* * * *
	59.00	1.910	0.0	3465.0	1	0	
	61.8	1.875	0.0	3465.0	1	0	
	63.3	1.857	0.0	3605.0	1	0	
	64.0	1.875	0.0	3565.0	1	0	
	64.6	1.913	0.0	3540.0	1	0	
	65.8	1.913	0.0	3465.0	1	0	
	67.6	1.888	0.0	3530.0	1	0	
	69.4	1.894	0.0	3505.0	1	0	
	70.8	1.910	0.0	3525.0	1	0	
	71.9	1.873	0.0	3450.0	1	0	
	72.7	1.925	0.0	3550.0	1	0	
	73.3	1.873	0.0	3460.0	1	0	
	73.9	1.894	0.0	3555.0	1	0	
	75.2	1.903	0.0	3465.0	1	0	
	76.2	1.943	0.0	3525.0	1	0	
	77.3	1.956	0.0	3390.0	1	0	
	78.0	1.928	0.0	3410.0	1	0	
	78.8	1.913	0.0	3485.0	1	0	
	85.2	1.913	0.0	3480.0	1	0	
	85.6	0.0	0.0	3480.0	1	0	
	85.9	0.0	0.0	3480.0	1	0	
	86.4	0.0	0.0	3435.0	1	0	
	87.4	0.0	0.0	3435.0	1	0	
* *	-----	-----	-----	-----	-----	-----	* *
***** END OF DATA *****							

VITA

Son of Mr. and Mrs. Manuel Casariego, Vicente Casariego G. was born in Yautepec, Mor., Mexico, February 9, 1944.

In the Fall of 1981, began working towards Ph.D. degree in Petroleum Engineering at Louisiana State University.

Master of Science in Petroleum Engineering, Louisiana State University, Baton Rouge, LA, Summer Commencement, 1981. Research work was on the determination of the velocity of large gas bubbles rising in annular geometries and the two-phase flow patterns present during well control operations.

Bachelor of Science in Petroleum Engineering, National University of Mexico, Mexico City, 1968.

Worked for the Mexican Petroleum Institute from 1968 to 1978. Work was focussed in the following areas:

Field: Design and supervision of pilot tests in the use of foam as a circulation fluid in workover operations in low pressure wells, in the southern oil fields of Mexico. Design and integration of experimental equipment to generate foam.

Research: Patented a foaming agent; study of foams and their application as circulating fluids in both well workover operations and drilling operations; laboratory evaluation of completion and workover fluids.

Married to the former Maria Teresa Hefferan and they have two children: Carla, 11 years old and Vince, 6 years old.